VU, NGOC H. M., Ph.D. Identification and Comprehensive Structural Characterization of Serum Lipid Markers to Type 1 Diabetes Progression. (2019)
Directed by Dr. Qibin Zhang. 171 pp.

Type 1 diabetes (T1D) is resulted from a self-destruction of insulin-secreting pancreatic β-cells, but the exact etiology remains unknown despite evidence indicating interaction between environmental and genetic factors. For the genetically predisposed individuals of T1D, islet autoantibodies are used for predicting the likelihood of T1D in the future, however, neither the appearance nor the titer can indicate the extent of the destruction of β-cells or quantify the remaining β-cell mass. Therefore, additional biomarkers are needed to monitor the health status of β-cell and the development of T1D.

Dysregulation of lipid metabolism exists in distinctive disease states. Several studies suggested lipids as a potential biomarker for T1D and the dysregulated profiles of lipids in T1D blood serum could predict the seroconversion of autoantibody positivity. However, many of the potential T1D lipid markers reported to date have not been validated in independent cohorts, and the structural identifications are ambiguous as only the total number of carbon atoms and double bonds in the fatty acyl chains were reported. There is no detailed structural information reported for the lipid species regarding the fatty acyl compositions and the location of C=C double bond- those fine structural details can determine the biological functions of lipids and help to elucidate the pathogenic mechanism of T1D. Based on these, we hypothesize that 1) lipid markers that either shed from diseased pancreatic β-cells or as a systemic response to autoimmune attack exist in

human serum; 2) dysregulation of lipid markers can predate the appearance of islet autoantibodies. Using advanced lipidomics tools and longitudinally collected sera from a well characterized T1D cohort, the primary goal of this project is to identify a panel of serum lipid markers correlated to T1D progression, with unambiguous characterization of their molecular structures.

In this dissertation, we are focusing on the following aims: *1)* Create a comprehensive human serum lipid library for high throughput LC-MS based lipidomics analysis; *2)* Identify candidate lipid markers to T1D progression through quantitative profiling of the temporal changes of serum lipids in T1D cohorts; and *3)* Comprehensively characterize the structures of the lipid markers. These aims were addressed in four projects that employed advanced instrumentation, sophisticated data analysis tools and precious human samples longitudinally collected from a T1D cohort. The first project generated a comprehensive library contains LC retention time and accurate mass of each lipid molecular species, and will be used for accurate and speedy identification of serum lipids in T1D subjects. In addition, this library can be implemented for an accurate and high throughput analysis of human serum lipids related to other diseases. The second and third project focused on development of Ozone-induced dissociation (OzID) on a high resolution MS to determine unambiguously the C=C double bond positions in unsaturated lipids. This technique is based on a highly selective gas phase reaction between C=C and ozone. We achieved high efficiency of OzID in both direct infusion- and RPLC-based workflows to effectively elucidate C=C

unsaturation in complex biological samples. Using the methodologies developed in the first three projects, the last project profiled temporal changes of lipidome in a T1D cohort, and identified a list of candidate lipid markers. These lipid markers showed a distinct profile prior to appearance of T1D as compared to healthy controls.

IDENTIFICATION AND COMPREHENSIVE STRUCTURAL CHARACTERIZATION OF SERUM LIPID MARKERS TO TYPE 1 DIABETES PROGRESSION

by

Ngoc H.M. Vu

A Dissertation Submitted to
the Faculty of The Graduate School at
The University of North Carolina at Greensboro
in Partial Fulfillment
of the Requirements for the Degree
Doctor of Philosophy

Greensboro
2019

Approved by

_____
Committee Chair

To my dear family, thank you for always be there for me and for raising me the way I am. To Uncle Toan and Aunty Lan Anh's family, without you, I wouldn't be where I am. Thank you for nurturing me and for believing in this kid……. To Grandama, I did it! Thank you!.....To my best friends, Thank you for counting the days for me and for assisting me with this journey….To some one special, Thank You, sincerely! I wouldn't be where I am without the love and support!

APPROVAL PAGE

This dissertation, written by NGOC H. M. VU, has been approved by the following committee of the Faculty of The Graduate School at The University of North Carolina at Greensboro.

Committee Chair _____

Committee Members _____

_____

_____

_____
Date of Acceptance by Committee

_____
Date of Final Oral Examination

ACKNOWLEDGMENTS

I would like to thank Drs. Nadja Cech, Nicholas Oberlies, and Norman Chiu for offering their guidance, expertise and precious time as committee members of my dissertation committee; Dr. Monica Narvaez-Rivas for training me in mass spectrometry and providing advices on my projects; Dr. Daniel Todd for assisting me in the mass spectrometry facility; Rodell Barrientos for his unsolicited support on my projects; Cherie Turner and Wendy Helton, for their thoughtful supports; all the faculty and staff of the Department of Chemistry and Biochemistry, and Center for Translational Biomedical Research for all the love and support. In addition, I want to thanks the collaborators for assisting me with samples, analysis and advice to finish the study: Dr. Kevin Giles, Dr. Jeff Brown, Dr. Marian Rewers and Dr. Wei Sha.

I especially want to express my gratitude to the Zhang research group including the past and current members for their continuous support. Thank you, Dr. Qibin Zhang for taking a faith in me, a newly-unexperienced student, to train me throughout my PhD journey.

This research was supported by the following grants from the NIH to Dr. Zhang: R21 GM104678 and R01DK114345.

TABLE OF CONTENTS

Page

LIST OF TABLES

Page

LIST OF FIGURES

Page

CHAPTER I

INTRODUCTION OF TYPE 1 DIABETES AND THE NEED OF ADDITIONAL BIOMARKERS

Background

Diabetes mellitus is a multifactorial and heterogeneous disorder that affects 415 million people worldwide and resulted in 1.6 million deaths in 2016, which is higher than the number of deaths from HIV and Malaria.[1] In total, diabetes gives rise to nearly $545 billion annual health care cost, with more than $100 billion from the United States alone.[2, 3] While Type 2 diabetes is more prevalent worldwide and constitutes 90% of the diabetic population, Type 1 diabetes (T1D), although occurs in <10% of the diabetics and mostly occurring in developed countries, is one of the most common chronic diseases in children, especially under the age of 5. There are approximately 1.25 million people in the United States with T1D, led to $14.4 billion in healthcare cost.[4, 5]

T1D is an autoimmune disease resulted from destruction of insulin-secreting pancreatic β cells, which can be triggered by environmental factors, such as diabetogenic enterovirus on genetically susceptible individuals; however, despite many decades of research, the exact etiology remains unknown.[6-8] It is commonly recognized that the progression of this disease depends on the remaining number of active β-cells, as illustrated in Figure 1.[8-10] In general, about half of the T1D subjects carry susceptible HLA loci and are predisposed to develop T1D.[8, 11, 12] During stage 1 of T1D progression

after exposure to an elusive environmental trigger, the immune tolerance to specific self-antigens is lost and T1D-susceptible individuals express multiple anti-islet autoantibodies. At this particular phase, a portion of β cells has already begun to undergo irreversible functional loss and self-destruction.[13, 14] However, it remains asymptomatic as there is no change physiologically to glucose tolerance. As the disease progress to stage 2, abnormal glycemia starts to appear with a more significant loss in functional β -cell mass. However, full-blown T1D symptoms won't appear until after reaching stage 3 of the disease when critical masses of β cells are being destroyed. At this stage of the disease, only up to 20% of β cells remaining, which leaves the individuals to rely on external insulin for their lifetime.[15]

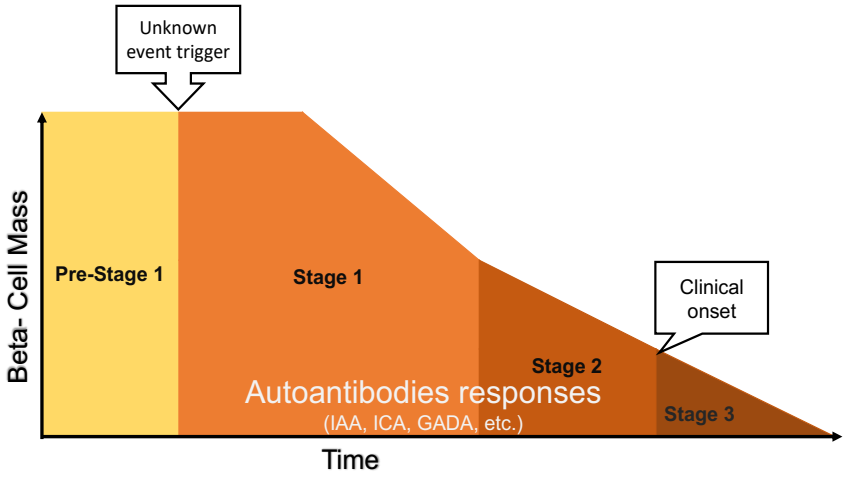

Figure 1. The Progression of T1D based on Time and The Beta-Cell Mass.

Current Biomarkers In Prediction of T1D

The progression of β-cell death is currently unpredictable, and the clinical symptoms of the disease are observed only when more than 80% of these cells are

dysfunctional or destroyed.[6, 7, 16] Hence, biomarkers that serve as predictive tools for the onset of clinical symptoms and indicators for the progression of the disease are in need.

Biomarkers are "substance, structure or process that can be measured in the body such as itself or its products can be used to predict the incidence of outcome or to monitor stages of a disease".[17] In addition to accurately diagnosis of T1D at its onset, good biomarkers of T1D should be able to quantify the risks of an individual during the different developmental stages of this disorder. Currently, autoantibody assays are clinically used as the diagnostic tool for those who have a family history of T1D. These assays can predict a 5-10 years window gap before the clinical onset of T1D.[12, 15] However, these biomarkers cannot predict when the clinical symptoms will present; nor tell what initiated the autoimmune attack on pancreatic β cells. [18, 19] Whilst the seroconversion of islet autoantibody can diverge from months to years before disease onset, the time point at which seroconversion occurs, may already be too late for preventing autoimmune-mediated β cell destruction or applying any therapeutic strategies to revert diabetes. As a result, there are insatiable interests and immediate needs in identifying biomarkers that can accurately indicate the initial process of β cell destruction process, and can be used for more accurate early diagnosis of T1D.

Lipids As Potential Biomarkers For T1D

In addition to being the main component of the cell membrane, lipids also play roles in signal transduction, and they are generally secreted into the bloodstream carrying information of tissues or cells' health status. Dysregulated lipid profiles are observed in different diseases,[20, 21] including T1D.[22-25] For example, studies conducted in Finland and

the United States showed that lipidomic profiles in the cord blood and blood serum/plasma of infants could differentiate T1D from healthy individuals.[23, 26] Oresic *et al*. showed that children who later developed T1D have lower levels of choline-containing phospholipids in their cord blood when compared to healthy children.[22, 27] Interestingly, they observed changes in *lyso*- and plasmalogen-phosphotidylcholine (PC) species prior to the appearance of islet autoantibodies in T1D patient.[27] Later, a follow-up study by the same authors focusing on children with HLA-conferred risk of T1D, investigated dysregulated lipidomic profiles at birth and during the development of β-cell autoimmunity and the progression of the disease. Agreeing with their previous results, they concluded that children who developed T1D had unique cord blood lipidomic profile, including a lower level of choline-phospholipids. Moreover, this newer study suggested that a panel of seven lipids could be used to predict the progression of T1D.[23] In addition to lacking the detailed molecular structure of the identified lipid species, most of the studies listed above used cross-sectional cohorts and samples collected from individuals with T1D clinical onset, it would be more informative if the lipidome during the different stages of T1D progression can be profiled longitudinally, so that the pathologically changes, even during the asymptomic period can be accurately captured to identify biomarkers indicating the early stages of T1D.

It is desirable to longitudinally profile lipid dysregulation during an individual's progression to T1D. As demonstrated in a very recent study, sera from 120 children from three groups (T1D progressor, non-progressor, and healthy control) were profiled for the changes in lipidome across 3 time points collected from <3 months up to 3 years of age.[25]

Comparison between time points showed that most of the changes in the lipidome were observed in a much younger age. Lower levels of sphingomyelins (SM) were observed in T1D patients when compared to healthy control and patients who developed autoantibodies but yet had a clinical onset T1D (non-progressor). The appearance of autoantibodies was associated with down-regulation of SMs and LPCs and up-regulation of cholesterol esters (CEs). Although validations are needed to further confirm the authenticity and utilities of these potential lipid markers, this study suggests that the concept that dysregulated lipidome exists at the early, asymptomic phases of T1D is valid, and it is feasible to identify novel lipid biomarkers predate the appearance of islet autoantibody for a very early prediction of T1D.

Conclusions

Biomarkers released from the pathological site or as systemic response to chronic diseases are at low level, which always pose a challenge to accurately determine the changes, especially considering many confounding factors such as age, gender, body mass index (BMI) are in play with the underlying disease biology. T1D is a polygenic autoimmune disease with an unknown etiology. Because of late intervention of the disease often leads to life-threatening complications, novel biomarkers are needed to monitor the disease progression and earlier disease intervention. Compared to cross-sectional studies, longitudinal studies can track the temporal changes of biomarkers on an individual basis by eliminating the large individual variations of human cohort. This requires high quality samples collected longitudinally from well characterized clinical cohorts. The samples of our study design were collected longitudinally from 5 months old

to 20 years old, which covers the span of T1D development and they were from age-matched individually from healthy controls, T1D progressors and autoantibody positive, non-progressors. By applying advanced technologies to profile the lipidomic changes in these samples, we are aiming to uncover the dysregulated lipids correlated well to the natural progression of T1D.

CHAPTER II

REVIEW OF LIPIDOMICS WORKFLOW: SAMPLE PREPARATION, SEPARATION AND MASS SPECTROMETRIC ANALYSIS

Introduction

Lipids are known to be ubiquitous molecules with a diversity of structures and are distributed throughout a wide range of organisms.[28] They are the primary component of membranes acting as the outer barrier for cells and organelles.[29] Moreover, lipids provide an appropriate hydrophobic environment for the interactions with membrane proteins.[30] Recently, evidence show that lipids play a vital role in many biological pathways, including transcription of genetic code to the regulation of pathway and physiological responses.[31] In the last decade, aberrant lipid metabolisms were observed in several human diseases such as diabetes, obesity, cancers and Alzheimer's disease.[32-35] The dysregulated profile of lipids provides a better insight into the biological pathways underlying the pathologies of these diseases and offers new directions for biomedical research.[36] Hence, lipidomics has attracted increasing attention from clinical studies. Taken all together, a systematic study of lipids has become the focal point in advancing the momentum of biosciences.[20]

The complexity in lipid structures, due to the number of different biochemical transformation happened during biosynthesis, has made lipids one of the most diverse

biomolecules. In 2005, LIPID MAPS consortium developed a comprehensive classification system and categorized lipids into eight categories based on their chemical structure and biochemical principles (Table 1).[37-39] Each category is further divided into classes and subclasses, based on the common functional groups or chemical "building blocks".[39] In this dissertation, we will focus on lipid categories and classes that are abundant and biologically significant in the mammalian systems. They are glycerophospholipids (GP) and glycerolipids (GL). GL are lipids including acylglycerols, in combination with alkyl and 1*Z*-alkenyl variants, and GP are lipids contains a phosphate group esterified to one of the glycerol hydroxyl groups.

Table 1. Lipid Categories and The Number of Structures Listed from the LIPID MAPS Database

Category	Abbreviation	Structure in Database
Fatty acyls	FA	2678
Glycerolipids	GL	3009
Glycerophospholipids	GP	1970
Sphingolipids	SP	620
Steol Lipids	ST	1744
Prenol Lipids	PR	610
Saccharolipids	SL	11
Polyketides	PK	132

In general, the biological function and activity of a molecule are based on its chemical structure. Thus, even a minor change in the structure can affect its physical and biochemical properties, as a consequence, influence the metabolism within a living organism.[40] The diversity in lipid function is reflected by an enormous variation in the structure of lipid molecules.[39, 41, 42] To better understand the roles lipids play in a

biological system, it is essential to characterize the accurate structure of individual lipid species, and on top of that, to determine changes of lipid metabolites associated with various pathophysiological conditions. Lipidomics, as the science for large scale study of lipid molecular species in biological systems, offers new opportunities for precision medicine by providing specific lipid molecular targets for disease diagnosis and prognosis.[43-45]

Overview Of Lipidomic Analysis

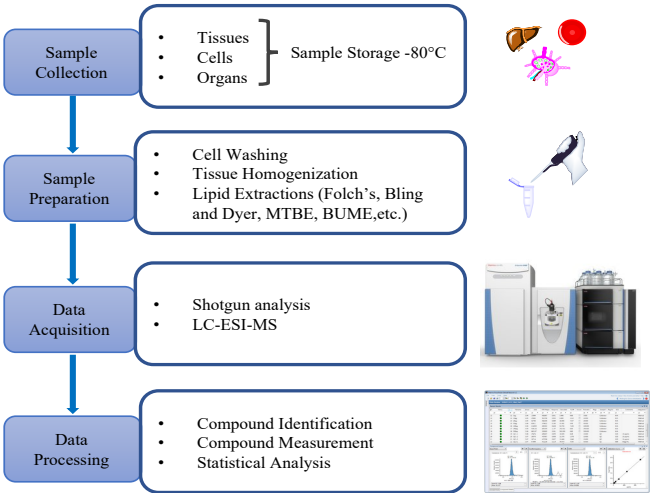

Figure 2. Standard Lipidomic Workflow including The Components of Sample Collection, Sample Preparation, Data Acquisition, and Data Processing.

The general lipidomic workflow includes lipid extraction, separation, structural characterization, feature identification, and statistical analysis (Fig.2). The type of samples and the purpose of the study should be taken into consideration for the experimental design. Hence, the lipidomic sample preparation should be tailored to the sample type, which is usually collected from a cell line, laboratory animals, or clinical hospitals and routinely stored at -80°C prior to analysis.

Total Lipid Extraction Methods

In biomedical research, the challenge has always been on how to efficiently collect the desired group or class of chemical compounds for the study. A critical step in lipidomic analysis is to effectively extract the majority of lipids representative in the sample without being biased, inducing, or promoting the degradation of lipids or contaminated with unwanted substances. The fidelity of the underlying biological study depends on the efficiency of the extraction method if one has a reliable analytical platform in the downstream sample analysis.

The main difference between lipids and other components of the biological sample (carbohydrates, proteins, and nucleic acid) is their hydrophobicity and solubility in an organic solvent.[46] The performance of the lipid extraction with a solvent system depends on the partitioning of different lipid classes into the organic solvent used. In most cases, the lipidomic extraction procedure involves a phase separation, where hydrophobic lipids partition into the hydrophobic phase, while the hydrophilic molecules remain in the aqueous phase.[47, 48] A good extraction process aims to recovery as many lipids as possible or to target the selected lipid classes with high specificity.

Folch Method And Bligh And Dyer Method

Folch and Bligh and Dyer methods were developed in the 1950s and have shown to be the most reliable and popular method used for lipid extraction for a variety of samples.[49, 50] In general, both methods share a similar workflow, as shown in Figure 3. Briefly, all samples, except biological fluids, are homologized and introduced to a monophasic chloroform/methanol (2:1,v/v) for Folch and (1:2,v/v) for Bligh and Dyer

method. The use of methanol results in disruption of hydrogen bonding networks or electrostatic forces between lipids and biopolymers, releasing the lipids into the organic layer. The introduction of chloroform formed the two-phase system, with lipids migrating into the chloroform layer at the bottom, and the polar biomolecules in the top layer. The simplicity and efficiency of the liquid-liquid extraction in these two methods were implemented in a variety of samples to extract a broad range of lipid classes.[47, 50, 51] Over the years, different modifications were done to these two methods, to make it more applicable for high throughput analysis. Overall, similar results were reported.[48] In terms of polar lipids, both methods have shown a similar recovery rate; however, Folch method indicates a better recovery for non-polar lipids, while Bligh and Dyer method is more popular in sphingolipidomic studies.[51] Thus, Folch method is the most popular procedure for total lipid extraction due to its recovery efficiency and the compatibility with a wide range of polarities of lipids.

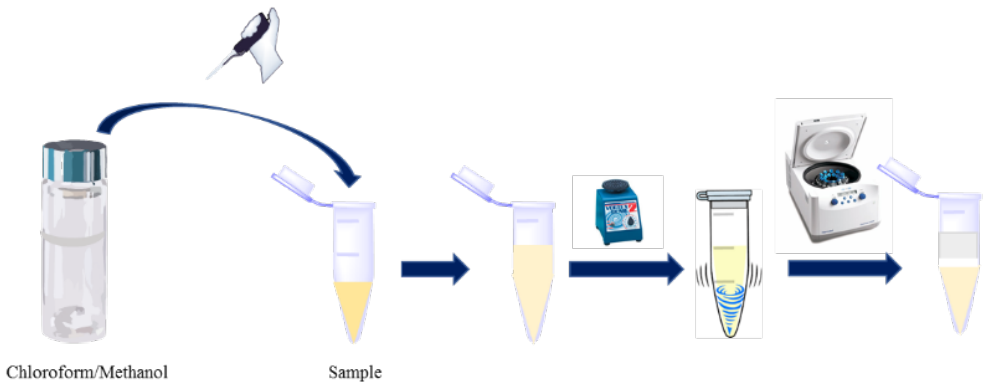

Figure 3. A Mixture of Organic Solvent (chloroform/methanol) was Added into The Sample, Vortexed, Incubated, and Centrifuged before Partition into Different Phases, Resulting Lipids Dissolved in The Bottom Layer, while The Middle Layer is The Protein and Top Layer is Water-Soluble Substances.

MTBE And BUME

One of the major drawbacks from the previous two extraction methods is the use of chloroform, which is a carcinogen and can be a health risk for lab personnel. In the last decade, different extraction protocols were proposed with the main objective of eliminating chloroform as the extraction solvent and having lipids dissolved in the upper organic layer to make it more amenable for automated liquid transfer. The most recent methods are methyl-tert-butyl ether (MTBE) and butanol and methanol (BUME) method.[52, 53]

MTBE was first introduced by Matyash et al. with the total lipids collected in the lipid-enriched upper phase using MTBE solvent in combination with methanol and water.[53] MTBE can offer a similar recovery when compared with the gold standard Folch method.[54] Hence, MTBE method showed its potential with automation and being considered for automated lipidomic extraction.[53] However, when taken with a high solvent/sample ratio, it is not compatible with the 96-well format. On the other hand, aiming for high throughput automated extraction of lipids, BUME method was proposed by Lofgren and coworkers to execute in 96-well format. [52, 55] The series of steps for sample preparation (sample collection, storage, homogenization, and extraction) were all performed in one single 2 mL polypropylene tube, hence the concept of "all-in-one-tube" concept. In terms of extraction efficiency, when compared with the gold standard Folch method, BUME obtained similar extraction efficiency for neutral lipids, sphingolipids and nonacidic phospholipids. [55] More evaluations between the three methods of MTBE, BUME and Folch could have been done to draw a more definitive conclusion.

Nevertheless, the Folch method remains the gold standard method in global lipidomics due to its unbiased recovery of all major lipid classes.

Major Separation Techniques Used In Lipidomics

Lipids are very heterogenous molecules, their diverse structures result into a wide range of chemical properties, from highly non-polar triacylglycerols to polar glycosphingolipids. As such, it is recommended to use a separation technique to increase the resolving power of analysis. In the past, thin-layer chromatography (TLC) or solid-phase extraction (SPE) was used to pre-fractionate lipids into classes prior to any measurement of lipids.[56] Since TLC and SPE are not as selective as liquid chromatography (LC), LC has been implemented to separate lipids based on their classes and/or molecular properties. Over the years, more researchers have adopted LC and developed different solvent systems to enhance the optimal separation of various lipids classes.

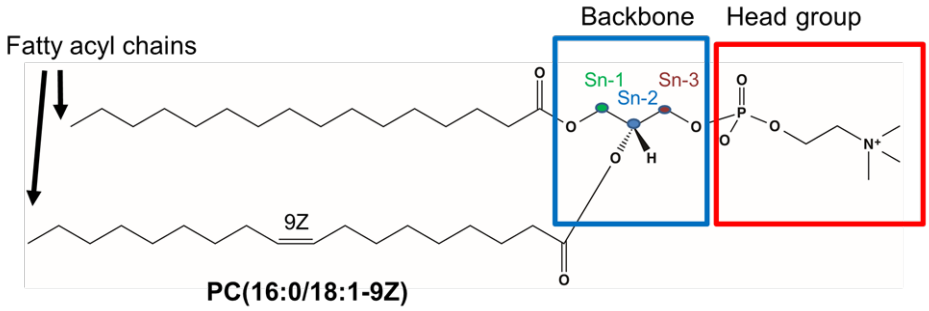

Figure 4. General Structure and "building blocks" of Lipids. Fatty Acyl Chains are Attached to *sn*-1 and 2 positions on the Glycerol Backbone of lipids, While the Head Group is Attached to The Backbone via Ester Linkage.

Liquid Chromatography

Liquid chromatography utilizes the competitive adsorption between the analyte, stationary phase, and liquid mobile phase for separation. Compared to other techniques, LC offers speed, resolution, sensitivity and specificity. There are three approaches of LC for lipidomic analysis. They are normal phase-LC (NPLC), hydrophilic interaction LC (HILIC), and reversed phase LC (RPLC).[57-60] These approaches separate lipids based on different mechanisms and can be tailored to separate the targeted analyte from a complex biological matrix.

Normal Phase Liquid Chromatography

NPLC separates lipids based on the polarity of the head groups (Figure 4),[61] and has the capability to resolve a wide range of lipid classes. In the 1980s, Christie was the pioneer in utilizing the polarity interaction of NPLC to separate class-based lipids in real samples.[59, 62] Throughout the years, modifications, including the introduction of aqueous and additives, improved the reproducibility and the peak shape of acidic phospholipids. Most importantly, the current approach in NPLC-based lipidomics uses a long, microbore silica column at a flow rate from 0.1-1 mL/min, and a higher flow rate for the desired study if there is a splitter. Typically, NPLC consists of a quaternary solvent system and uses highly non-polar solvents. The separation starts with a weak mobile phase such as heptane, isooctane, chloroform or a mixture of these solvents, and gradually introduces the stronger mobile phase for the elution of polar lipids. The stronger mobile phase comprises of methanol, IPA/MTBE, isooctane/IPA, acetone, IPA/MeOH, etc.[61] Triethylamine has been used to minimize the influence of fatty acyl chains in the

retention of the column particles.[61, 63] Depending on the type of detector, different additives may be needed. Additives can be salts such as ammonium acetate, ammonium formate, diethylamine, formic acids. In NPLC, the analysis time is typically longer (30-60 mins) than other techniques, primarily due to the choice of a longer column and the large particle-size sorbents and the time it takes for column re-equlibration. With the continuous development of NPLC, the number of lipid classes separated in a single run, increased from <10 lipid classes to more than 20 lipid classes and sub-classes, covering from non-polar to polar GL lipids in biological samples.[59, 63-65]

Hydrophilic Interaction Liquid Chromatography

Another approach that applies similar principle as NPLC to separate lipids is HILIC. Different from NPLC, HILIC uses non-polar solvents with the addition of water in the mobile phase to maintain a stagnant enriched water layer on the surface, which may attract the analyte.[66] Moreover, a stronger solvent system is used, which improves the separation of more polar lipids such as GP subclasses. HILIC uses a shorter column with a smaller ID, operated at a similar flow rate of NPLC, resulting in a shorter analysis time (15-60 mins). Usually, with HILIC, ACN or the mixture of ACN are used in the system to resolve the non-polar lipids, while the more polar solvent presented at the end disrupts the bonding between polar lipids and particles inside the silica or the BEH column. The additive used for HILIC is the same as NPLC. HILIC has been implemented on the separation of polar lipids,[67] and becomes a fundamental technique in the separation of sphingolipids while NPLC has more applications on a broader range of lipid classes and sub-classes in biological samples.

Reversed-Phase Liquid Chromatography

RPLC is the most popular LC technique and has been most widely used for analysis at molecular level-based separation because of the high demand in studying lipids at the molecular level.[63, 68, 69] The mechanism of RPLC separation of lipids is based on the interaction between the lipophilicity of the fatty acyl chains and the hydrophobic stationary phase (Figure 4).[70, 71] Lipophilicity is primarily determined by the length and the number of double bonds in the acyl chains. Thus, a lipid species contains a longer fatty acyl chain will stay in the column longer than the one with a shorter chain, and the saturated lipids will elute later when compared to lipids with mon- or poly-unsaturated analogs. Previous studies showed the use of long, narrow column with 2-5 μm particle size, operating at high UHPLC back pressure range while maintaining the high resolution. Lately, the new technology of using porous shell fused to a solid core decreases the diffusional mass transfer path at high speed, resulting in a high-resolution chromatogram at shorter time of separation. The standard RPLC columns used in lipidomics are Acquity UPLC BEH C18, HSST3, BEH C8, Kinetex C18, and Accucore C30. These columns can endure a high-pressure flow rate while maintaining the well-separated chromatogram. In RPLC, a weak mobile phase is applied at the beginning of the gradient which is made of water mixed with organic solvents such as water/acetonitrile (ACN), water/iso-propanol (IPA), or water/methanol/tetrahydrofuran, and gradually the gradient transits to a stronger mobile phase consists of high percentage of IPA. Based on its capability of separating lipids at the molecular level, RPLC is the primary tool for high-throughput separation and analysis of lipidome in biomedical

research.[57] Over the years, deciphering the complexity of molecular lipids has highlighted the need to resolve isomers and isobars within a lipid class or from different lipid classes, especially the isomeric lipids that have different biological functions. With the most recent developments in column chemistry and solvent system optimization, RPLC is capable of separating lipids with varying compositions of fatty acyls, *sn*-positional isomers, and some isobaric species.[72, 73] For example, application of RPLC in human plasma samples resulted in 300-400 lipid molecules identified, yet there are a high number of co-eluting peaks that can't be determined to their molecular levels.[26, 74, 75]

Two-Dimensional Liquid Chromatography

While each LC approach has its advantages, there are inherent limitations in each approach if using alone, which can be overcome by integrating with other approaches. For example, NPLC and HILIC are good at separating lipids based on their classes, while lacking the separation power of individual lipid species; on the contrary, RPLC can provide molecular level separation, but lipid species with the same or similar fatty acyl chains but belonging to different lipid classes can co-elute. Therefore, pairing LC techniques together can leverage more separation principles and results in a better separation.[60, 63, 76-78] This so called 2D-LC can be performed on-line (such as HILIC-RPLC) or off-line (such as NPLC-RPLC). The off-line mode offers a full optimization of separation in each of the dimension, even though it might be labor-intensive. The on-line approach, on the other hand, can be automated, but the separation is not as comprehensive as what off-line mode can deliver, due to the restrictions in sampling time and solvent compatibility. For a comprehensive identification of lipid species in the

lipidome of a complex biological sample, 2D-LC is frequently recommended.[63, 77, 79-81] This not only can uncover the low abundant lipid species that typically would be masked by the high abundant lipids, doing so would also enhance the confidence in assignment of the molecular structure of lipids.

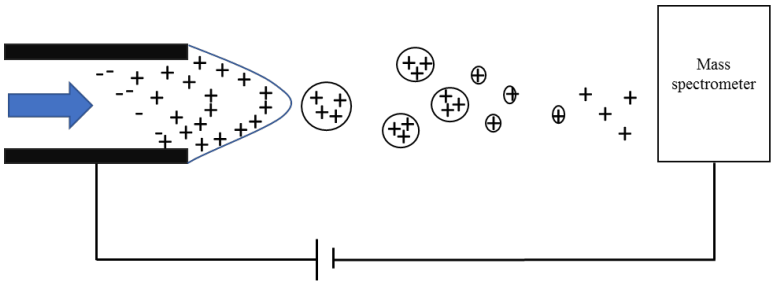

Figure 5. Mechanism of Electrospray Ionization.

Mass Spectrometric Analysis Of Lipids

Ionization Of Lipids

Concurrent with the development of mass spectrometric technologies, various methods have been applied to ionize lipids. In the 1980s, the popular method for ionization of biomolecule is fast atom bombardment (FAB), as such FAB was used in generating lipid ions for mass spectrometric analysis, but it has low sensitivity and is contaminated with ions from the insource fragmentation and matrix ions.[82] The need for a soft ionization technique resulted in the development of electrospray ionization (ESI) in the 1990s.[83] Compared to FAB, ESI offered up to 1000 times more sensitivity, enabled a rapid growth in the number of lipids identified in biological samples.[83]

Fenn and colleagues first developed ESI.[84] To analyze polar compounds, ESI uses a strong electric field under the atmospheric pressure to assist the transfer of ions from

solution into the gaseous phase prior to the mass spectrometric analysis. Compounds analyzed by ESI are converted to ionic form by protonation/deprotonation or ion adductation. To do so, a solution of compounds is dispersed to a fine spray of charged droplets, followed by solvent evaporation using nebulizing gas, and finally ejection from the highly charged droplets and desolvation into ions (Figure 5).

ESI-MS is a highly sensitive and efficient method, as long as a sufficient dipole potential is presented in a molecule to interact with the charge, ions can be formed and analyzed. ESI-MS-based shotgun lipidomics was first proposed by Han and Gross in 2003,[85] to directly analyze lipids from biological samples without any LC separations. In shotgun lipidomics, additives were added into the solution of lipid extract to assist the ionization of lipids. Positive ESI-MS yields abundant $[M+H]^+$ and $[M+X]^+$ (X= metal adducts such as Na, K, Li, etc.), while negative ESI-MS yields $[M-H]^-$ and other adducts. The results obtained by Han and coworkers were impressive and high throughput; however, there were challenges in working with a biological sample without any separation techniques. With the separation power provided by LC, ESI was also used to couple LC separation and MS analysis as it is a natural interface between these two techniques. For enhanced performance, the LC mobile phase needs to be a volatile solvent to preserve the ionization efficiency of ESI. NPLC uses apolar solvents; hence, the low conductivity of these solvents are not suitable with ESI-MS. In contrast, HILIC and RPLC are more compatible with ESI due to the organic-rich aqueous mobile phase can readily induce the ionization and desorption in the source.

Another well-known ionization technique is matrix-assisted laser desorption ionization (MALDI), which has been used for direct lipid analysis of a vast array of biological samples such as tissues.[86-88] MALDI has been applied in studying a variety of lipid classes, from non-polar lipids such as triacylglycerols to highly polar lipids of glycosphingolipids.[89-91] There are many applications of MALDI in biomedical research of lipidomics, especially when it comes to imaging lipid species in brain-related diseases.[92-94] The advantages of MALDI lie in its tolerance of impurities and less labor-intensive in terms of sample preparation. Moreover, it was observed that MALDI is more sensitive to phospholipids in the positive mode compared to ESI, resulting in multiple adducts for one lipid species in a single spectrum.[95] This can be an advantage but also a disadvantage because of the complexity of the spectrum and the competition for ionization between phospholipids and other lipids, making it difficult for identification as well as quantification.[96] Besides, MALDI is not compatible with LC technique. These shortcomings limit the application of MALDI in non-imaging-based lipidomics studies, where ESI is still dominated.

Tandem Mass Spectrometry For Structure Characterization Of Lipids

Confident identification of a lipid species requires accurate measurement of the molecular weight, isotopic pattern and very informative sub-structural information, with the former ones provided by high resolution MS and the latter one tandem mass spectrometric techniques. Tandem mass spectrometry or MS/MS is the basis for structural characterization of lipids, different scanning approaches such as product ion

scans, precursor ion scans, neutral loss scans, and multiple reaction monitoring scans are routinely used in shotgun and targeted lipidomics studies.[97-103]

Collisional induced dissociation (CID) is the default technique in commercial mass spectrometers for performing tandem mass spectrometry and the most commonly used fragmentation technique for structural analysis of lipids. To perform CID, mass selected ions are collided with inert gas molecules through either potential-driven ion acceleration or excitation at resonant frequency of ion motion, which leads to increased ion internal energy and bond cleavage. Lipid species within the same class often follow the same fragmentation pattern under CID, whilst different lipid classes having different headgroups present unique class-characteristic fragment ions. In positive ionization mode, GPs form protonated or ammonium adduct $[M+H]^+$ or $[M+NH4]^+$, or a wide range of metal adducts including $[M+Na]^+$, $[M+K]^+$ and $[M+Li]^+$, etc. Although the protonated adducts can form product ions resulting from neutral loss of fatty acyls, their relative abundance is very low, which makes it difficult for assignment of the structures. Alternatively, fragmentation of metal adducts showed more information-rich fragments that can indicate the *sn*-position on the glycerol backbone. However, their applications are not popular in the biomedical research due to the overcomplicated spectra.[104-107]

For acidic GPs that favor negative ionization, they generally form deprotonated ions [M-H]-. For example, CID fragmentation of PS (16:0_18:1) produces the carboxylate anions $[RCO_2]$- at m/z 255 and 281, known as fatty acyl substituents. These two product ions also present concomitantly with anions of the fatty acids RCO_2H or ketene derivatives R'CHCO. Moreover, the precursor ions of PS easily lose the serine

moiety (-87 Da) under the influence of CID. From these fragments in a spectrum, one can conclude the lipid class, as well as the composition of the acyl chains (number of carbon and double bonds). Meanwhile, PCs and SMs cannot be easily deprotonated, instead, they form acetate $[M+CH_3CO_2]^-$, formate $[M+HCO_2]^-$, or chloride adduct $[M+Cl]^-$. CID of these adducts generates neutral loss of the methyl group $[M-CH_3]^-$, and further disassociates to $[RCO_2H]^-$ or $[R'CHCO]^-$ to reveal the structure of the fatty acyls. Moreover, the relative abundances/ratio between two fatty acid ions $[R_1CO_2]^-$ and $[R_2CO_2]^-$ in GPs can be used for *sn*-assignment. For instance, the PC (16:0_18:0) yielding two fatty acid ions at m/z 255 (FA (16:0)), and the more abundant at m/z 281 (FA (18:1)). This result indicated the FA (16:0) belongs to *sn*-1 position while FA (18:1) attached to *sn*-2 position, so this lipid is reported as PC (16:0/18:1) with clear sn-annotation. Hence, the ratio of $[R_1CO_2]^-$ / [R2CO2]- <1 has been used to characterize the *sn*-assignment of lipids. The combined use of CID-MS/MS in both ionization modes can provide both the head group and fatty acyl information and to a certain degree, the stereo-specificity of *sn*-position; therefore, it has been increasingly applied to lipidomic studies. It is of note that a different version of CID is implemented in the high resolution orbitrap instruments; this higher energy collisional dissociation (HCD) performs similarly to the CID in other mass spectrometers. Both techniques produce very similar fragments, with a slightly different relative ratio.

Although CID/HCD has been the main tool for structural elucidation of lipids, the fragmentation can only provide the head group (lipid class), the composition of fatty acyls (total number of carbons and double bonds), and *sn*-assignment in some cases.

Direct CID/HCD of lipid ions has not been able to form fragments that can indicate the unsaturation site on acyl chains, or the C=C stereochemistry, which are level 4 and 5 of lipid structural identification as illustrated in Fig. 6. This has remained as the major challenge in the structural elucidation of lipids. Nonetheless, various approaches have been developed to overcome this challenge.

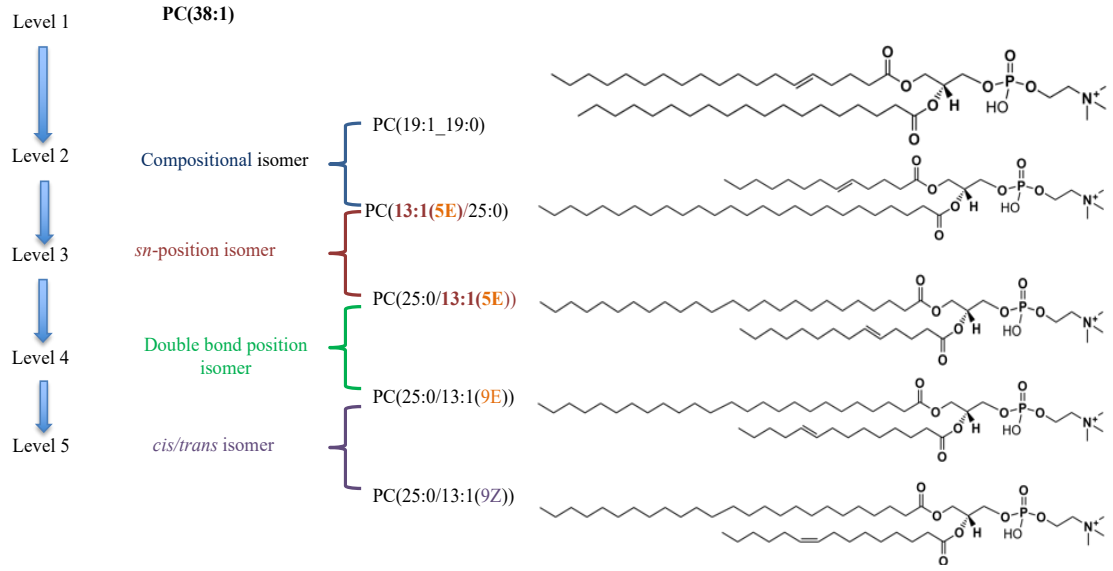

Figure 6. Summary of The Levels of Structural Identification in Lipids using PC 38:1 as an Example. Level 1 contains Information of Total Number of Carbon and Double Bond; Level 2 presents Compositional Isomers with The Composition of Fatty Acyl Chains; Level 3 contains *sn*-assignment of Fatty Acyls; Level 4 represents Lipids with information of Double Bond Positions; and Level 5 contains *cis/tran* information.

One of the approach is to derivatize unsaturated lipids using olefin-specific photochemistry or chemistry, such as using Paterno-Buchi,[108] and most recently, m-CPBA epoxidation[109] to enable a selective reaction to the C=C, which is carried out either in solution or during ionization process, then using CID-MS/MS of the derivatized ions to generate fragment ions specific to C=C position. In Paterno-Buchi reaction, a carbonyl

and an olefin produce a four-membered oxetane ring via UV irradiation during ESI, and CID-MS/MS of the oxetane ring-containing derivative subsequently yields diagnostic ion pairs with 16 Da different. Although this reaction is implemented explicitly for pinpointing the double bond position, its reaction efficiency is rather low, resulting in a mixture of reacted and non-reacted lipids, which overcomplicates the interpretation of mass spectra. m-CPBA, on the other hand, utilizes the highly reactive epoxidation reaction of C=C to form an epoxide product in solution, which subsequently is being ionized and fragmented under CID-MS/MS to form aldehyde and olefin diagnostic ions (16 Da mass different). While the reaction is reported to have a complete conversion after 10 min and the diagnostic fragments are easy to generate and interpret in any commercial mass spectrometers, the epoxide intermediate is induced prior to the ESI, and can be an isobar to other lipids if studied in a complex mixture. In addition, this technique is still under development to be compatible with polyunsaturated lipids. Overall, both techniques can pinpoint the position of unsaturation in lipids and use routine CID-MS/MS for dissociation of derivatized ions, their application to complex biological sample may be limited as the low reaction efficiency, or the newly formed products can introduce additional species, sometimes isomeric or isobaric to the species in the already complicated lipidome.

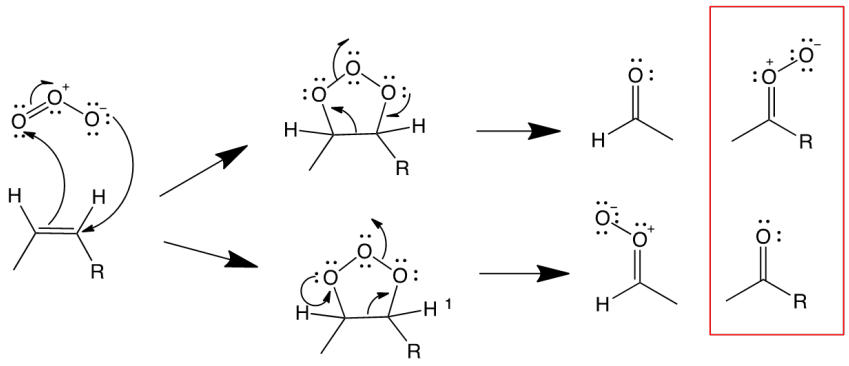

Figure 7. Mechanism of The Ozonolysis Reaction. *1,3*-Dipolar Cycloaddition of Ozone to The Alkene Leading to The Primary Ozonide, Which Decomposes to give a Carbonyl Oxide and a Carbonyl Compound.

Gas Phase Ion Chemistry

The reaction between ozone and olefin is also very specific and ozonolysis has been used in organic chemistry for many decades to oxidize alkenes in solution. This reaction was first used in solution for lipid unsaturation analysis using a mass spectrometer by Murphy and coworkers in 1996.[110] Ten years later, Blanksby and coworkers revisited the same subject and initiated ozonolysis in the gas phase, by generating ozone using the high voltage corona discharge in the ESI source.[111, 112] Once ozone attacks the alkene double bond, it follows the Criegee mechanism (Fig. 7),[113] and dissociates the ozonide into a carbonyl oxide diradical and an aldehyde. The ions observed in the spectra are the ones that carry the charge and form the paired products. They are the charge-bearing Criegee intermediate and aldehyde, with 16 Da mass difference (Fig. 8). While OzESI-MS offers high selectivity to the C=C double bonds, their applications are limited to individual lipids or simple lipid mixtures because the reaction happens with every unsaturated lipids at the source and therefore lacks

selectivity with targeted lipids, in addition to the low reaction efficiency.[112] Moreover, the OzESI products are isobaric with other oxidized lipid ions directly from the lipid extract, and the assignment of fragment ions to their respective precursor ions becomes ambiguous as the complexity of the mixture increases. To further improve gas phase ozonolysis in mass spectrometry, Blanksby and his team brought ozone gas into an ion trap of a mass spectrometer and utilized the ion trap as a gas chamber/reaction cell.[114] This approach kept the selectivity of ozonolysis to only the C=C of mass-selected lipid ions. This technique was first introduced in 2008, and termed ozone- induced dissociation (OzID).[114] In the last ten years, OzID-MS was implemented on a few different instrument platforms, from low resolution ion trap instruments to high resolution Q-TOF based mass spectrometers, and from studying only lipid standards to application of biological samples (Fig. 9).[115-119] Moreover, OzID can be hyphenated with CID in tandem dissociation to get more informative structural information of lipids. The improvement in its efficiency has also moved from being only applicable with direct infusion to compatible with LC-based separation.[115-117, 120-125] OzID-MS also is promising in distinguishing between the *cis/trans*-isomers;[119, 126] however, reference lipid standards are suggested to be compared with before a definitive assignment of the structure can be reached.

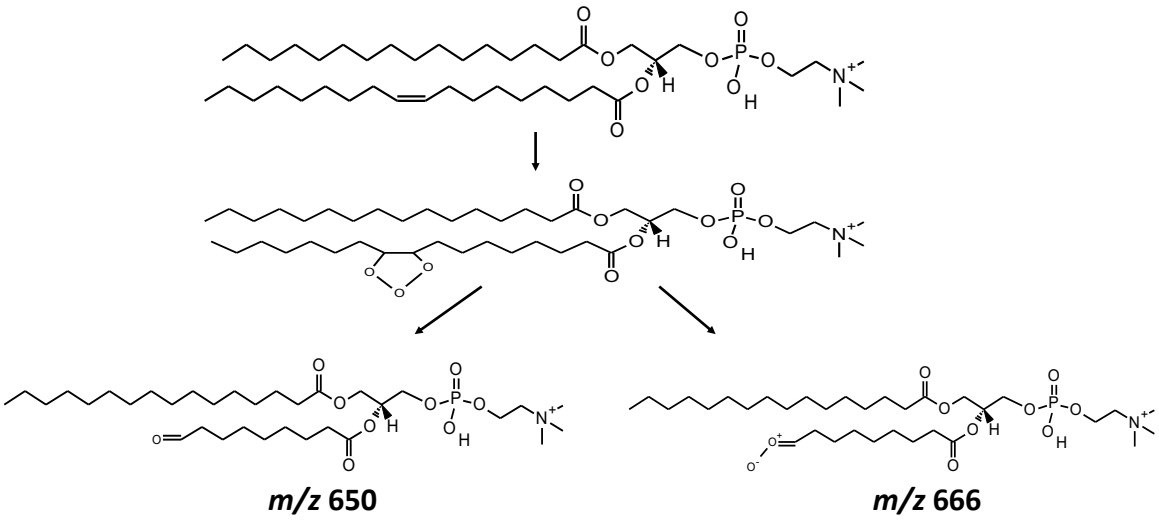

Figure 8. OzID-MS Spectra of PC (16:0/18:1). Ozone Attacked the C=C Double bond on The FA (18:1) of the Lipid, to Form Primary Ozonide, and Subsequently Cleaved to Form Aldehyde Product (*m/z* 650) and the Criegee Product (*m/z* 666). These Two Product Ions are 16 Da apart.

Figure 9. The Revolution of OzID-MS over the last 10 years.

Conclusion And Future Directions

Biological samples are complex. Lipids are immersed in and also bound to other biological molecules, such as proteins. High structural diversity of lipids itself already poses a significant challenge as many isomeric lipid species exist in a biological sample.

In addition, high abundant lipid species can mask the detection of low abundant ones. Similarly, lipid classes with high ionization efficiency can mask the detection of the classes with lower ionization efficiency. As such, comprehensively profiling the lipidome and establishing the structure-function relationship of lipids require optimal extraction of lipids from the biological matrix, integrated use of separation methods to reduce the complexity of lipids prior to structural analysis, and combined use of positive and negative ionization modes and tandem mass spectrometric techniques, including both CID/HCD and OzID to thoroughly and confidently characterize the structure of lipid species. This is the strategy that we have adopted in this dissertation to identify lipid biomarkers for T1D, and will be presented in detail in the following chapters.

CHAPTER III

ACCURATE MASS AND RETENTION TIME LIBRARY OF SERUM LIPIDS FOR TYPE 1 DIABETES RESEARCH

This chapter is published at journal *Analytical and Bioanalytical Chemistry* and is presented in this style.

Introduction

Besides of being essential structural components of cell membrane, lipids have other distinctive biochemical roles in providing a hydrophobic environment for membrane proteins, assisting cell signaling process, regulating action of hormones, and storing biochemical energy.[31, 127] Dysregulation of lipid metabolism has offered critical insights into the pathogenesis of complex diseases, and lipids are identified as biomarkers to cancers, diabetes, Alzheimer's and other inflammatory diseases.[128, 129] While clinical type 1 diabetes (T1D) features metabolic dysregulation of some serum lipid species, interestingly, changes in lipidome appear to precede hyperglycemia or even the appearance of islet autoimmunity.[25, 26, 130]

Biomarkers can be either secreted or leaked from pathologic tissues to bloodstream. Although cell, tissue and biofluid samples are routinely used to study diseases, blood plasma and serum are the most commonly used specimen for clinical diagnostics because of their availability.[131] However, significant analytical challenges are associated with this type of complex specimen, namely the identification of the low

abundant lipids and the differentiation of isobaric and isomeric species commonly exist in glycerophospholipids and glycerolipids classes. Because of these, most of the lipids reported in the literature were characterized to the level of summed composition, i.e. total number of carbon and double bonds in the fatty acyls, which results in ambiguity in characterizing the exact molecular structure and, in turn, hinders further investigation into the roles of these lipids in biological processes.[28]

Liquid chromatography coupled with tandem mass spectrometry (LC-MS/MS) is increasing used for untargeted lipidomic analysis owing to the increases in LC resolving power, decreasing particle size, novel column chemistry and new separation mechanisms.[58, 63, 73, 80, 132, 133] The popularity of RPLC-MS based method can be further explained by several advantages such as more reliable identifications of individual lipid species exist at trace level and the separation of isomeric and isobaric lipids with reduced ion suppression.[63, 132] Software, such as LipidBlast, LipidSearch, LipidMiner, and MzMine2 were developed to process LC-MS/MS based untargeted lipidomics data and to handle the need of automated data processing.[134-137] These software use in-*silico* generated mass fragment libraries - many based on LIPID MAPS (https://www.lipidmaps.org/) - for lipid spectrum annotation. The drawback of providing a large database for lipidomic profiling in compound identification is the prevalence of false positive identifications. Incorporating LC retention time information into the database search could greatly reduce the search space and improve the search accuracy. In this respect, accurate mass and time tag approach has been developed for

proteomics,[138, 139] and more recently applied to metabolomics,[140] but rarely this approach has been used in lipidomics.[141]

Previously, we developed an offline two-dimensional LC-MS/MS method for untargeted lipidomic profiling.[63] In this approach, a mixed-mode LC and RPLC coupled to a high resolution mass spectrometer was demonstrated to double the lipidomic coverage for complex tissue and plasma samples in comparison to RPLC-MS/MS alone. More importantly, very reproducible retention time and high mass measurement accuracy was achieved for each lipid molecular species. In current work, we apply this approach for a comprehensive identification of lipids in T1D patient sera. Total lipids extracted from pooled sera were fractionated using mixed-mode LC based on the head group of each lipid class, collected fractions were further separated on a RPLC-MS/MS platform k cohort. The DAISY study protocol was approved by the Institutional Review Board of the University of Colorado and detailed study design and methods have been previously published.[142, 143] Written informed consent were obtained for all study participants from a parent or legal guardian. Samples were stored at -80º C prior to analysis. Analysis of these samples was also approved by the Institutional Review Board of the University of North Carolina at Greensboro. All research was performed in accordance with relevant guidelines/regulations.

In total, serum samples from 50 subjects were selected from two groups: Type 1 Diabetes (T1D) group comprised of children who developed islet autoimmunity and progressed to T1D and the control group from children who remained negative islet autoimmunity at all times. Four time points (0.7 to 14.7 years of age) during the disease

progression in the T1D group were selected for this study, which include the earliest time point possible in the longitudinal study, the time point prior to and after appearance of persistent islet autoimmunity, and the time point of clinical diagnosis. Sample selection of the control group was age and sex matched to the T1D group.

Pooled samples were created to represent different stages of disease development and also reflect the nature of each group. Aliquot of 5 μL from each sample within the first two time points of each group were pooled, so were the last two time points. Extraction of serum lipids was carried out following a modified Folch method.[63] Briefly, pooled samples were diluted with cold (-20º C) chloroform/methanol (2:1, v/v) at ratio of 5:1 (solvent/sample ratio). The mixture was vortexed for 10 s, then set at room temperature for 10 min and vortexed again before centrifuging for 10 min at rate 10,000 RPM. The chloroform phase was collected to a glass vial, followed by evaporation of the extracted lipids to dryness under vacuum, and stored at -80° C in nitrogen gas prior to further analysis.

Materials and Methods

Chemical Reagents And Standards

Ammonium formate, *n*-heptane, acetone, methanol, isopropanol (IPA) and water (Optima® LC-MS grade) were provided by Fisher Scientific (Fair Lawn, NJ). Acetonitrile (ACN) and formic acid were of LC/MS quality and acquired from Fluka (Germany). Chloroform (HPLC grade) and ammonia solution were purchased from Merck (Germany).

Lipid standards were purchased from Avanti Polar Lipids (Alabaster, AL), which include Cer d18:0/24:1, PC 18:0/18:1, PE 16:0/18:1, PG 16:0/18:1, PS 16:0/18:1, PI 21:0/22:6, PC P-18:0/20:4, PC O-18:0/20:0, PE P-18:0/22:6, PE O-18:0/18:0, SM d18:1/12:0, and d5-TG ISTD Mix I. The acylglycerols, fatty acids, cholesterol and cholesterol esters were obtained from Nu-Chek Prep, Inc. (Elysian, MN).

Mixed-Mode LC Fractionation Of Lipid Classes

The mixed-mode LC separation was performed according to our previous published method using an Agilent HPLC equipped with a quaternary pump, and an Agilent 1260 Infinity evaporative light scattering detector (ELSD) (Palo Alto, CA, USA).[63] The method was run on a Chromolith Performance Si column (100mm×4.6mm, macropores size 2.1μm and mesopores size 13nm, Merck, Darmstadt, Germany). The autosampler was set up at 23º C and the injection volume was 10 μL, equivalent to 100 μL of serum.

Overall, all lipid classes were collected into these fractions with the following order: CE and TG from 1- 3.2 min; Chol and *1,3*-DG from 3.21-4.1; *1,2*-DG *from 4.11*-5.5 min; MG from 11-13.6 min; Cer from 13.61- 15 min; FAs from 15.01- 17 min; PG from 20.51- 22 min; PE from 26.01- 28 min; PI and PS from 28.01-30.5 min; PC from 30.51- 35 min; SM from 35.01- 39 min; *sn-1* LPCs from 39.6-41 min; *sn-2* LPCs from 41.5-42.4 min.

RPLC- MS/MS Analysis

The RPLC-MS/MS analysis was performed as we reported previously,[73] using a Vanquish UHPLC system coupled to a high resolution hybrid Quadrupole-Orbitrap mass

spectrometer (QExactive HF, ThermoFisher Scientific, USA). The separation was achieved using an Accucore C30 column (ThermoFisher Scientific) maintained at 40º C and the gradient was delivered at a flow rate of 350 µL/min. The mobile phases A and B were ACN:H_2O (60:40, v/v) and IPA:ACN (90:10, v/v), respectively, both containing 10 mM NH_4HCO_3 and 0.1% HCOOH.[63, 73] The sample tray was set at 15°C with the injection volume of 5 µL.

The following parameters were used in electrospray ionization: the spray voltage, the capillary temperature and the heater temperature were at 3 kV, 350 °C and 400 °C, respectively, for both ionization modes; the S-Lens RF level was set at 50. The Orbitrap mass analyzer was operated at a resolving power of 120,000 in full-scan mode (scan range: 114 – 1700 m/z; automatic gain control target: $1e^6$) and of 30,000 in the Top20 data-dependent MS2 mode (HCD fragmentation with stepped normalized collision energy: 25 and 30 in positive ion mode, and 20, 24 and 28 in negative ion mode; maximum ion injection time: 100 ms; isolation window: 1 m/z; automatic gain control target: $1e^5$ with dynamic exclusion setting of 15 s).

Fatty Acid Analysis

The method for total fatty acid analysis was described in our previous work.[63] Briefly, total lipids were extracted from human serum and dried prior to hydrolysis and derivatization with 2M KOH/CH_3OH. The resulted fatty acid methyl esters (FAMEs) were extracted and profiled using an Agilent 7890 GC system (Agilent Technologies, Santa Clara, CA) coupled to a Leco Pegasus HT time-of flight MS (Leco, St. Joseph, MI). A HP-88 column (100 mx 0.25 mm) with a film thickness of 0.2 µm (Agilent

Technologies) was utilized for separation of FAMEs. Commercial FAMEs standard mixture (Agilent) was used as reference standards.

Data Processing

All LC-MS/MS data files were processed using LipidSearch software (version 4.1) (ThermoFisher Scientific) to identify lipid molecular species within each lipid fraction. Settings of LipidSearch were as follow: precursor tolerance: 5 ppm; product tolerance: 5 ppm; product ion threshold: 5%; m-score threshold: 1; Quan m/z tolerance: ± 5 ppm; Quan RT (retention time) range: ± 0.5 min; use of main isomer filter and ID quality filters A, B, C and D; Adduct ions: +H and $+NH_4$ for positive ion mode, and -H, +HCOO and -2H for negative ion mode. The lipid classes selected for the search were: LPC, PC, LPE, PE, LPS, PS, LPG, PG, LPI, PI, LPA, PA, SM, MG, DG, TG, CL, So, Cer, CE. The same lipid annotations identified within ± 0.1 min were merged into the aligned results. LipidSearch results were manually inspected for *sn*-positional assignment of fatty acyls according to corresponding fragment ion intensities in tandem mass spectrometry. Identification results were further filtered using the retention time -total fatty acyl chain length correlation and, confident identification was also restricted to fatty acyl compositions provided by GC-MS-based total fatty acid analysis.

The resultant raw data files of the pre-T1D sample were processed using Progenesis QI (Nonlinear Dynamics, UK) for peak detection with the following parameters: peak percentage 0.04%, retention time windows from 1 min to 25 min. All detected features were searched against our human serum lipid AMT library with matching tolerances of 0.2 min in retention time and 10 ppm in mass accuracy.

Results

Isomeric and isobaric lipid species are dominant in highly complex blood serum samples, in addition, highly abundant lipid species can mask the low abundant lipid species, similarly the high ionization efficiency species can interfere the detection of species with low ionization efficiency. Therefore, to broaden the coverage of serum lipidome and to provide highly confident lipid identification, a mixed-mode-LC coupled with an ELSD detector was used to fractionate the total lipid extract into different lipid classes according to the polarity of lipid head group, which is followed by further separation of the collected fractions into individual molecular species and structural characterization using RPLC-MS/MS analysis (**Fig. 10**).

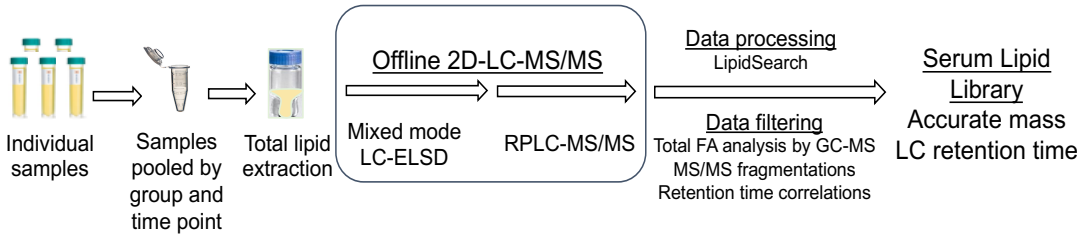

Figure 10. Workflow to Create The Accurate Mass and Time Tag Library for Serum Lipids. Total Lipids were Extracted From Pooled Samples. In the First Dimension of LC Separation, Fractions Containing Lipid Classes from Total Lipid Extraction were Separated and Collected using Mixed-Mode LC-ELSD, and further Analyzed at the Molecular Level in The Second LC Dimension using RPLC-MS/MS. Putative Identifications Obtained from Automated Data Processing Software LipidSearch were Manually Validated using Multiple Data Filtering Criteria (total fatty acid analysis by GC-MS, MS/MS profile and LC Elution Order), Only The Verified Lipid Identifications were Curated into The Final Lipid Library with Each Species Annotated With Accurate Mass and RPLC Retention Time.

Fractionation Of Total Lipid Extracts Using Mixed-Mode LC To Simplify The Sample Complexity Of Downstream RPLC-MS/MS

We applied a previously optimized mixed-mode LC-ELSD method for class-level separation of lipids from total lipid extract of serum.[63] In total, 18 lipid classes and subclasses were detected and eluted in the order of increasing polarity (**Fig. 11**), namely: cholesterol ester (CE), triacylglycerol (TG), cholesterol (Chol), phosphatidylglycerol (PG), phosphatidylethanolamine (PE), phosphatidylethanolamine plasmalogen (p-PE), lysophosphatidylglycerol (LPG), phosphatidylinositol (PI), phosphatidylserine (PS), lysophosphatidylethanolamine (LPE), phosphatidylcholine (PC), phosphatidylcholine plasmalogen (p-PC), sphingomyelin (SM), *sn2*-lysophosphatidylcholine (*sn2*-LPC) and *sn1*-lysophosphatidylcholine (*sn1*-LPC); ceramide (Cer), *1,3*-diacylglycerol (1,3-DG) and *1,2*-diacylglycerol (*1,2*-DG) existed only in low level in serum, therefore they were not labeled on the chromatogram. Because of the low level of LPG, LPE and LPI in serum, they co-eluted with other glycerophospholipids, but this did not pose a challenge in downstream RPLC-MS/MS analysis as the co-eluting classes do not share isobaric species (**Fig. 11)**. Although mixed-mode LC-ELSD analysis can distinguish disease-associated dysregulation of metabolism at the lipid class level, overall, there were no noticeable class-level changes between the disease groups or between the early and late time points of each group.

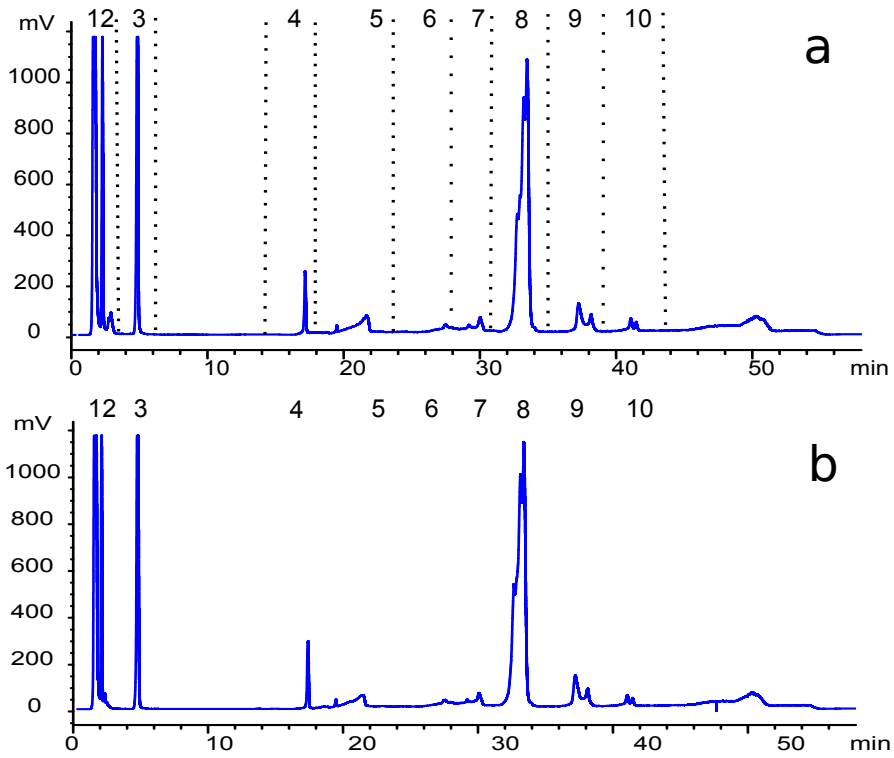

Figure 11. Mixed-Mode LC-ELSD Chromatograms Obtained from Total Lipid Extract of Human Sera. a) Pre-T1D Samples and b) Healthy Control Sample. Both Chromatograms Showed Similar Lipid Profiles at Lipid Class Level. 1: CE, 2: TG, 3: Chol, 4: FA, 5: PG, 6: LPG, PE, p-PE, 7: PI, PS, LPE, 8:PC, p-PC, LPI, 9:SM, 10: *sn2*-LPC, *sn1*-LPC.

RPLC-MS/MS Analysis Of Lipid-Class Fractions Improved Confidence In Structural Identification Of Lipid Molecular Species

With mixed-mode LC separation, the cross-class, isobaric species used to co-elute were separated into different fractions for further downstream RPLC-MS/MS-based molecular level separation and identification. This greatly improved the confidence of structural assignment. For instance, a full scan MS of PC fraction showed a lipid species with a neutral mass of 755.5465 Da. According to Human Metabolome Data Base (www.hmdb.ca) and LIPID MAPS (www.lipidmaps.org), 32 and 28 isomeric lipid

species from different lipid classes are associated with this mass, respectively, each with a unique composition. However, because this species was from the PC fraction, we limited the database search space of LipidSearch to PC when processing the RPLC-MS/MS raw data of this fraction. Specifically, the precursor ion at *m/z* 756.5529 ($[M+H]^+$) was selected for MS/MS fragmentation in positive ionization mode. As shown in **Fig. 12a**, the base peak at *m/z* 184.0733 - a signature ion of phosphocholine head group confirmed the identity of the fraction collected in the mixed-mode LC separation as PC. Similarly, *m/z* 800.5445 ($[M+HCOO]^-$) was selected in the negative ionization mode for MS/MS, and it aligned well in retention time (<0.1 min) with the positive mode data. As shown in **Fig. 12b**, prominent ions at *m/z* 253.2172 and 279.2329, corresponding to the ions of $[FA(16:1)-H]^-$ and $[FA(18:2)-H]^-$, respectively, demonstrated that the fatty acyl composition of this species is 16:1 and 18:2. The *m/z* 279.2329 as the base peak indicated that FA 18:2 located at *sn-2* position on the glycerol backbone, as it is known that fragment ion ratio of $[FA_1-H]^-/[FA_2-H]^-$ is less than 1.[72, 73, 144] Hence, we concluded the identification for the species with neutral mass of 755.5465 Da with the retention time of 9.61 min to be PC 16:1/18:2.

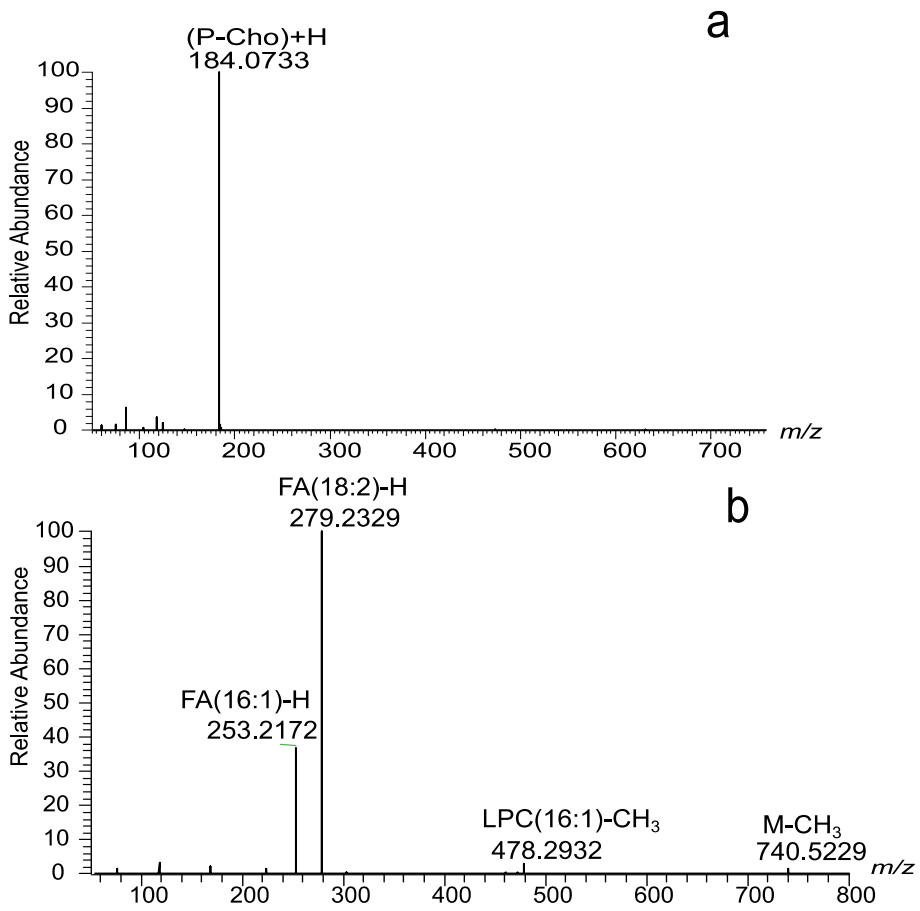

Figure 12. MS/MS Spectra of PC 16:1/18:2 in a), Positive ion Mode and b), Negative ion Mode. m/z 184.0733 in a) Shows the Signature ion of PC , Which also Confirmed The Accuracy of Mixed-Mode LC Fractionation, While m/z 253.2172 and 279.2329 in b) Reflect the Composition of the Two Fatty Acyl Chains and The sn-position assignment.

Although fragment ion ratio of $[FA_1\text{-}H]^-/[FA_2\text{-}H]^-$ <1 has been commonly used to assign the *sn*-positions, there are reported exceptions to this rule and it casts doubt on solely relying on this ratio to assign the *sn*- position when using different collision energies.[98, 145-147] Therefore, we performed MS/MS for glycerolphospholipids and triacylglycerols standards containing different compositions of fatty acyl chains. These standards were studied with the stepped collision energy listed in the method section,

under both direct infusion and LC-MS conditions. In agreement with the literature,[73, 104, 106, 107, 146, 148] our data suggested that for most of the phospholipids, generation of $[FA_2\text{-}H]^-$ is more favorable than $[FA_1\text{-}H]^-$ and the ratio of $[FA_1\text{-}H]^-/[FA_2\text{-}H]^-$ is consistently smaller than 1 at different normalized collision energy. As a result, majority of the lipid species identified in this work have clear annotation of *sn*-positions using the "/"; for lipids with uncertainty in assigning the *sn*-position, we annotated it with "_".[149, 150]

Elution Order Of Lipids On RPLC Column Depends On The Total Carbon Number And Degree Of Unsaturation Of The Fatty Acyls

Relative retention on RPLC column depends on the hydrophobicity of analyte, the more hydrophobic, the later it elutes. In the case of lipids, this is determined primarily by the length and saturation of fatty acyls. This rule is especially true for the molecular species within the same class of lipids, where all species share the same head group.[71, 151] We plotted the retention time versus the total carbon number of fatty acyls and observed, as shown in **Fig. 13**, a relationship of second degree polynomial regression for the fully saturated species of the abundant serum lipid classes: TG, SM, PC, LPC and Cer, with each class having a different slope reflecting the actual gradient conditions experienced by species in each class. In these plots, we observed species with the same number of total carbon but different retention time. By studying their MS/MS profile in both positive and negative mode, we confirmed they are *sn*-position isomers. Nevertheless, the correlation coefficients R^2 are greater than 0.99 in all plots. To our knowledge, this is the most comprehensive determination of the dependence between elution order and total carbon number of various species of different lipid classes.

A similar correlation was observed for the fatty acyls containing one, two and multiple double bonds (**Fig. 14**). Compared with lipids containing fully saturated fatty acyls, more lipid molecules with the same total number of carbon and double bond exhibited different retention time (vertically lined dots). These species are isomers with different compositions of fatty acyl chains, in particular the C=C positional isomers, as the interactions are slightly different between different locations of C=C double bond and the C30 RPLC column. As a result of the presence of these isomeric lipid species, the correlation R^2 are slightly lower than the values of the fully saturated lipids in **Fig. 13**, but still are greater than 0.97 with the species having less than 3 double bonds. When the lipid species have at least 3 double bonds, the correlation R^2 were generally reduced, with the SM and TG lipids significantly reduced to >0.80. Overall, PC had the highest correlation between retention time and total carbon number, even when the degree of unsaturation increased; while TG and SM had a lower correlation coefficient due to the complexity of the structures and a higher number of isomers (more vertical dots) for each species.

In addition, higher degree of unsaturation resulted in the lipid species eluting earlier when comparing the lipid species with the same total number of carbon and different number of double bonds, i.e. for the same lipid class, the X:2 lipid species eluted earlier than X:1 when X is identical (**Fig. 14**), which is in agreement with previous report.[71] It is of note that the excellent correlation observed between the retention time on RPLC and the length and degree of unsaturation of fatty acyls provide a way to filter the

output of LipidSearch software. As a result, those putative lipid identifications that deviated from the established regression curves were further filtered out and not counted as valid.

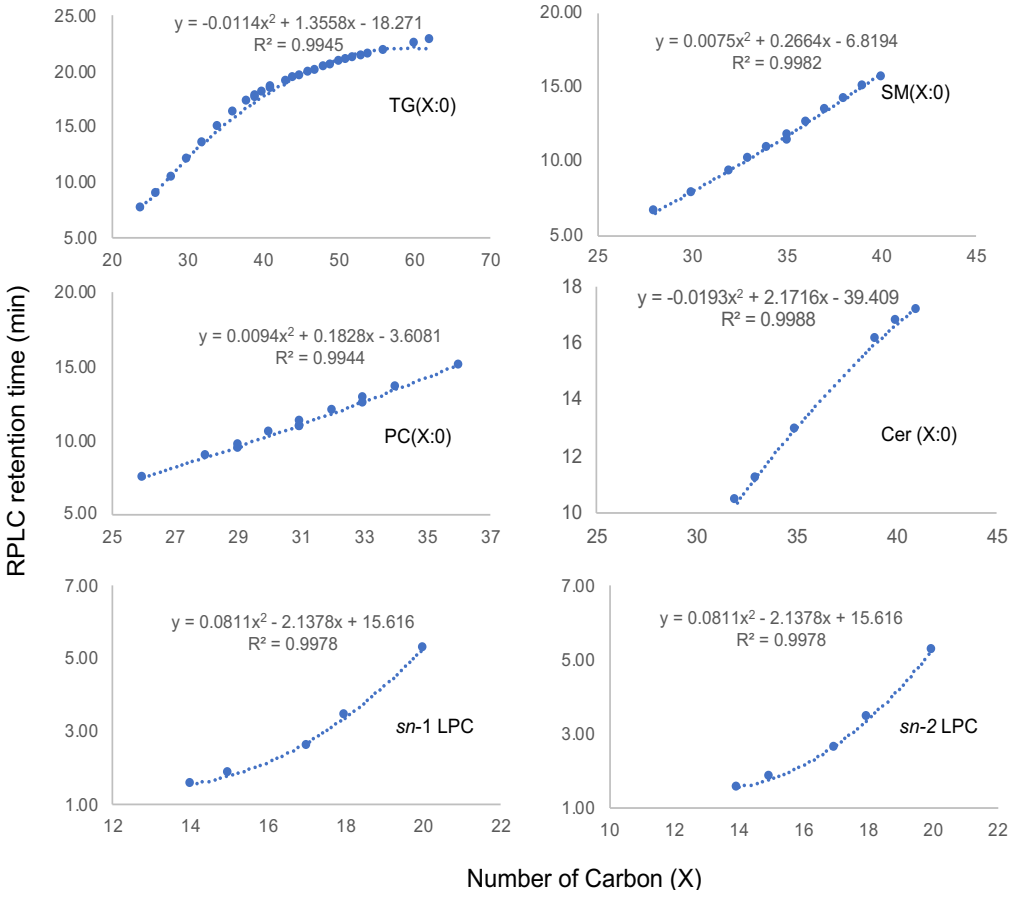

Figure 13. Plots Showing Dependences of RPLC Retention Times of Saturated Lipids to The Total Number of Carbon, each Panel is a Different Lipid Class (TG, SM, PC, Cer, and LPC). Lipid Molecules with longer fatty acyl chain (larger number of total carbon) are less polar and elute later from column.

GC-MS Based Fatty Acyl Analysis Improved Confidence In Identification Of Fatty Acyl Composition Of Lipids

Lipidomics research requires automated data annotation software, particularly at the initial identification stage. LipidSearch software is highly sensitive in peak detection, hence, often times, species in the noise were considered as identifications. Another observation from using LipidSearch as well as other automated software is the ability to identify "biological impossible" lipids due to the input of the *in-silico* library. The large number of putative identifications resulting from combinatorial enumeration inevitably generates large number of false positive identifications. To this end, we performed fatty acyl methyl ester analysis using GC-MS by derivatizing the fatty acyls hydrolyzed from lipid backbone under alkaline methanol condition. Using methyl ester derivatives of fatty acid standards as reference, fatty acyl chains of serum lipids were analyzed. Results showed that the fatty acyl chain lengths varied from 8 to 24 carbons, including the odd numbered chains, and the degree of unsaturation varied from 0 to 6. While it is possible that serum lipids contain unique fatty acyls of odd numbered carbon (>21 carbons) or more than 6 double bonds, their low abundance in these serum samples did not provide strong enough justification for the inclusion of these fatty acyls as valid lipid identifications. Based on the results of fatty acyl analysis, we filtered out the putative lipid identifications to limit the valid identifications only to those ones containing the detected fatty acyls.

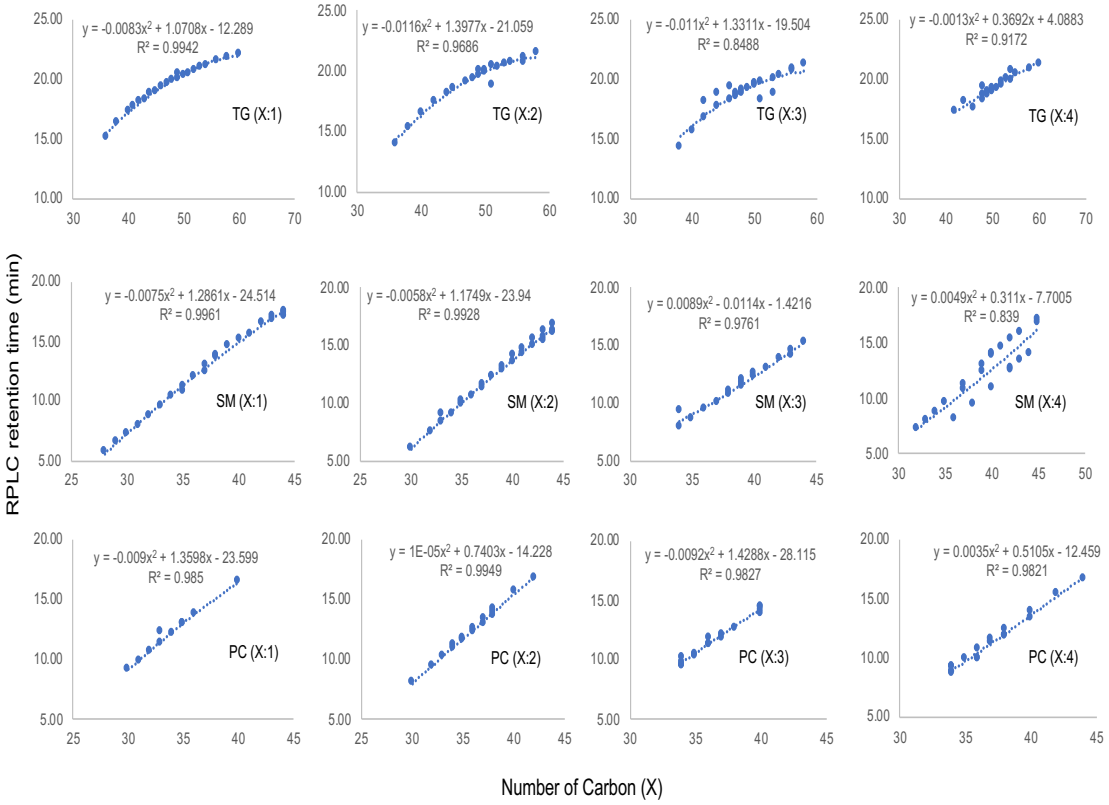

Figure 14. Plots Showing Dependences of RPLC Retention Times of Unsaturated Lipids to The Total Numbers of Carbon, with each Panel Showing a Different Lipid Class (TG, SM, and PC) or Degree of Unsaturation (1 to 4). Within each class, slightly different retention times were observed between different C=C positional isomers and *sn*-position isomers (vertically lined dots).

Contents And Characteristics Of The Human Serum Lipid Library

Using the offline 2D-LC-MS/MS approach and the data filtering and validating approaches mentioned above, we confidently identified 753 lipid molecular species in healthy control and pre-T1D human sera. The curated library, as provided in Table S1, contains information of accurate mass, RPLC retention time for each identified species. Overall, these 753 lipid molecules belong to 13 major lipid classes: Cer, DG, LPC, LPE, LPI, LPG, TG, PC, PI, PE, PS, PG and SM (**Fig. 15**). The sub-classes including plasmalogen and *sn*-position (*1,3*- and *1,2*-DG and *sn-1/sn-2* LPC) were combined and

reported under their corresponding representative classes such as DG, PC, PE, LPE and LPC. Every lipid class was detected in both positive and negative ionization mode, except TG and Cer, which were solely in positive mode. $[M+H]^+$ and $[M+NH_4]^+$ are the dominant ions in positive ionization mode, whilst $[M-H]^-$ and $[M+HCOO]^-$in the negative mode. In total, 88% of the lipids within our human serum lipid library are unsaturated lipid species, with 83% of them being polyunsaturated (degree of unsaturation $\geq$2). Majority of the species observed belong to TG, SM, PC and PE classes. Cer species are composed of fatty acids of 16 to 24 carbons, with the majority having one to two double bonds and an appearance of the odd long chain base d17:1. Both *1,2*-DG and *1,3*-DG were detected, with a predominance of polyunsaturated *1,2*-DG species. Lyso-glycerophospholipids (LPLs) including LPC, LPI, LPG, LPE were also found in the serum sample with a diverse fatty acyl chain length of 12-22 carbon. LPC is the most dominant LPLs with the strong preference of *sn-1* over *sn-2* isomers. Moreover, we were able to clearly identify plasmanyl and plasmenyl PLs using their distinct MS/MS fragments.

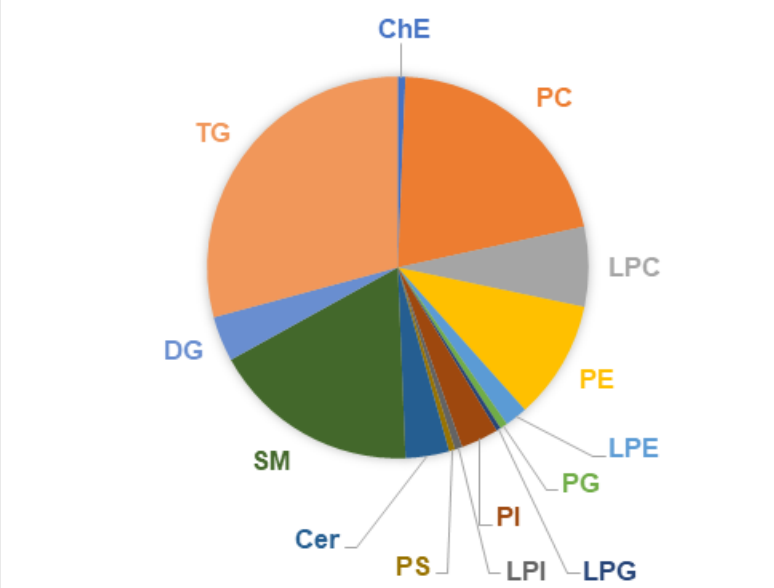

Figure 15. Relative Distribution of Lipid Species contained in The Serum Lipid Library.

We further plotted the spatial distribution of all lipids included in the library in the two dimensional spaces of RPLC-retention time and m/z. As shown in **Fig. 16**, clusters of lipids with mass ranges from 400-600 Da, 500-900 Da and >900 Da eluted in the following order: earlier than 5 min, 5.5-17 min, and after 17 to 25 min, respectively. Clearly, many isobaric and isomers species overlapped and it would be challenging to identify them if only using RPLC-MS/MS. The only lipid class that was separated well from others on RPLC is the highly non-polar TG. Lipid species belonging to LPLs eluted together, and GPLs (PC, PE, PI, PS) co-eluted with the DG, SM and Cer species. However, DG and Cer species have a different mass range from phospholipids. Conversely, with mixed-mode LC, we increased the level of confidence in lipid identification because a correct identification needs to come from the right fraction (lipid class), and match with the accurate mass and the elution order.

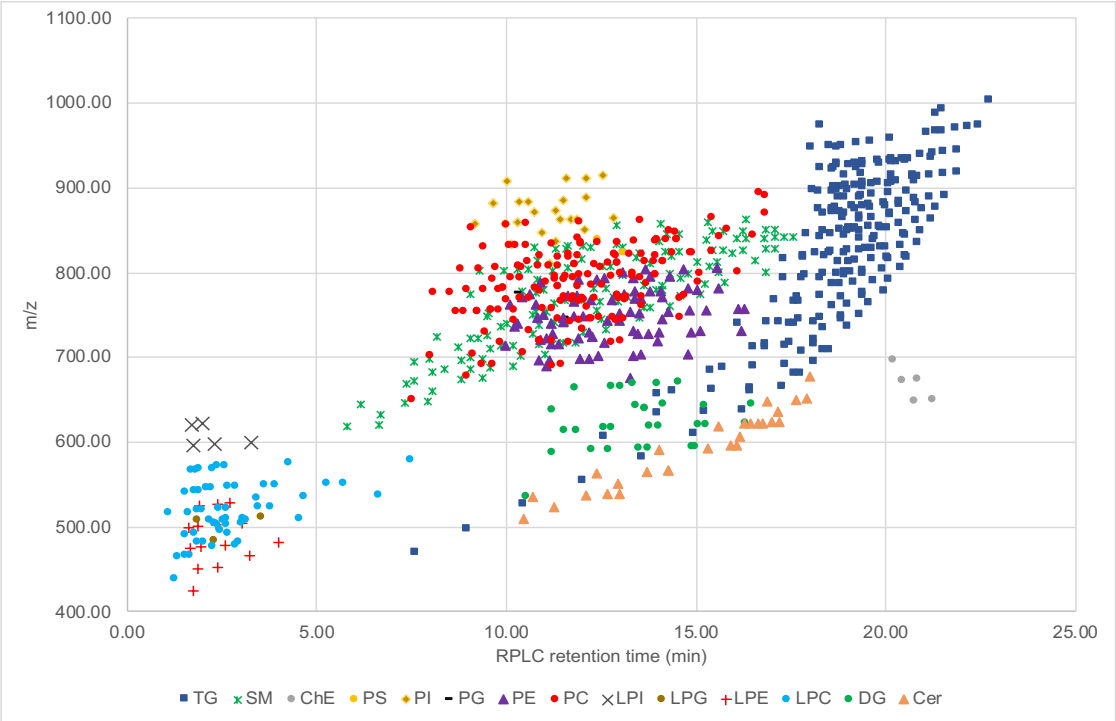

Figure 16. Individual Lipid Molecular Species Identified in Human Sera, Plotted with Their Respective *m/z* and Retention Time (min) on the RPLC. Identification of These Lipid Molecular Species was Facilitated by Lipid Class Level Fractionation using Mixed-Mode LC-ELSD, and Molecular Species Level Separation using RPLC-MS/MS.

Application Of The Lipid Library To Identify Lipids From Serum Sample

As a demonstration of the utility of the curated library in identification of lipids from biological sample, total lipids extracted from one individual pre-T1D serum sample were directly analyzed by RPLC-MS/MS without fractionation at lipid class level and raw data files were processed using two approaches - without and with our AMT serum lipids database. In the first approach, the raw data were processed directly using LipidSearch software resulting into 217 lipid species identified with assignment of *sn*-positions. In the second approach, the resultant raw data were processed using Progenesis QI software. Detected features from Progenesis QI were searched against the curated

human serum lipid library based on the accurate mass and RPLC retention time of each lipid molecular species. In total, we identified 412 molecular lipids in one individual pre-T1D serum sample, as summarized in **Fig. 17**. Majority of the species identified are in the class of TG, PC, SM, PE and LPC, which is proportional to the composition of lipid library. The profile of carbon length and degree of unsaturation for each fatty acyl in T1D lipidome varied from 10-22 carbons, including some odd chains (15 and 17 carbons), and 0-6 double bonds C=C. Hence, with the use of our AMT lipid serum database, we are able to increase the number of identification significantly, mostly from the low abundant species.

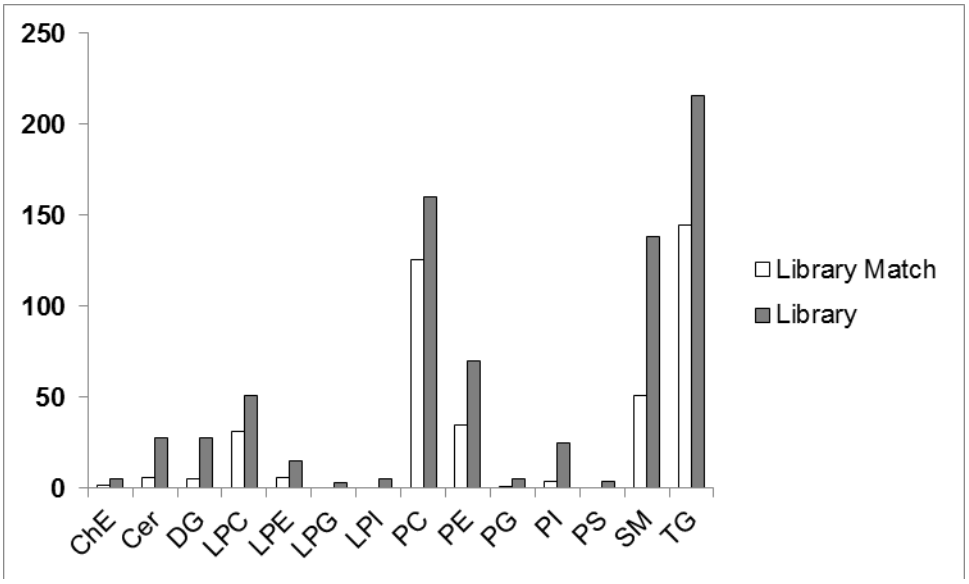

Figure 17. Number of Lipid Species identified from a T1D Serum Sample. Progenesis QI was Used to Match the LC-MS Profiles of The T1D Serum Sample to the Serum Lipid AMT Library.

Discussion

There has been an increased interest in comprehensively characterizing the human serum lipidome for its use in disease diagnosis. However, due to the complexity of blood serum samples, it is commonly recognized that many lipid species are unlikely to be detected due to their low abundance in serum, which is further hindered by the limited resolving power of one-dimensional LC separation and the under-sampling issue of data-dependent MS/MS. The accurate mass and time (AMT) tag approach was initially developed for high throughput proteomics to provide extensive coverage of complex peptide mixtures by taking advantage of the high resolution and wide dynamic range of the MS scans, which largely overcame the under-sampling issue in MS/MS-based peptide identification.[139] The concept employed in AMT tag based-proteomics studies could be applied to study other biomolecules, such as lipids.[141] Specifically, if an AMT tag library can be generated for various lipid species using a reproducible and robust LC-MS platform, then lipids from different samples of the same type of specimen could be analyzed in high throughput using the identical platform, where the AMT tag library would serve as a look-up table for lipid identification using LC retention time and accurate mass instead of relying on the MS/MS spectrum.

To achieve this, we employed offline two-dimensional LC separation,[63] which used mixed-mode LC in the first dimension to fractionate the total lipid extract into lipid classes, followed by reversed phase LC separation to further separate lipids in the same class into molecular species. The chromatographic separation and mass spectrometric detection conditions have previously been optimized in our laboratory, which doubled the

coverage of rat serum and liver lipidome compared to using RPLC-MS/MS alone. Fractionating total lipid extract into different lipid classes prior to the 2nd dimensional RPLC-MS/MS analysis is critical for building the library, as it greatly increased the confidence in lipid identification process by limiting the cross contamination of co-eluting isobaric/isomeric species between different lipid classes. For example, isobaric PC and SM can be challenging to differentiate when co-eluted on RPLC column because they share the common characteristic fragment ion (phosphocholine head group) in positive ionization mode.[101] However, the ambiguities in identification can be eliminated with additional dimension of separation provided by mixed-mode LC on which SM is clearly separated from PC.

Automated lipid identification programs, such as LipidSearch, are powerful in identification of lipid molecular species based on pre-configured fragmentation rules.[135] However, not all MS/MS spectra acquired from real biological samples are of high quality, which can be further complicated by lipids co-eluted and co-fragmented within the precursor ion selection window. This undoubtedly poses a challenge in structural elucidation when only head group-specific ions can be observed. As an effort to improve the confidence of identified lipids, we did total fatty acyl analysis using GC-MS to limit the composition of identified lipids only to those detected fatty acyls. We also observed a rigorous dependence between the RPLC retention time and the sum composition of total carbon number of all fatty acyls, which was used to further remove the putative lipid identifications not following the trend line.

The ratio of $[FA_1\text{-}H]^-/[FA_2\text{-}H]^-$ has been used for *sn*-positional assignments; however, relative intensities of the two carboxylate anions can vary depending on length and unsaturation, as well as the collision energy used in fragmentation.[72, 147, 152, 153] In this respect, it has been reported that different fragmentation patterns originated from different cleavage sites could be formed as a result of very different collision energies,[154] or the ratio of $[FA_1\text{-}H]^-/[FA_2\text{-}H]^-$ could be altered with the collision energy.[146, 147] Hence, to confidently identify the *sn*-position assignment of fatty acyls, we studied the relative ratio of $[FA_1\text{-}H]^-/[FA_2\text{-}H]^-$ using a list of representative lipid standards with different fatty acyl chains for each class, and concluded that $[FA_1\text{-}H]^-/[FA_2\text{-}H]^- < 1$ can be used to assign the fatty acyl positions in most of lipid classes under our experimental conditions, i.e. NCE 20–30 under HCD. Thus, within the stepped collision energies used in this work, we ruled out their effects on reversing the ratio of carboxylate anions.

Results from mixed-mode LC separation showed that there were no noticeable lipid class-level changes between healthy and T1D group or between the early and late time points of each group. Considering the samples used in this study were collected from patients older than 8 months and pooled from 25 subjects and two time points, our observation is somewhat in agreement with the serum lipid profile changes reported for the Finnish Type 1 Diabetes Prediction and Prevention cohort (DIPP) study, where the lipidomic profile changes associated with the progression of T1D appear to be most pronounced in children at 3 months of age.[25] Nevertheless, no change at the lipid class level further underline the importance of separating lipids at the molecular species level.

In agreement with the literature, our finding revealed that TG, PC, and SM are predominant lipids in human serum, with TG comprising over 50% of lipids having more than 52 fatty acyl carbon atoms.[155, 156] Compared to the previous published human plasma/serum lipidome, our lipid library provided unambiguous identifications at the level of *sn*-assignment for most of the glycerolphospholipids.[81, 156, 157] Although generally not native to mammalian cell lipidome, glycerolphospholipids containing odd chain fatty acyls and longer chain fatty acyls on the *sn*-1 position were also observed and passed our validation criteria. It is of note that, despite cholesterol and fatty acids being abundant classes observed in the mixed-mode LC (**Fig. 11**), we didn't perform identification of these two classes at the molecular level. Cholesterols have been known to ionize poorly with electrospray ionization unless derivatized to cholesterol esters[158] and therefore traditionally cholesterols are ionized with chemical or photo ionization techniques and not suitable for detection using our electrospray ionization-based platform. With respect to identification of free fatty acids, the main fragment ions resulted from CO_2 loss requires NCE > 50,[159] which greatly exceed the NCE used for other lipid classes.

In summary, using orthogonal and highly resolving separation methods of mixed-mode LC and RPLC in conjunction with high resolution tandem mass spectrometry and multiple levels of data filtering and validation, we have created a comprehensive human serum lipid library containing 753 lipid molecular species, with accurate mass and retention time annotated for each lipid molecule and with confident assignment of fatty acyl sn-positions for most of the species. This library not only

provides a comprehensive resource for studies of T1D, it will also be valuable for biomarker studies of other childhood diseases.

Acknowledgement

The work was partially supported by National Institutes of Health (NIH) grants R21 GM104678 and R01 DK114345. Clinical sample collection was supported by NIH grant R01 DK32493.

Compliance With Ethical Standards

a) The authors declare no competing interests. b) This research analyzed de-identified human serum samples collected from clinical studies and has IRB approval as stated in the Materials and Methods Section. c) All authors have read and agreed to the final version of this manuscript.

CHAPTER IV

OZONE-INDUCED DISSOCIATION ON A TRAVELING WAVE HIGH RESOLUTION MASS SPECTROMETER FOR DETERMINATION OF DOUBLE BOND POSITION IN LIPIDS

This chapter has been published in journal *Rapid Communication in Mass Spectrometry* and is presented in that style. Vu, N., Brown, J., Giles, K., Zhang, Q. *RCMS*. **2017**, 30, 1415-1423

Introduction

Lipids are involved in a wide range of biological processes from being a major component of cell membranes to regulation of metabolic pathways. Changes in lipids are reflected in various pathological and physiological conditions.[39, 160-163] Consequently, lipids have been implicated as biomarkers and major contributors to diverse diseases such as obesity, diabetes, cancers and Alzheimer's.[21, 36]

The function of a lipid depends on its molecular structure. Lipid isomers that differ only in their fatty acyl C=C position can have very distinctive roles functionally. For example, free fatty acids (FFAs) that contain double bonds at ω6 or ω9 positions inhibit the activity of nicotinic acetylcholine receptor, while the ω11 and ω13 isomers have no such effect.[164] Similarly, FA (18:1, ω3) prevents cardiovascular disease whilst its ω6 double bond positional isomer worsens this disease.[165] Thus, detailed characterization of lipid structures would aid in understanding their biological functions.

Recent advancements in the field of mass spectrometry (MS) have greatly improved the field of lipidomics, as a result more lipids have been identified with better structural annotation.[73, 166-169] However, the determination of carbon-carbon double bond locations within the unsaturated fatty acyl chains still remains a challenge. Different hyphenated mass spectrometry techniques have been used to localize lipid double bond positional isomers. In gas chromatography coupled with mass spectrometry (GC-MS), lipid molecules are derivatized to form methyl esters for volatilization, which is followed by fragmentation with high energy electron ionization. Although this GC-MS analysis can pinpoint the location of a double bond that is closest to the methyl end of the fatty acyl chain, it only allows confident identification of the location of double bonds in monounsaturated lipid species.[170] In addition, the *sn*- substituent information is lost during the hydrolysis process and therefore GC-MS is incapable of determining C=C positions from intact lipids. On the other hand, the commonly used low energy collision induced dissociation (CID)-MS, is able to assign the *sn*- positions and identify the total number of carbon on each fatty acyl chain along with their total degree of unsaturation from intact lipids, but struggles to characterize the locations of double bonds without using multistage ion activation techniques on lipid-metal adduct ions.[171-175] Alternatively, high energy CID-MS has been applied to study the structural variation of the fatty acyl chains, yielding a highly complicated fragmentation spectrum embedded with structurally diagnostic product ions.[176-178]

C=C selective ion-molecule reactions are promising techniques that largely overcome the above mentioned limitations. They also offer increased sensitivity and the

ability to provide detailed structural information of a given lipid molecule when coupled with mass spectrometry. Xia and co-workers coupled a photochemical reaction online with tandem mass spectrometry. [179-182] When the Paternò-Büchi (PB) reaction product between a lipid ion and acetone is activated using CID, it generates a pair of diagnostic ions originating from the C=C location. Using 193 nm laser, Brodbelt and co-workers implemented ultraviolet photodissociation on an Orbirap mass spectrometer to localize C=C in lipids.[183] Another well-known ion-molecule reaction is the Ozone-induced dissociation (OzID) pioneered by Blanksby and co-workers, which uses the ozonolysis reaction of C=C to pinpoint the location of double bonds based on the neutral loss of diagnostic fragment ions (aldehyde and Criegee ions).[114, 116, 121, 126, 170, 184] OzID has been implemented in both shotgun and LC-MS based lipid analyses, mainly using ion trap MS platforms (Thermo LTQ and AB QTRAP) to characterize the lipid double bond positional isomers; however, the presence of ozone/oxygen results in decreased resolution for helium filled ion traps when ozone/oxygen concentration exceeds a certain percentage in helium.[114] In addition, most of the OzID-MS experiments carried out so far were focused on the sodiated adducts of lipids owing to their stability and predominant presence in shot-gun based lipidomics workflow;[31, 32] fragmentation of the most commonly observed protonated ions generated in LC-MS based lipidomics workflow has been less explored.

In this work, we demonstrate the ozonolysis of protonated lipid ions in a high resolution MS instrument platform to elucidate the locations of double bonds on the lipid fatty acyl chains. The experimental arrangement was based on a Synapt G2 HDMS

instrument (Waters Corp., Milford, MA), a MS with high resolution and accurate mass capability that employs Traveling Wave-based stacked ring ion guides (SRIGs) for ion transfer.[185] By modifying the default potential settings, we improved the OzID efficiency by increasing the reaction time between lipid ions and ozone gas in the TriWave region whilst maintaining the duty cycle of the scan. This approach is promising in both shotgun and LC-MS based lipid analysis to fully characterize the structure of unsaturated, intact lipids.

Experimental

Chemicals

C18:2 (10*E*,12*Z*) methyl ester was purchased from Nu-Chek Prep, Inc (Elysian, MN). All phospholipid standards were obtained from Avanti Polar lipids, Inc (Alabaster, AL). HPLC grade methanol, acetonitrile (ACN), and isopropanol (IPA) were purchased from Sigma-Aldrich (St. Louis, MO). LC-MS grade ammonium formate and formic acid were provided by Fisher Scientific (Pittsburgh, PA).

Sample Preparations

C18:2 (10*E*,12*Z*) methyl ester standard solution was prepared in methanol at a concentration of 12.5 μM. Phospholipid standard solutions were prepared in the solvent of ACN/IPA/H_2O (65/30/5, v/v/v) at a concentration of 25 μM. To aid the formation of protonated, 10 mM of ammonium formate and 0.1% formic acid were added into each standard solution. All standards were stored at -20°C. A solution of 2 ng/μL leucine encephalin (Waters, UK) in ACN/H_2O (50/50, v/v) with 0.1% formic acid was used as the lock mass for instrument calibrations.

In-line Ozone Generation

An O_3MEGA Integrated Ozone Delivery System (MKS Inc, Andover, MA) was used for in-situ production of ozone from high purity oxygen. The oxygen pressure was set to 15 psi and the ozone system was set to output up to 18 wt% of ozone at a flow rate of 0.5 slm. The generated ozone/oxygen mixture was connected to the mass spectrometer Trap/Transfer gas supply, with the excess guided to an Ozone Destruct Module (MKS Inc.) to convert ozone back to oxygen before venting to the laboratory exhaust system (Fig. 1). To ensure safe operation of the ozone delivery system, an Ozone Leak Detector/Monitor (Ozone Engineering Inc., El Sobrante, CA) was installed to alarm and shut down ozone production if room ozone concentration exceeded safe levels.

Mass Spectrometry

OzID-MS experiments were performed on a Waters Synapt G2 HDMS (Milford, MA) with MassLynx v4.1 instrument control and data acquisition software. The Synapt G2 HDMS has a TriWave region positioned between a quadrupole mass analyzer and an orthogonal time-of-flight (oa-ToF) mass detector (Fig. 18). The TriWave region is comprised of traveling wave-based SRIGs which have confining radio frequency and superimposed transient DC voltages for ion propulsion. These serve as: collision cell (Trap); ion mobility separator (IMS) and ion transport device (Transfer) delivering sophisticated ion manipulation functions, including ion accumulation, collision induced dissociation, ion mobility based separation and high speed ion transfer for TOF based detection. In the trap and transfer regions, ions can be manipulated to accumulate or fragment using CID prior or after the IMS region.[186, 187]

The Argon collision gas inlet of the mass spectrometer was connected to a stainless-steel T union to accept both Argon and Ozone, with each line having its own shutoff valve. This inlet supplies collision gas to both Trap and Transfer cells as configured by the manufacturer (Fig. 18). The trap and transfer gas flow was maintained at 2.0 mL/min using a flow controller (Bronkhorst, Suffolk, UK) operated via MassLynx. At this gas flow rate, pressures at the trap and transfer regions were at ~1.0 e-2 and 1.0 e-4 mbar, respectively. The effective ozone concentration during OzID was at 6.0 %, which can be achieved by either diluting the in line generated high concentration Ozone with Argon or by directly generating Ozone at this concentration.

Sample was directly infused using a syringe pump at a flow rate of 5 μL/min, and ionized using the electrospray ionization source. The parameter settings for ionization were: source capillary voltage 2.70 kV; sample cone voltage 30V and extraction cone voltage 6.0V; source and desolvation temperature at 40°C and 80°C, respectively; the cone gas and desolvation gas flow rate at 50 L/h and 500 L/h of nitrogen respectively. Precursor ions were mass selected in the quadrupole and reacted with ozone gas in the trap and transfer regions before reaching the ToF detector. Full MS spectra were acquired for every sample. The scan rate was set at 0.2 s/scan.

The default trap and transfer collision energy were at 4.0 and 2.0 V, respectively. The Wave height and velocity in the trap region were set at 0.5 V and 300 m/s; in the transfer region were set at 0.2 V and 247 m/s. Additionally, the TriWave DC conditions were set as follows: for the trap region: trap DC entrance 2.0 V, trap DC -2.0 V, Trap DC

exit 0.0 V; for the transfer region: transfer DC entrance and exit at 5.0 V and 15.0 V, respectively.

Results and Discussions

Performance Of OzID At The Default Trap And Transfer Settings

All OzID performances of lipid standards were first studied using default acquisition settings of the Synapt G2 HDMS. In our experimental design, ozone gas was supplied in the trap and transfer regions to perform ozonolysis (Fig. 18). Ion residence time within the TriWave region can be estimated from the traveling wave velocity, which is derived from the distance between pairs of electrodes divided by the time the pulse remains on each pair. For example, the spacing between each electrode pair in the trap and transfer regions is 3 mm; therefore, a 10 μs pulse time gives rise to an average velocity of 300 m/s. Under these default settings, it takes 946 μs for an ion beam to transmit through the trap and transfer regions while interacting with neutral gas before reaching to the ToF detector.[187]

The conjugated lipid standard FAME C18:2(10*E*,12*Z*), previously shown to readily undergo ozonolysis was initially used to study OzID efficiency under the instrument default settings.[184] When oxygen was employed as the collision gas, the sodium adduct (*m/z* 317) alone was observed in MS/MS spectrum under default minimal collision energy used for ion transmission (Fig. 19A). In contrast, when ozone gas was introduced into the collision cells, OzID aldehyde product ions at *m/z* 223 and 249 were generated with low intensity (Fig. 19B). These ions are specific to the 10 and 12th position of the double bond location, respectively. Likewise, ozonolysis reaction of the

protonated ions of PC (16:0/18:1(9*Z*)) (*m/z* 760) resulted in the characteristic neutral loss of 110 Da and 94 Da at the position *n*-9, which yielded the aldehyde and Criegee products ions at *m/z* 650 and 666, respectively (Fig. 20A). Compared to conjugated C=C (Fig. 19B), the monounsaturated C=C has ~ 30 times lower OzID efficiency. This is in line with what reported previously on the reaction rate difference between conjugated and single C=C when taking into consideration of the double bond conformation.[188] It should be noted that these product ions were very weak and could only be observed in the spectra under high magnification. Nevertheless, these results indicated that OzID-MS could be implemented in the Traveling Wave mass spectrometer.

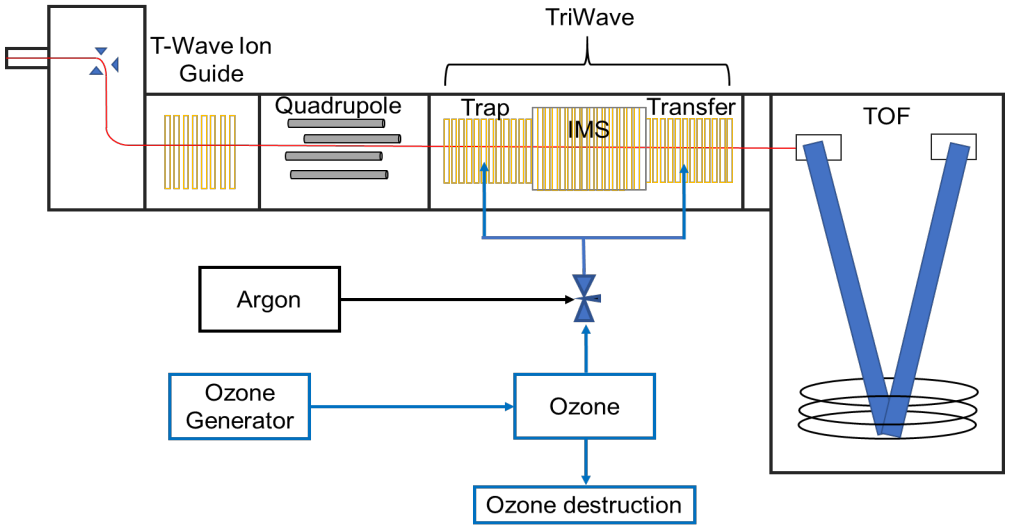

Figure 18. Schematic of The Traveling Wave Q-TOF Mass Spectrometer (Synapt G2) Modified to Allow OzID in The Trap and Transfer Cells. IMS was Off during Experiment.

Optimization Of Traveling Wave Height And Velocity In Trap Region To Improve OzID Efficiency

Under the default instrument settings, the traveling wave is set at an elevated wave velocity and wave height in order to reduce ion transmission times whilst maintaining sensitivity.[186] Although this default setting is very beneficial for normal applications, it depresses ozonolysis of unsaturated lipid ions due to the short reaction time with ozone. Thus, modifying the wave height and wave velocity would effectively allow control of the movement of ions across the trap and transfer regions and their reaction time with ozone.

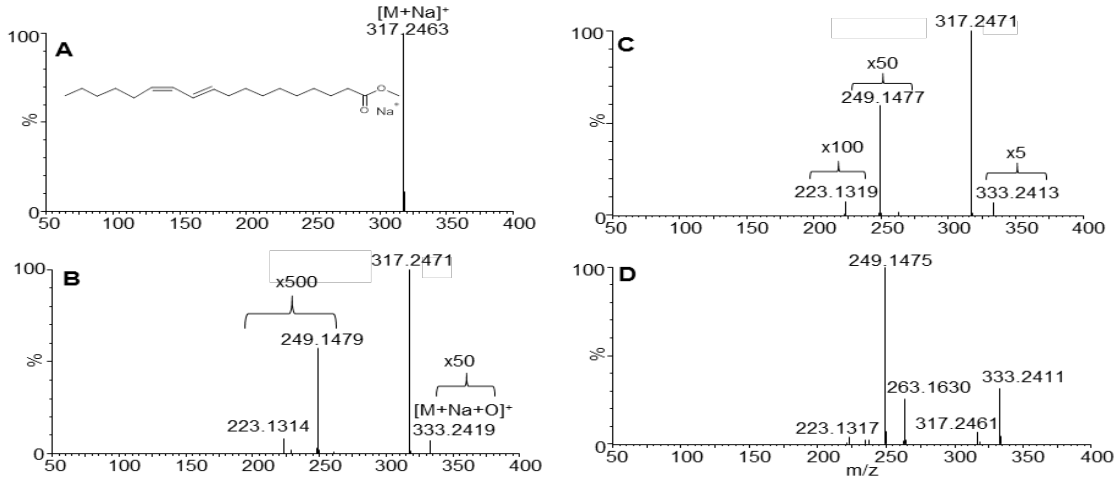

Figure 19. OzID-MS Spectra of FAME C18:2 (10E,12Z) under Different MS Settings: A, Oxygen, MS/MS at default settings; B, Ozone, MS/MS at Default Settings; C, Ozone, Trap wave height = 0.2 V; D, Ozone, Trap Wave Height = 0.2 V, Trap Wave Velocity = 8 m/s, Transfer Wave Height = 0.4 V and Transfer Wave Velocity = 247 m/s.

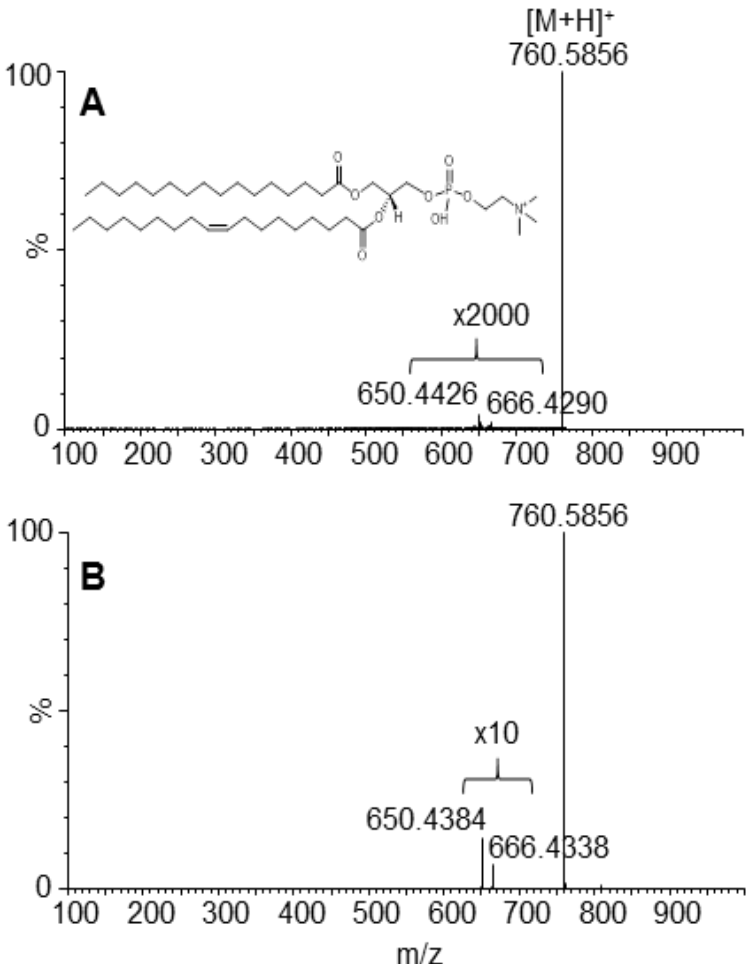

Figure 20. OzID-MS Spectra of PC (16:0/18:1(9Z)) under Different MS Settings. A, Ozone, Default Settings. B, Ozone, Trap Wave Height = 0.2 V, Trap Wave Velocity = 8 m/s, Transfer Wave Height = 0.4 V and Transfer Wave Velocity = 247 m/s

Increasing the height of traveling wave reduces the chance of ions 'rolling-over' the waves and so reduces residence time in the collision cells. Based on this, a series of trap wave heights were applied from 0.0 V to 0.5 V (at fixed 300m/s wave velocity) to study the effect on ozonolysis of the sodiated ion of FAME C18:2 (10*E*,12*Z*). In Fig. 21A it can be seen that 0.2 V wave height produced the highest yield of the OzID products and the spectrum is shown in Fig. 19C, which showed a 10x increase in OzID product yield

compared to OzID spectrum under default settings (Fig. 19B). Additionally, when the wave height was < 0.2 V, ion impulses were not sufficient to allow the ions to keep up with the traveling wave through the SRIG, leading to significant loss of signal intensity. This is possibly due to the transit time being too long and ions not exiting the TriWave before the interscan period during which a sweep-out pulse is applied. Likewise, trap wave velocity could be decreased to enhance the OzID reaction (Fig. 21B). Results showed that trap wave velocity of 8 m/s (at fixed 0.2 V wave height) produced the highest relative intensity of the OzID product ions because lipid precursor ions remained in the trap and transfer regions together with ozone gas for 16.65 ms, which is significantly longer than the 946 μs of the default setting. A slight enhancement to the OzID efficiency was observed in the transfer region by altering the wave height to 0.4 V while keeping the defaulted transfer wave velocity at 247 m/s (Fig. 19C &D); however, unlike the trap region, overall there was no significant change in OzID efficiency when varying the wave height or wave velocity in the transfer region. This may be explained by 1) the lower pressure (1.0 e-4 mbar) thus lower effective ozone concentration in the transfer region; and 2) ions having higher velocity (i.e. reduced residence time) in the transfer cell, likely as a result of the trap bias applied in TOF mode which effectively adds to the traveling wave velocity in the transfer region.

Using FAME C18:2 (10E,12*Z*) as a conjugated C=C containing standard, the optimized traveling wave velocity and height in both trap and transfer regions increased OzID efficiency ~1000x when compared with the result obtained under the default settings (Fig. 19D vs Fig. 19B). Identical experiments were performed on PC

(16:0/18:1(9*Z*)) to ensure the improvement of ozonolysis also worked on lipids containing a single C=C (Fig. 20B). Results showed a ~600x improvement in OzID efficiency using optimized trap and transfer traveling wave height and velocity settings for a monounsaturated lipid (Fig. 20B vs Fig. 20A). The different OzID yield for conjugated and mono C=C is a result of their different reactivity with ozone, as it is known that the former has much faster reaction rate than the latter one.[188]

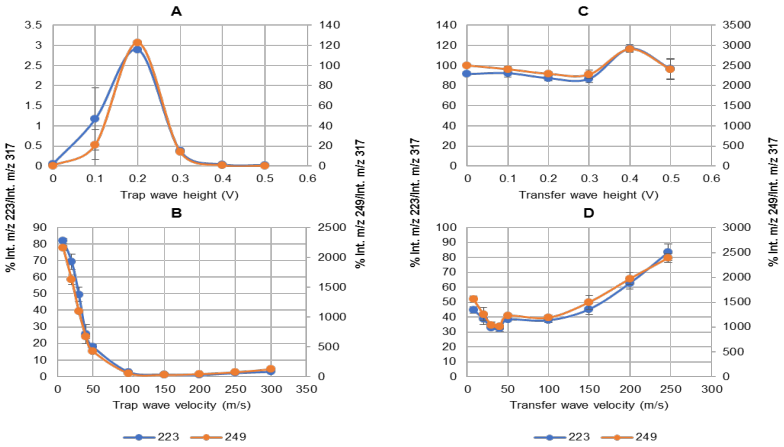

Figure 21. Effects of Changing Traveling Wave Height and Wave Velocity on OzID Efficiency: A, Trap Wave Height Effect; B, Trap Wave Velocity Effect; C, Transfer Wave Height Effect; D, Transfer Wave Velocity Effect. Data obtained by direct infusion of FAME C18:2 (10E,12Z).

It is of note that an ion with m/z 263.1630 appeared when FAME C18:2 (10*E*, 12*Z*) reacted with ozone under optimized trap and transfer wave height and velocity settings (Fig. 19D). A radical cation of m/z 262 was reported previously from OzID of this compound,[188] however, the accurate mass that we measured for this ion preclude its identity as this radical cation. The exact identify of this ion remains to be determined; it is likely a result of hydrogen abstraction by the radical cation from other gas molecules in the vacuum environment (mass measurement error ppm).

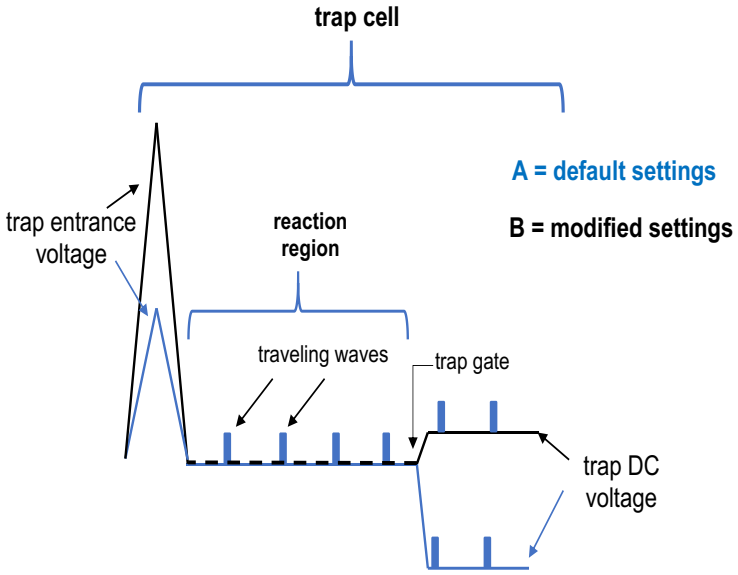

Figure 22. Diagrams Illustrate The Transmission of Ions Through The Trap Cell in The TriWave Region and The Effect to Gas Phase Ozonolysis by Changing Trap Entrance Voltage and Trap DC Voltage. Potential Hills are Based on Trap Wave Height at 0.2 V. Trap Entrance DC and Trap DC are The Voltage Applied at The Entrance, and The End of Trap Cells (before Ions entering the IMS), respectively. Under the default setting (A) of trap entrance (2V) and trap DC (-2V), ions can easily transmit through trap cell. Upon the increase of trap entrance and trap DC voltage (B), an artificial "ion dam" is created in the trap region to hold ions in this region to react with ozone.

Optimization Of Trapping DC Bias And Entrance Potential To Further Improve OzID Efficiency

An alternate strategy that could prolong ion transit time is to increase the trap entrance voltage and trap DC. The trap entrance voltage is the voltage applied to the differential aperture at the entrance to the trap region, immediately after precursor ion selection in the quadrupole section. Trap DC is the potential of the post gate transport region of the trap cell. In the default setting, the trap entrance voltage and trap DC are set at 2V and -2 V, respectively relative to the main trap SRIG, to facilitate transmission of accumulated ions to the IMS cell (Fig. 22). However, these settings adversely decrease reaction time between ozone and lipid precursor ions, reducing efficiency. Alternatively,

these settings can be modified to analogously create a “water dam” for the incoming ions, in order to increase residence time and boost the ozonolysis efficiency while maintaining the signal intensity of the spectrum (Fig. 22). Trap entrance and trap DC were optimized at 7V and 0.2V (Fig. 23), respectively, for maximum ozonolysis yield. The high trap entrance voltage would slow/hold the stream of ions at the entrance to the trap region, therefore, lengthen the reaction time of precursor ions with ozone gas exiting the trap. Once the number of ions built up at the trap entrance space charge effects would overwhelm the “dam”, precursor ions and OzID product ions would travel through trap and transfer cells to reach to TOF detector, while OzID was further performed during their transit. It is of note that these optimal ion dam settings are at the expense of reduced overall ion transmission and signal intensity, therefore, we used trap DC of 0.2 V instead of 0.4 V because higher OzID yield but significantly lower ion transmission was present in the latter (Fig. 23A).

The OzID-MS spectrum of protonated PC (16:0/18:1(9*Z*)) generated using these settings had sufficiently high intensity and signal-to-noise ratios to make OzID product ions the base peak in spectrum (Fig. 24A). To our knowledge, this is the first time that ozonolysis of a protonated monounsaturated lipid ion has been demonstrated with such high reaction efficiency, by simply passing the ions through the ozone gas at a slower rate. Compared to the spectrum acquired under the default acquisition setting (Fig. 20A), the aldehyde product ion (*m/z* 650) represents >40,000x improvement in OzID efficiency (A_{650}/A_{760}). Even considering all the ion transmission losses with ion dam settings, the

absolute intensity of the aldehyde ion under ion dam settings still has~300x increase to that of the default settings.

In addition to the commonly observed OzID products – the aldehyde and Criegee ions, we observed another abundant product ion at *m/z* 636.4240 (Fig. 24A). This ion is likely to be the further oxidation product of the vinyl peroxide structure of the Criegee ion as illustrated previously.[126] Under the environment of high concentration ozone, the vinyl peroxide ion lost a formaldehyde (H_2CO) to form the unique product observed , which has similar mass to the direct C=C cleavage product (m/z 636.4599) generated using a high energy collision (~10 keV) either on magnetic sector or TOF/TOF instruments.[176] Because the default collision energy in our OzID settings was at 4 eV and the high mass measurement accuracy of the Synapt G2, we were able to assign the product ions correctly as further oxidation product of vinyl peroxide (theoretical mass 636.4240) , not of C=C bond direct cleavage.

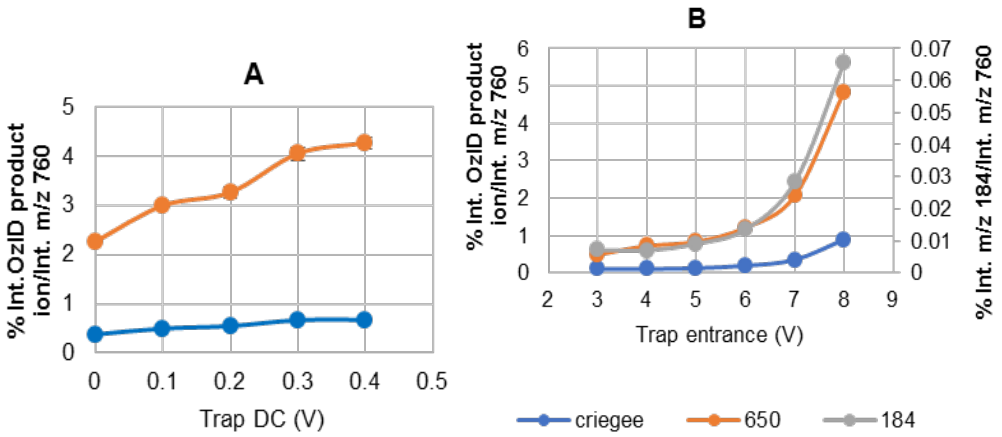

Figure 23. Effects on Changing Trap Entrance and Trap DC on OzID Efficiency: A, Trap DC Effect; B, Trap Entrance Effect. Data Obtained by Direct Infusion of PC (16:0/18:1(9*Z*)).

Overall, the enhancement in efficiency and sensitivity of OzID on the traveling wave mass spectrometry system illustrates the benefit of prolonged reaction time with ozone, and suggests the potential for its integration with a shotgun-based high throughput lipidomics workflow. Application of these settings to differentiate lipid regioisomers was performed below.

Difference In The Yields Of OzID Products Can Distinguish Isomeric Lipids

It has been reported that lipid isomers can be distinguished using OzID fragment ions of sodiated adducts.[114, 116, 121, 126, 184] To see if similar patterns can be observed using protonated lipid ions on this traveling wave-based OzID-MS, we selected four monounsaturated lipid standards: PC (16:0/18:1(9*Z*)), PC (18:1(9*Z*)/16:0), PC (18:1(9*E*)/18:1(9*E*)) and PC (18:1(9*Z*)/18:1(9*Z*)), with the former two representing *sn*-positional isomers and the latter two as *cis*-*trans* configurational isomers. Due to the solvents used, protonated ions were the most abundant ions for these lipids and the experiments were performed on them.

***sn*-positional Isomers**

The OzID-MS spectra of the $[M+H]^+$ ions of the two *sn*-positional isomers: PC (16:0/18:1(9*Z*)) and PC (18:1(9*Z*)/16:0) were acquired under identical ozone concentration and MS instrumental parameter settings (Fig 24A & 24B). The pairs of aldehyde (m/z 650) and Criegee product ions (m/z 666, very weak) observed in each of these spectra are characteristic of the expected neutral loss of 110 Da and 94 Da, resulting from the cleavage at double bond position *n*-9. Given the same OzID-MS settings, it is reasonable to compare the relative reactivity of these two isomers with ozone based on

the ratio of product ion intensity to the precursor ions. Both of the isomers showed the aldehyde ion as the base peak at *m/z* 650, whereas the precursor ion for each isomer had different relative intensity. For the PC (16:0/18:1(9*Z*)), the relative intensity of precursor ion (*m/z* 760) was ~20%, whereas the intensity of the counterpart ion was ~50% of the base peak for PC (18:1(9*Z*)/16:0) isomer. This observation suggests that ozonolysis rates of the C=C depends on the substitution position of the fatty acyl moiety, and that the C=C in the protonated ions for PC (16:0/18:1(9*Z*)) isomer reacts ~1.5x faster than that in the PC (18:1(9*Z*)/16:0). The same observation was made by Poad et al. when they compared the reaction rates using the OzID approach with the additional supplemental voltage.[126]

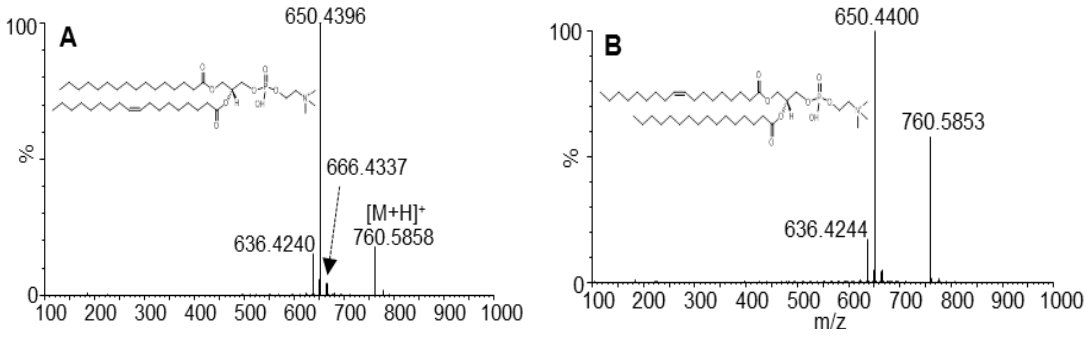

Figure 24. OzID-MS Spectrum of (A) PC (16:0/18:1(9Z)) and (B) PC (18:1(9Z)/16:0) Obtained Under Optimized OzID Settings: Trap Wave Height = 0.2 V, Trap Wave Velocity = 8 m/s, Transfer Wave Height = 0.4 V and Transfer Wave Velocity = 247 m/s, Trap Entrance = 7 V and Trap DC = 0.2 V.

cis/trans Configurational Isomers

The OzID-MS spectra obtained from the reaction of ozone with the $[M+H]^+$ ions of the stereoisomeric PC (18:1(9*E*)/18:1(9*E*)) and PC (18:1(9*Z*)/18:1(9*Z)*) (m/z 786.58) are shown in Fig. 8. The spectra were obtained under the same OzID settings as described in the analysis of PC (16:0/18:1(9*Z*)). Since the C=C position is at *n*-9, the expected

neutral losses for the aldehyde (m/z 676) and Criegee ions (m/z 692, weak) are 110 Da and 94 Da when there is a cleavage of only one C=C from either of the fatty acyls. Moreover, we observed the abundant neutral losses of 220 Da, which is dual aldehyde (m/z 566) from the cleavage of double bonds from both *sn*-1 and *sn*-2 acyl chains. Comparing the OzID-MS spectra of the two configurational isomers in Fig.25 A & B, it is also interesting to note that the relative abundance of the OzID aldehyde products resulted from the cleavage of two double bonds (*m/z* 566) and one double bond (m/z 676) differed significantly between the *cis*- and *trans*- forms. The base peak in the OzID-MS spectrum of the *trans*-isomer was at *m/z* 566 (Fig. 25B), whilst under the same conditions, the *cis*-isomer spectrum presented a base peak at *m/z* 676 (Fig. 25A). This clearly indicates the *trans*- isomer has a higher reaction rate with ozone. Similar observations have been reported by Poad.et al for the OzID of the sodiated adducts of these phosphatidylcholine stereoisomers, in which the reaction rate of *trans*-isomers to ozone is 2.5 times that of the *cis*-isomers. [31] Our observation is also in agreement with the known stability of *trans*-ozonide as supported by a higher steric hindrance imposed by *cis*-alkenes when the gas phase kinetics of ozone reaction with neutral *cis*- and *trans*-alkenes were measured.[189, 190] This is also consistent with detailed theoretical calculations which show that product branching in ozonolysis reactions are sensitive to the structure of the primary ozonide, which in turn is influenced by the double-bond geometry. Interestingly, we observed an abundant product ion at *m/z* 552.2938, which is likely to be an aldehyde arising from further oxidation of the Criegee ion in the form of formaldehyde loss under high ozone concentrations, as suggested above. In addition, the signature ion

(m/z 184) from the phosphocholine head group loss can be observed, its low intensity and the facile cleavage under CID conditions further confirms the minimal collision energy applied in our experiments.

Conclusions

The data presented here demonstrated that high quality OzID-MS spectra of protonated lipid ions can be obtained routinely from a traveling wave high resolution mass spectrometer. The modification of traveling wave height and velocity, as well as trap DC bias and entrance potential in the TriWave regions provided a significant enhancement in the ozonolysis efficiency in comparison to the default settings. As demonstrated, the relative abundances of the OzID characteristic aldehyde and Criegee ions can differentiate *sn*- positional and *cis/trans* isomers for standard lipids. In addition, the higher ozone concentration used in the current implementation of OzID further oxidizes the Criegee ions to form new product ions as a result of the loss of one formaldehyde from the metastable vinyl peroxide ions. Besides the enhancement of ozonolysis, the high mass accuracy achieved through a high-resolution measurement in Synapt G2 MS enables the assignment of OzID fragments without ambiguity.

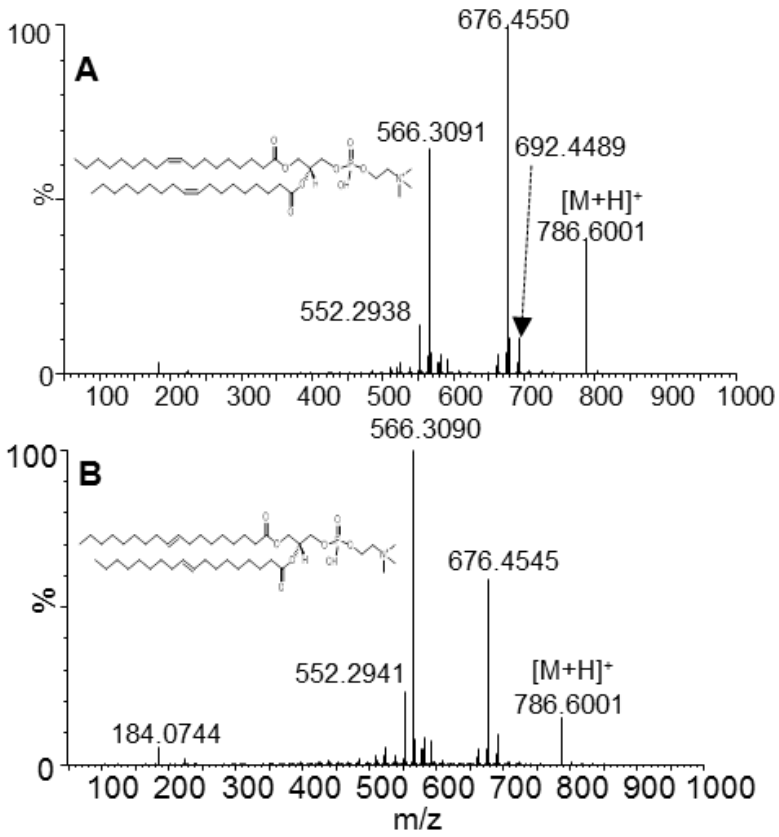

Figure 25. OzID-MS Spectrum of (A) PC (18:1(9Z)/18:1(9Z)) and (B) PC (18:1(9E)/18:1(9E)) Obtained Under Optimized OzID Settings: Trap Wave Height =0.2 V, Trap Wave Velocity = 8 m/s, Transfer Wave Height = 0.4 V and Transfer Wave Velocity = 247 m/s, Trap Entrance = 7 V and Trap DC = 0.2 V.

While our work was under review, implementation of OzID on a similar platform (Synapt G2 Si) has been reported,[191] which explored traveling wave velocity and height for prolonged reaction time between Ozone and lipid ion in the IMS region. Although the trap and transfer regions are shorter in dimension compared to the IMS region and higher vacuum (1.0 e-2 mbar in trap and 1.2 e-4 mbar in transfer with IMS off) is also present in these regions, by creating an ion dam to trap ions to elongate their reaction time with Ozone, we achieved the highest efficiency OzID reported to date without sacrificing

spectrum acquisition rate (total trapping time is only 16.65 ms). On the other hand, Poad et al. implemented OzID in the high pressure (~ 3 mbar) IMS cell, significant improvement in OzID efficiency has been achieved during ion transmission through this region (20 - 200 ms) for its practical application in LC-MS based lipid analysis. This, together with the manipulation of OzID reaction in the trap and transfer region detailed in our work, makes the Q-IMS-TOF MS a very versatile platform to implement this C=C specific dissociation technique for unsaturated lipid isomer analysis.

Acknowledgement

This work was supported by the National Institutes of Health grant (GM 104678). The authors thank the Triad Mass Spectrometry Facility at the UNCG Chemistry and Biochemistry Department and Dr. Daniel Todd for help with this work. The authors also thank reviewers of this manuscript for their insightful comments.

CHAPTER V

SERUM ISOMERIC LIPID IDENTIFICATION FACILITATED BY LIQUID CHROMATOGRAPHY-OZONE INDUCED DISSOCIATION-MASS SPECTROMETRY

This chapter is intended for submission to journal *Rapid Communication in Mass Spectrometry* and is presented in that style.

Introduction

Blood plasma and serum contain a vast array of biomolecules that are either as systemic response to disease or being secreted or leaked from pathological tissues into circulation. The dysregulation of these biomolecules reflects the disease status, as such, they are being suggested as biomarkers to either diagnose the onset of disease or monitor the therapeutic outcome.[131, 155, 192, 193] As one of the major compositions of human serum, lipids have been proposed as biomarkers for various diseases, including cancers,[194] diabetes,[33] Alzheimer's disease,[32] etc.[28, 157, 195, 196] Lipids have enormous structural diversity, with variations in backbone, headgroup, fatty acyl composition and their positions on the backbone, as well as the location and stereochemistry of C=C unsaturation. It is known that the function of lipids depends on their structures,[28] therefore, better understanding the roles lipid biomarkers play in disease pathogenesis requires detailed, unambiguous elucidation of their structures.[80, 156]

Majority of the lipids can be easily fragmented using collision-induced disassociation (CID) or higher energy collision-induced dissociation (HCD)- tandem mass spectrometry, [80, 141] which reveals the head group information and the composition of fatty acyls, if both positive and negative ionization modes are used in combination.[120] Although CID/HCD fragments can indicate the degree of unsaturation of the fatty acyls, they are not useful to determine the double bond positions. As a result, most of the plasma/serum lipidome profiled in the past reported only the summed composition of carbon number and double bonds of the fatty acyls.[156, 197]

Various CID-MS/MS-based approaches were developed to determine the position of C=Cs in lipids, such as dissociation of Paternò–Büchi reaction or epoxide products resulted from photochemical or chemical derivatization of C=C.[108, 109, 198, 199] Ozone-induced dissociation mass spectrometry (OzID-MS), on the other hand, does not require any derivatization of lipids, and relies on gas-phase ozonolysis reaction inside mass analyzer to pinpoint the C=C position using characteristic Criegee and aldehyde ions.[114, 118, 119, 123] The simplicity of spectrum interpretation is a clear advantage, but the efficiency of the ozonolysis reaction is an issue in the earlier implementations of this technology, which prevented it from being integrated into high throughput lipidomics workflows.

We have previously increased the OzID efficiency in the shotgun analysis of phospholipids and applied the high-efficiency OzID-MS to elucidate detailed structures of sphingolipids in porcine brain sample.[118, 119] To leverage both the power of LC separation and OzID-MS in the determination of C=C unsaturation, others have coupled LC with OzID-MS in a few instrument configurations.[123, 125, 191, 200] Here we report the

coupling of UPLC with OzID-MS in a high-resolution Synapt G2 mass spectrometer, the high-pressure ion mobility cell enabled high ozonolysis efficiency for effective coupling with LC separation, which facilitated clear differentiation of isomeric lipids in human serum.

Materials and Methods

Materials

All solvents used were Optima LC/MS grade and purchased from Thermo Fisher Scientific. Formic acid and ammonium formate were purchased from Sigma-Aldrich. Oxygen gas was provided by Airgas. Synthetic lipid standards including PC 16:0/18:1, PC 18:1/18:1, LPC 18:0, SM d18:1/12:0, SM d18:1/18:1, and TG 22:1/22:1/22:1 were acquired from Avanti Polar Lipids (Alabaster, AL). Human sera were purchased frozen from BioIVT (Westbury, NY, USA).

Sample Preparation

Individual lipid standard solutions were prepared at 15 μM in 2-propanol/acetonitrile/water (65/35/5, v/v/v) with 10 mM ammonia formate and 0.1% formic acid, for direct infusion ESI-MS experiments. The lipid standard mixture for LC-MS analyses was prepared in the same solution and at the same concentration of 15 μM for each lipid.

The total lipids of human serum were extracted using methanol/chloroform according to a modified Folch method as reported previously.[63, 73] After extraction of the lower organic phase containing lipids, the solution was dried under a stream of nitrogen and finally reconstituted in 100μL of 2-propanol/acetonitrile/water (65/35/5, v/v/v) with

10 mM ammonium formate and 0.1% formic acid. All lipid standards and lipid extract were stored at -80°C until analysis.

Reversed-Phase Liquid Chromatography

All chromatography was performed using a Waters Acquity UPLC system (Waters, Milford MA, USA) coupled with a high-resolution time of flight mass spectrometer. Lipid extract and standard mixtures were analyzed using a core-shell Accucore C30 column (1.5 x 2.1 mm, Thermo Fisher Scientific) at 40°C. A binary solvent system of A (ACN:water, 60:40, v/v) and B (IPA:ACN, 90:10, v/v), both containing 10 mM ammonium formate and 0.1% formic acid and the following gradients were used: 0-5 min with 30% - 43% B; 5.1-14 min, 50-70% B; 14.1-21 min, 70-99% B; 21.1-24, 99% B; 24-24.1 mins, 99-30% B; 24.1-31 min, 30% B. The flow rate was set to 350 μL/min and the injection volume was 5 μL.

Mass Spectrometry

Mass spectra were acquired using a Synapt G2-HDMS (Waters, Wilmslow, UK). The typical parameter settings for ionization were: source capillary voltage 2.70 kV; sample cone voltage 50 V; source temperature 40°C; the cone gas flow rate 50 L/h. Precursor ions were mass selected in the quadrupole, passed through the trap region to enter and react with ozone gas in the IMS cell, then transmitted through the transfer region with or without collisional dissociation before reaching the TOF detector. MS spectra were acquired at a rate of 1Hz.

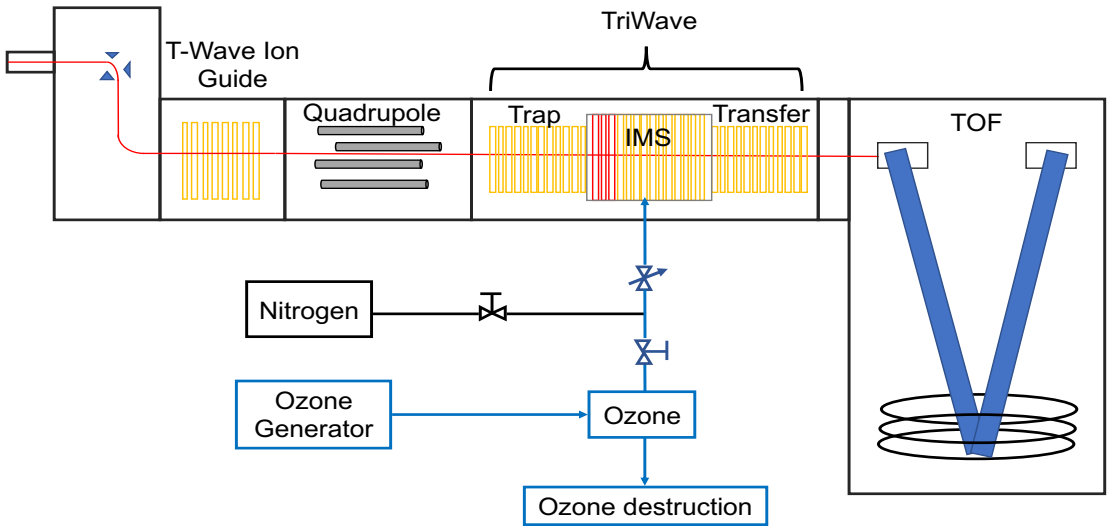

Figure 26. Schematic of Traveling Wave Q-TOF HDMS Synapt G2 MS Modified to Allow OzID to Replace Nitrogen Gas in IMS Cell. Red region in the IMS cell indicated the He cell with He gas remained as default setting.

The nitrogen gas inlet of the mass spectrometer was connected to a stainless-steel T union to accept both nitrogen and ozone with each line having its own shutoff valve. This inlet supplies drift gas to the IMS cell as configured in Fig. 26. The gas flow was maintained at 62 mL/min, which resulted in pressue in the IMS region as 2.13 mbar. The effective ozone concentration during OzID was at 6.1%. The transmission time for ions in the IMS cell was controlled by varying the amplitude and velocity of the traveling wave.

Results

OzID-MS studies in the Synapt G2 and G2-Si HDMS mass spectrometer can be implemented in either trap/transfer or IMS regions of the instrument.[118, 119, 191] The significant difference between the trap/transfer cell versus the IMS cell is the gas pressure. At the default settings, the pressure at trap/transfer region is 0.018 mbar and

IMS region 3 mbar, ~200 fold higher in the latter as required for ion-mobility separation applications.[185] Noted the helium cell is designed to maintain the ion transmission while limiting the fragmentation and ion losses when ions transmitted into the high-pressure IMS cell. Helium pressure was set as default throughout this study and maintained at 1000 mbar.

In this study, we implemented the OzID-MS in the IMS cell, and coupled it to the front end LC separation for analysis of blood serum lipids. Parameters for OzID-MS were first optimized using lipid standard PC 16:0/18:1 in direct infusion and mixture of lipid standards in LC separation conditions. Then, we focused on using LC-OzID-MS to elucidate C=C positions to differentiate isomeric lipids in human serum, where LPC, PC, SM, and TG lipid classes are dominant with isomeric species and it can be challenging to distinguish if using traditional LC-CID-MS/MS alone.

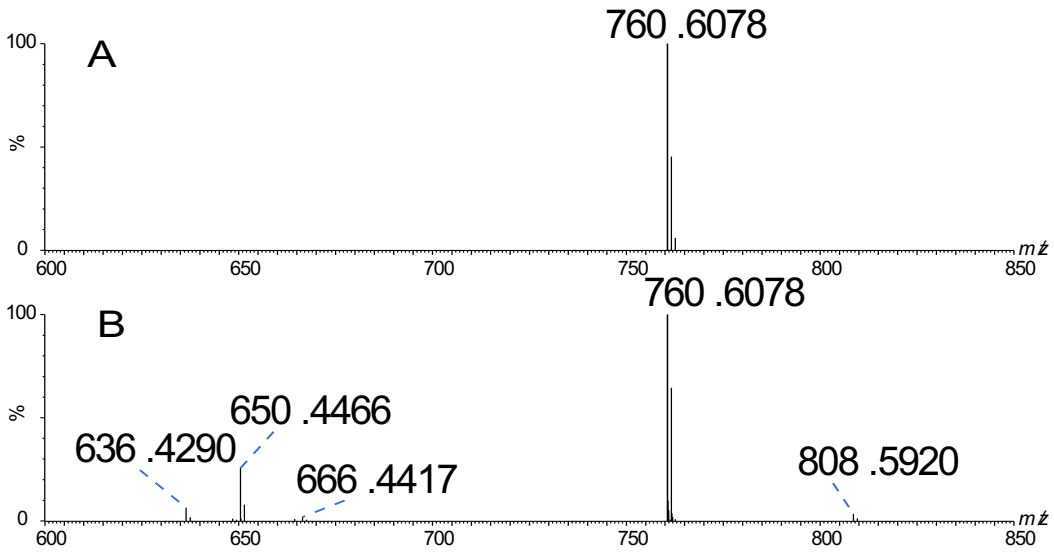

Figure 27. Analysis of PC 16:0/18:1(n-9) in A) OzID-MS of IMS cell Under The Default Setting and B) Under The Optimization Setting with Ozone as The Mobility Gas (setting listed in the method).

To optimize the conditions for OzID, a solution of synthetic standard PC 16:0/18:1 was directly infused into the ESI source operating in positive ion mode. The precursor ion, observed at *m/z* 760.58 as the $[M+H]^+$, was subsequently mass selected for gas phase ozonolysis under the default settings. As previously reported, lowering traveling wave amplitude and velocity in the reaction region can increase the efficiency of OzID by prolonging the ozonolysis time.[119, 191] Therefore, these two parameters were lowered to 21.6 V and 8 m/s, respectively. Under these settings, we calculated the targeted ions interacted with O_3 in the IMS for approximately 33 ms instead of ~386 μs as under the default settings. However, a drop in signal intensity was encountered as a result of ion scattering when operating at these low settings.[185, 186, 201] Thus, further optimization was done on the pressure of the IMS cell, by varying the flow rate of helium and IMS gas. These optimized settings offered a high-quality OzID-MS mass spectra of PC 16:0/18:1. As shown in Figure 27B, m*/z* 650 is the aldehyde ion resulted from ozonolysis because of the neutral loss of 110 Da from the precursor ion; *m/z* at 636 is differed by 30 Da from the Criegee product (m/z 666), suggesting it to be the further oxidation product of vinyl peroxide of Criegee ion as observed previously.[119, 202] These two product ions at *m/z* 650 and 636 can be observed clearly in the spectrum without zooming; at 26%, the relative intensity is especially high for the m/z 650 ion. This result indicates a higher OzID-MS efficiency was achieved than previous experiments conducted in the same region.[191]

LC-OzID-MS of Lipid Standards Mixture

The design of the instrument to have two collision cells in the front and back of the IMS, can offer CID capability without interfering the ozonolysis reaction. Hence, we can explore CID (Transfer cell) and OzID (IMS cell) either individually or in combination for the same precursor ion .

A mixture of lipid standards was analyzed using LC-OzID-CID-MS to determine the double bond positions of lipids and to validate the OzID settings optimized in the direct infusion experiments. The mixture contains PC 16:0/18:1, PC 18:1/18:1, LPC 18:0, SM d18:1/12:0, SM d18:1/18:1 and TG 22:1/22:1/22:1, which were separated on a reversed phase Accucore C30 column. Based on the choice of salts, the abundant adducts for PC was $[M+H]^+$, and for TG was $[M+NH_4]^+$.

The targeted analyte was mass selected by the quadrupole and transmitted through the trap cell for ion activation in IMS cell, where the gas phase ozonolysis took place. After the formed ozonide fragmented into the unique OzID product ions, both unreacted precursor ions and product ions left the IMS cell to enter the transfer cell, which was set to 16 eV to produce the lipid class-characteristic CID products. This unique set up allows us to generate both OzID and CID ions in a single spectrum. While OzID can determine the C=C double bond location based on the neutral loss from the methyl end of the fatty acyl, the CID products can assist in annotating lipid classes based on their unique head group-specific ions.

The total ion chromatogram (TIC) constructed from the abundance of all ions detected in the OzID scans of targeted masses of lipid standards were presented in Fig. 28A. Integration of OzID scans obtained across each of the chromatographic peaks gave the OzID mass spectra, and XIC of unique OzID products from different spectra was showed in Figure 28B. As seen, XIC at a particular *m/*z of OzID product ions aligned perfectly with the TIC of the precursor ions.

Fig. 28C showed clear evidence that OzID is only selective to the unsaturated lipids, as no OzID products were observed since LPC 18:0 doesn't contain any C=C for ozonolysis reaction. Fig. 28D showed the OzID-MS spectra of SM d18:1/12:0 without any evidence of product ion resulted from cleavage of C=C at *n-14* on the long chain base. Fig. 3E showed the OzID-CID-MS spectrum of SM d18:1/18:1; *m/z* at 184 is the fragment of choline generated by CID. OzID-MS product was observed clearly at m/z 619, which corresponds to the NL of 110 of *n-9* position on the fatty acyl chain 18:1. The poor efficiencies of OzID in the unsaturated long chain base observed in SM standards agree with what we reported previously.[112, 118]

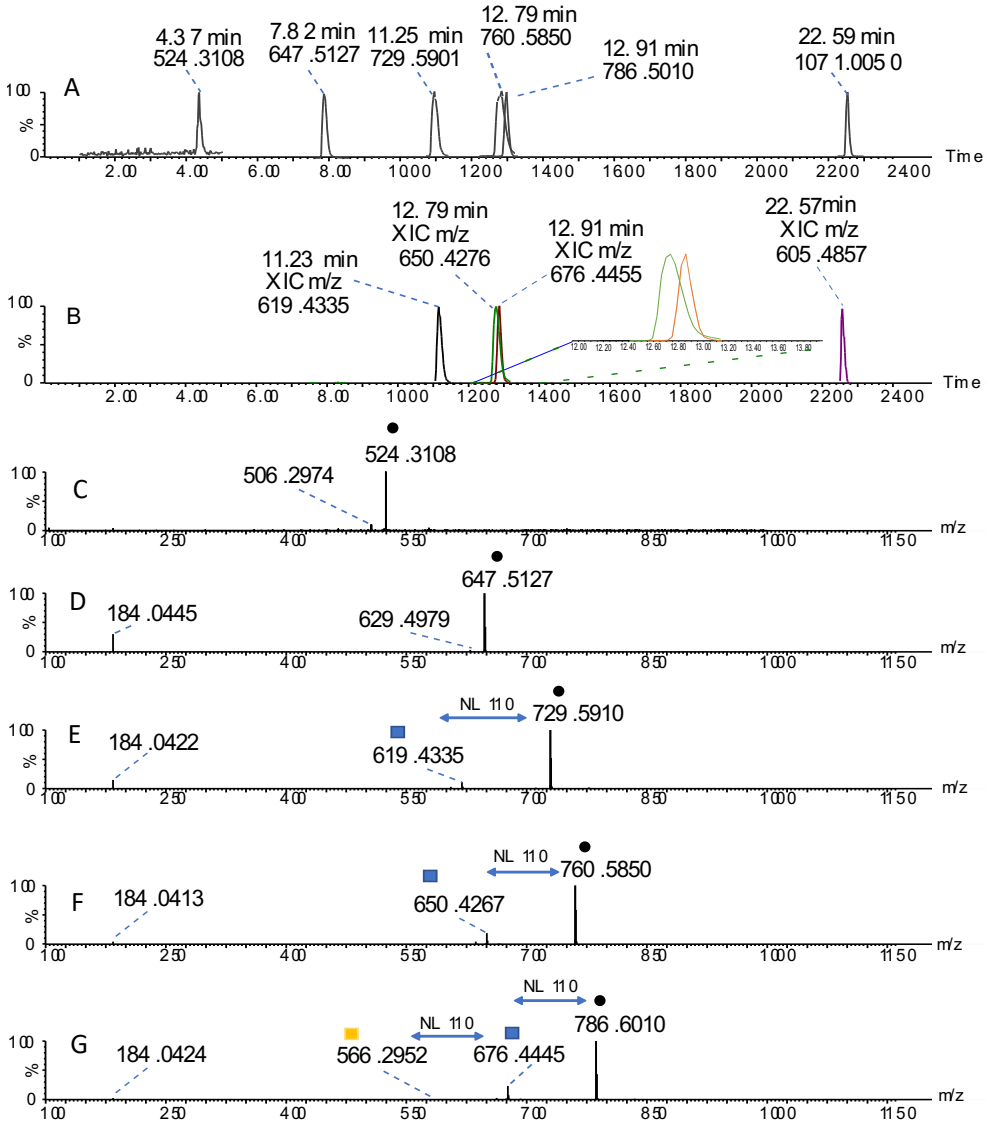

Figure 28. XIC of The Targeted Lipid Standards at The Known *m/z*. (A), and The XIC of OzID Products for The Unsaturated Lipid Standards (B). Integration of OzID Scans Obtained Across Each of The Chromatographic Peaks gave The OzID Mass Spectra Showed in here. OzID-MS of the following standards: C) LPC 18:1, D) SM d18:1/12:0, E) SM d18:1/18:1, F) PC 16:0/18:1, G) PC 18:1/18:1.

Fig. 28F and 28G showed the OzID of PC 16:0/18:1 and PC 18:1/18:1, respectively. *M/z* 184.04 was observed in both spectra, which is the diagnostic ions of choline head group for PC/SM class under the CID condition. It is of note that the

relative intensity of this ion (*m/*z 184) is lower in PC class than the ones from SM (Fig. 28D and 28E), which differentiates the two lipid classes. Distinguished OzID product ions were observed in the respective spectrum at m/z 650 and m/z 676. Both product ions confirmed C=C at *n-9* for both PC standards because of the 110 Da neutral loss from their respective precursor ions. In Fig. 28G, ion at *m/z* 566 showed a NL of 110 and 220 from *m/z* 676 and precursor ion at *m/z* 786, respectively. This ion reflects the OzID cleavage of two double bonds at the same location (*n-9*) of different fatty acyl chain. Also of note that a similar pattern and identical OzID product ions were generated using this LC-OzID-MS approach when compared with the data acquired previously using direct infusion and OzID implemented in the trap cell.[119]

LC-OzID-CID-MS Of Isomeric Lipids In Human Serum: OzID-MS Provides Informative Compositions Of Fatty Acyls In Serum Phosphatidylcholine

PC is one of the major lipid classes in human serum, and many isomers exist that are structurally very similar and challenging to differentiate.[38, 156] Taking advantage of the reactivity of PC lipids with ozone, we explored using RPLC-OzID-MS to confidently identify conformational isomers and double bond positional isomers of PC in human serum. OzID-MS confidently characterized the position and degree of unsaturation in fatty acyl chains of the interested lipids.

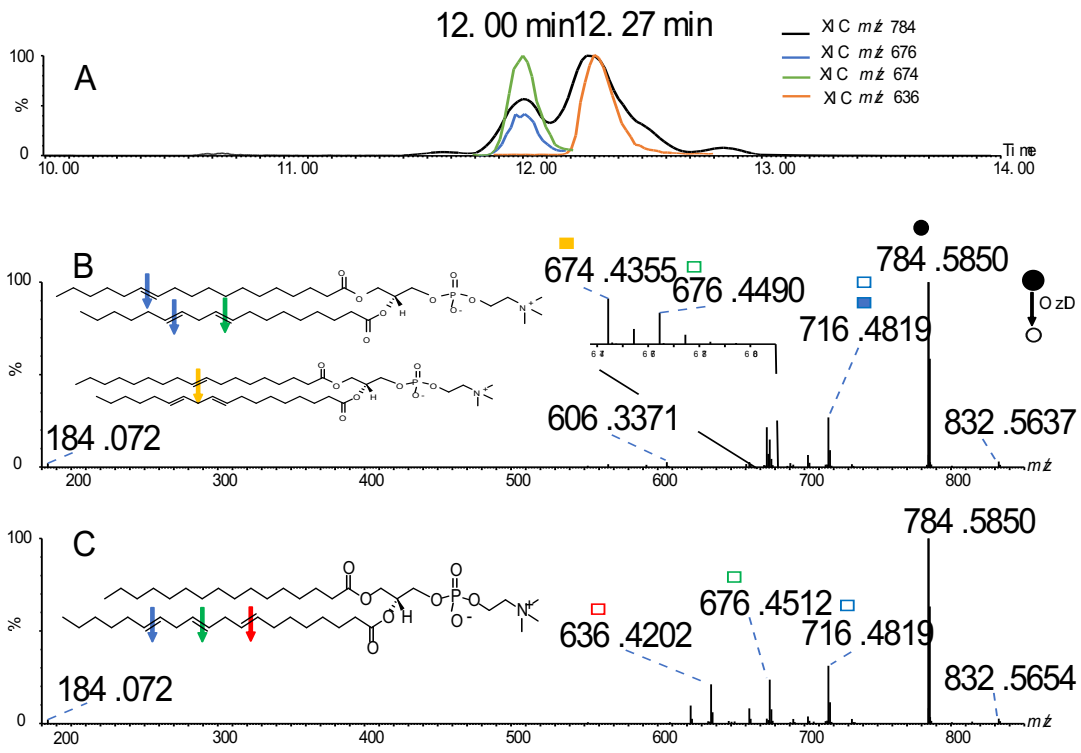

Figure 29. A) XIC of m/z at 784 was extracted (solid black line), and XIC of OzID Products at m/z 674, 676 and m/z 636 (color coded lines), Represented for Parent Ion PC (18:1_18:2) and PC (16:0_20:3), respectively at 12.00 min and 12.27 min; B) OzID-MS spectra of PC (18:1_18:2) Showed The Result of Two Possible Double Bond Positions on a Fatty Acyl Contains a Mono-unsaturated DB at n-6 and n-9 at m/z 716 and m/z 674, while a pair of ions at m/z 676 and 716 indicated a polyunsaturared double bonds at n-6 and 9 on the other acyl; C) OzID-MS spectra of PC(16:0_20:3(n-6,9,12)).

For instance, PC 36:3 can be composed of two isomers: PC 18:1_18: 2 and PC 16:0_20:3, with the fatty acyl composition identified from LC-CID-MS/MS under negative ionization mode. When the corresponding $[M+H]^+$ ion (m/z 784.59) was selected in LC-OzID-MS analysis under positive ionization mode, as shown in Fig. 29A, two closely eluting chromatographic peaks appeared (black line). The OzID-MS spectra for the peak at 12.00 min showed major products at m/z 674 and 716, corresponding to NL of 110 and 68 Da from the precursor ion, indicating mono-unsaturated double bond at

n-9 and *n*-6 position in fatty acyls (Fig. 29B, solid squares). Interestingly, we also observed ion at m/z 676, which cannot be the $[M+2]^+$ isotopic peak of m/z 674 since it did not follow the isotopic distribution pattern. The appearance of *m/z* 676 and its corresponding neutral loss of 108 from precursor ion indicate that di-unsaturated C=Cs exist in the lipid species and one of the C=C is at *n*-9 position.[121] Based on these two lines of evidence, we assigned this isomer to be PC (18:1_18:2) with the C=C in FA 18:1 at *n*-9 and C=C in FA 18:2 as *n*-6 and *n*-9, respectively. OzID-MS spectrum of the later eluting isomer is shown in Fig. 29C, which is significantly different from the patterns observed in Fig. 29B. Three OzID products were observed at *m/z* 716, 676, 636 correspondings to neutral losses of 68, 108, 148 from the *m/z* 784 precursor ion. These neutral losses correspond to C=Cs at *n*-6, *n*-9 and *n*-12 in poly-unsaturated fatty acyl, therefore the 2nd chromatographic peak was assigned as PC 16:0_20:3.

OzID-CID-MS Resolves The Double Bond Position Isomers Of PC In Serum Lipid Extract

RPLC has been known to resolve different PC isomers, especially for *sn*-positional isomers when the length of the two fatty acyls varies to a large degree.[72] However, resolving double bond positional isomers remains as the major challenge in lipidomic analysis, which can result in unambiguous structure assignment for lipids derived from complex biological extracts. The data presented above primarily showcased using OzID-MS to determine the degree of unsaturation and the location of C=C in fatty acyls of lipids, here we show that for certain C=C positional isomers, OzID-MS can help

to differentiate them. Moreover, the highly OzID efficiency setting resolved the co-elution of these peaks, giving us an additional orthogonal separation.

An example is Fig. 30 , which is LC-OzID-MS analysis of precursor ion *m/z* 788.6209 from human serum lipid extracts (Fig. 30). Under the high OzID efficiency we obtained, each scan can provide a high level of confidence for structural elucidation of double bond positional isomers. Two product ions, *m/z* 678 and 706 dominated in two subsequent scans, which is the neutral loss of 110 and 82 Da from the precursor ion, respectively. Hence, based on the accurate mass of the precursor and the OzID product ions, we confidently assigned these two spectra to be double bond position isomers of PC 18:0_18:1 at *n*-9 and *n*-7, respectively (Fig. 30B and 30C). Moreover, in Fig. 30B one can see the appearance of both OzID product ions at *m/*z 678 and 706 because XIC of these two product ions shown PC 18:0_18:1(*n*-9) cannot be fully resolved from PC 18:0_18:1(*n*-7). RPLC-MS chromatogram clearly showed the coelution of these two isomers. Without OzID, it is impossible to acknowledge the presence of these two isomers.

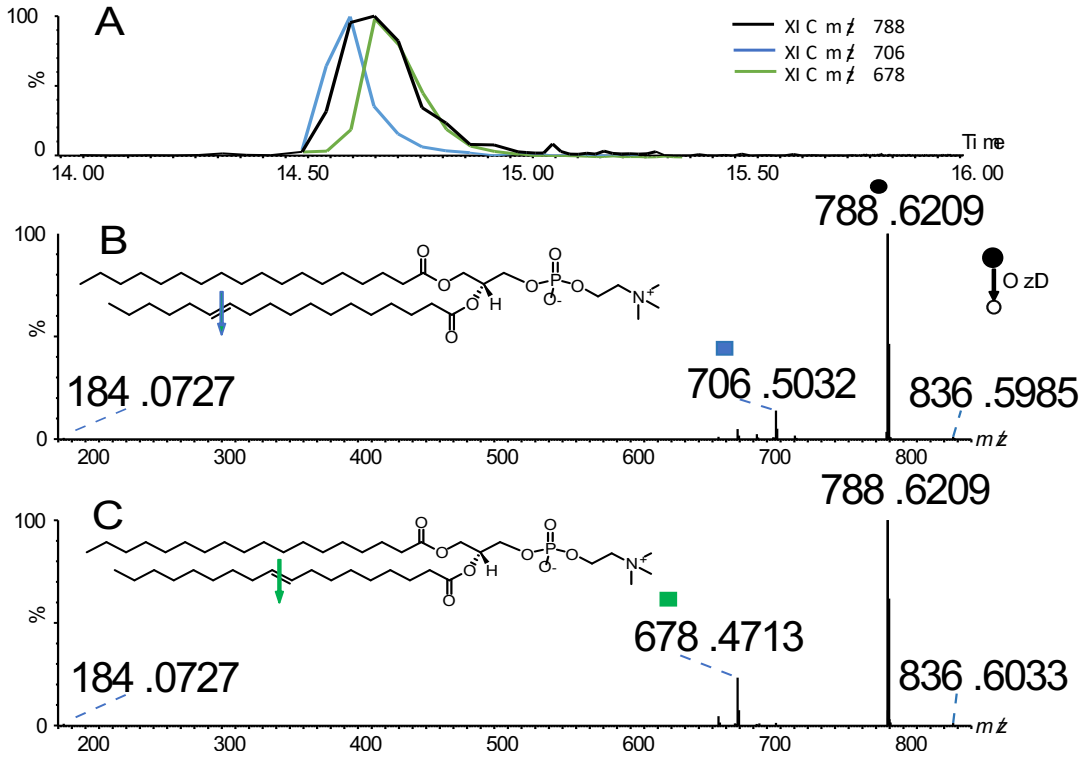

Figure 30. LC-OzID-MS of PC 18:0_18:1. A) XIC of the parent ion at m/z 788 (solid black line); XIC of OzID product ions m/z 678 and m/z 706 (color coded); mass spectra of B) PC(18:0_18:1) indicated a mono- double bond at n-7; mass spectra of C) PC 18:0_18:1 indicated a mono-double bond at n-9, coeluted with its double bond positional isomer at n-7.

OzID-CID-MS Resolves The Double Bond Position Isomers Of LPC In Serum Lipid Extract

LPC presents another interesting case to determine the double bond positional isomers. Shown in Fig. 31A is LC-OzID-MS analysis of m/z 522.3642, corresponding to LPC 18:1. Fig. 31B and 31C were acquired at 3.11 min and 3.15 min, respectively. OzID product ions were observed at *m/z* 440 and 412, corresponding to neutral losses of 82 and 110 Da, expected for a monounsaturated double bond at n-9 or n-7, respectively. Taken the data together, they suggested two double bond positional isomers of LPC 18:1 presented in the human serum sample, namely LPC 18:1(*n*-7) and LPC 18:1(*n*-9).

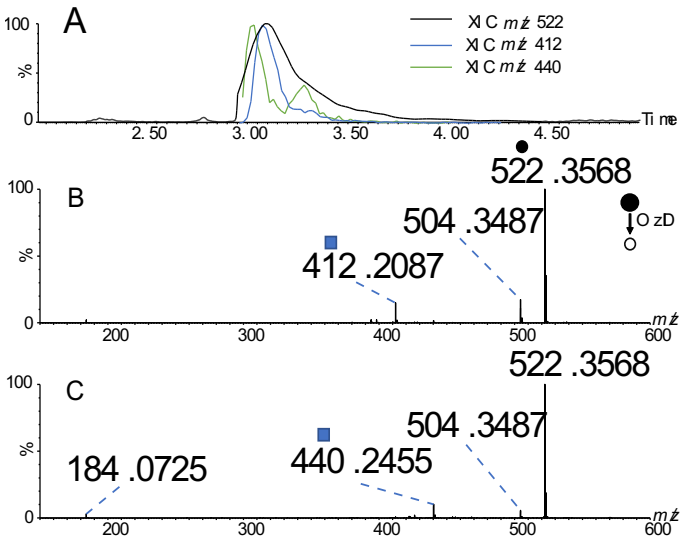

Figure 31. LC-OzID-MS of LPC 18:1. A) is the XIC of m/z 522 (black solid line), of m/z 440 (green line), of m/z 412 (blue line); B) OzID mass spectra of LPC 18:1 revealed the double bond at n-7; OzID mass spectra of LPC 18:1 revealed the double bond at n-9.

Discussion

LC-OzID-MS has been implemented on QTrap and Synapt G2 Si mass spectrometers, [115, 191] in particular in the latter case, high duty cycle that is compatible with high-resolution LC separation was achieved. The results presented here confirmed the practicality of implementing LC-OzID-MS on an IMS cell-equipped mass spectrometer for high OzID efficiency, in addition to the benefit of performing OzID and CID concurrently for more informed structural elucidation of lipids due to the unique configuration of Synapt G2 system. With this, as illustrated in this work, isomeric species in a complex matrix of serum lipid extract, previously masked or unidentified by LC-CID-MS/MS based approaches, now can be differentiated and structurally identified with more certainty.

Unlike the work of Blanksby and co-workers that primarily used sodiated adducts for OzID-MS, our focus for LC-OzID-MS-based lipidomics is on the protonated and ammonium adducts, for which we have already developed high throughout workflows for comprehensive profiling of the lipidome in complex biological samples.[63, 73] Despite the generally lower efficiency of OzID product ions from protonated/ammonium adducts,[114] we achieved higher OzID reaction efficiency, which is compareable to OzID data of metal ion lipids, as demonstrated by presence of abundant OzID product ions without spectrum magnification. This result greatly facilitated data interpretation for biomedical applications of OzID-MS.

Differential reactivity of C=C with ozone were observed in the long chain base and in the fatty acyl when analyzing SM, with the latter one having much higher yield, while the former one almost no reactivity. This observation is similar to what we have reported previously on OzID-MS of glycosphingolipids, where the ozone reactivity with C=C of fatty acyl is eight times higher than that of long chain base.[118] The differential reactivity likely can be explained by charged-induced fragmentation mechanism, where the gas phase conformation of protonated SM induces hydrogen bonding to their allylic alcohol, this results into limited interaction between C=C of the long chain base, ozone and the charge.[112, 118]

Taken together, by utilizing the high pressure IMS cell in Synapt G2 as the reaction chamber for ozonolysis and the unique capability of concurrent OzID and CID, LC-OzID-CID-MS implemented here has largely overcome the deficiencies of LC and LC-CID-MS/MS in resolving C=C positional isomers in human serum lipids. Together

with the work reported by others, application of OzID-MS to high throughput LC-MS based lipidomics has become a reality, and more detailed structural characterization of the lipidome will establish unequivocally the lipid structure and biological function and uncover new biology at the system level.

CHAPTER VI

IDENTIFICATION OF SERUM LIPID MARKERS TO TYPE 1 DIABETES PROGRESSION

Introduction

Type 1 diabetes (T1D) is a chronic childhood autoimmune disease. T1D is characterized as insulin deficiency due to the selective death of pancreatic β-cells. Although both genetic and environmental factors have been considered as the possible pathogenic mechanisms of the disease, their exact etiology remains unknown.[15, 203-205] The currently detectable signal indicating the initiation of autoimmune attack in T1D is the appearance of autoantibodies. However, it might be too late for therapeutic intervention when seroconversion of islet autoimmunity is detectable. Hence, biomarkers that reflect and predate the disease progression, while provide an insight into the underlying causes of disease are of great need.[15, 18, 19]

Lipids have recently emerged as promising markers for T1D.[22, 23, 25-27, 206, 207]. As the main component of the cell membrane, lipids are typically secreted into the bloodstream carrying information of tissue or cell health. Multiple evidences suggest a disturbance of lipid profile in T1D patients, and lipids can even indicate the appearance of islet autoantibodies.[23, 26] For example, phosphatidylcholines (PC) are down-regulated at birth, and triacylglycerol (TG) and ether phospholipids are also decreased with the progression of T1D.[27] A recent study also showed increasing level of proinflammatory

lysophosphatidylcholine (LPC) several months prior to the seroconversion of autoantibody positivity.[207] Another report found that higher concentrations of odd-chain TG and polyunsaturated glycerophospholipids are in those who developed T1D and were positive to autoantibody tests.[24] Therefore, profiling lipids at different T1D stages could uncover lipid markers indicating the natural progression of the disease, and changes of some of these markers may even predate the process of seroconversion to islet autoimmunity.

The main biofluid sample used for T1D studies is human blood plasma and serum. Different lipidomic analysis strategies were introduced to discover and characterize lipid markers of T1D.[25, 26, 75, 208] These studies have not only expanded our knowledge of the dysregulated lipidome of T1D, but also provided insightful information that can help understanding the underlying pathology, diagnose the disease at the earlier stage and, potentially predict the progression of this disease. However, limitations in technologies used to measure the lipidome led to an ambiguous structure characterization of lipid markers.

Most of the T1D studies were focusing on cross-sectional characterization of serum/plasma lipidome after T1D is diagnosed. These blood-derived samples were often collected at a single time and reflected late stage of the disease after the development of hyperglycemia. Recently, a lipidomic study containing a series of samples collected chronologically between ages 0 to 3, reported some distinct lipid profile observed at the very young age of T1D patients.[25] Despite the importance of this result, the sampling time points were inconsistent which may not truly capture the progressive nature of T1D.

To identify the biomarkers for T1D progression, samples that contains the temporal changes of lipids during the different developmental stages of T1D is required. In this respect, the longitudinally collected serum samples were carefully selected from a well-characterized T1D cohort - Diabetes Autoimmunity Study in the Young (DAISY).[142, 209] Moreover, a comprehensive lipidomic workflow, and advanced software such as Progenesis QI were used to analyze, process, and identify human serum lipids in T1D samples.[63] As a result, we accurately profiled the temporal changes of lipidome during the natural progression of T1D, and further investigated the significant differences between T1D and healthy controls at a young age, and identified a panel of potential lipid markers predicting the development of islet autoimmunity after the age of three.

Experimental Section

Sample And Study Design

Participants were selected from the Diabetes Autoimmunity Study in the Young DAISY cohort, with T1D susceptible HLC-DR/DQ alleles through genotyping at birth and followed prospectively. Informed consent was obtained from the parents of each study subject. The Colorado Multiple Institutional Review Board and the University of North Carolina at Greensboro approved all study protocols, respectively.

Islet autoantibodies GAA, BDC512, MIAA, and ZnT8 were measured at the Barbara David Center in Denver. In total, 292 serum samples of 75 subjects from three groups: Healthy control, T1D and AB group. T1D group contains children who developed islet autoantibodies and progressed to T1D; AB group are children who developed islet autoimmunity but have not yet progressed to T1D. Healthy controls are

children who have not developed islet autoantibodies or T1D and are frequency matched on age to the combined case groups. Venous non-fasting blood samples were collected at each study visit and plasma and separated and stored at -80˚. Three to four longitudinal samples were collected from 1995 to 2011. Frozen serum samples were transferred to our lab for sample processing and measurement. At the end, 90, 106 and 104 samples from T1D, AB and Healthy control group, respectively, were processed according to the experimental workflow Fig. 32 .

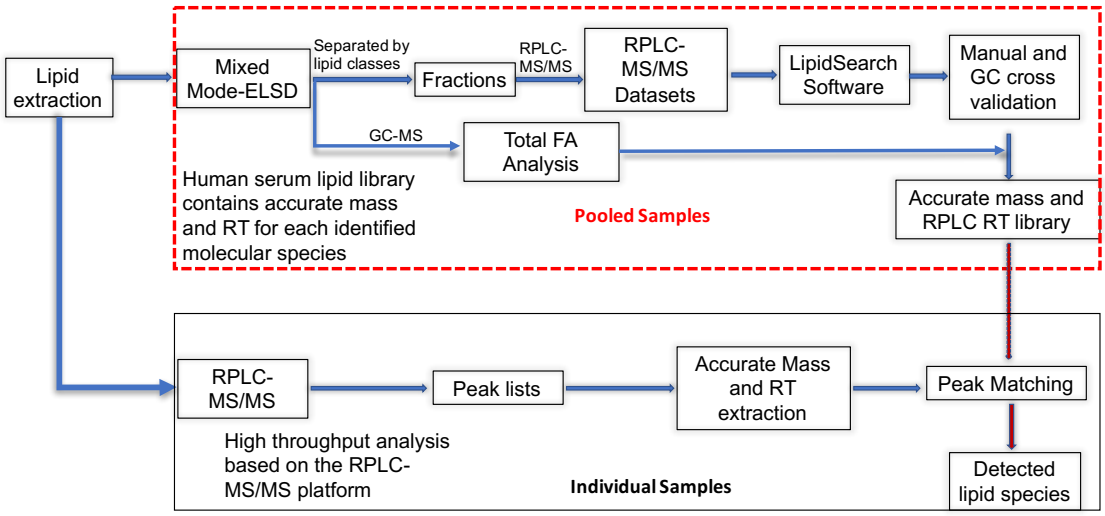

Figure 32. The Overal Work Flow of The AMT Approach. Samples from the DAISY Cohort was Pooled together to Create a Comprehensive Human Serum Lipidome Library using the Offline 2D-LC-MS/MS Aproach. Subsequently, a high throughput analysis of individual samples was done using the identical RPLC-MS/MS conditions used to generate the human serum AMT library. Raw data was processed by matching features with the AMT library before further statistical analysis.

Analysis Of Molecular Lipids

All reagents and chemicals used in this study were purchased from Sigma Aldrich St. Louism, MO , and lipid standards were purchased from Avanti polar lipids. A total of 292 serum samples were randomized and extracted using a Folch's procedure that

previously published.[63, 73] All the samples were prepared in the same batch by the same researcher to minimize the variations in sample preparation. For each sample, 25 µL of serum sample were performed Folch's method using 125 µL methanol/chloroform (1:2,v/v), 190 uL of organic layer were collected, dried under nitrogen gas and reconstituted in 50 uL of IPA/ACN/H_2O (60/35/5; v/v/v) for the subsequent high throughput analysis using RPLC-MS/MS.

Quantitative LC-MS/MS Analysis

The samples were analyzed using an ultrahigh performance liquid chromatography coupled with a hybrid Q-orbitrap high resolution mass spectrometer (UHPLC-QEHF). The separation was performed using an Accucore C30 column (ThermoFisher Scientific). The column oven temperature was 40˚C and the gradient was delivered at a flow rate of 350 µL/min with mobile A (ACN:H_2O) and B (IPA:ACN), respectively, both containing 10 mM NH_3HCO_3 and 0.1% HCOOH. The sample tray set at 15˚C with the injection volume of 5 µL.[63]

The following parameters were used in electrospray ionization: the spray voltage, the capillary temperature and the heater temperature were at 3 kV, 350 °C and 400 °C, respectively, for both ionization modes; the S-Lens RF level was set at 50. The Orbitrap mass analyzer was operated at a resolving power of 120,000 in full-scan mode scan range: 114 – 1700 m/z; automatic gain control target: 1e6 and of 30,000 in the Top*20* data-dependent MS2 mode HCD fragmentation with stepped normalized collision energy: 25 and 30 in positive ion mode, and 20, 24 and 28 in negative ion mode;

maximum ion injection time: 100 ms; isolation window: 1 *m/z*; automatic gain control target: $1e^5$ with dynamic exclusion setting of 15 s.

Database Search For Identification

All raw files obtained from LC-MS/MS analysis were analyzed using Progenesis QI ver 2.3 separately in positive and negative ion mode, search against in-house curated human serum lipids database. The parameter for peak detection was 400<*m/z*<1200, RPLC retention time between 1-25 min, peak sensitivity was set at 0.04% base peak. Peak alignment was set at default for all the files in each mode. Progenesis QI detected the features in the chromatogram, assigned the identification and extracted the peak area for each feature. Raw data was exported in excel format for subsequent statistical analysis.

Statistical Analysis

Data normalization was done using Perseus software ver 1.6.2.2 https://maxquant.org/perseus/ and Metaboanalyst. Raw data was imported in the software without any missing value, then log2 transformation, and mean centering normalization. An ANOVA test with FDR <0.05 was adapted from significant analysis. Volano's plot and Hierarchical clustering was done to observe and obtain the changes within and from three groups. Linear mixed model, t-test and ANOVA were done using SAS ver 9.4 (SAS Institute, Cary, NC, USA). Separation model of PLS-DA and OPLS-DA was done using SIMCA ver 16 (Umetrics, Umea, Sweden).

Results

Comprehensive Coverage Of Human Serum Lipidome

Human serum from 75 subjects belonging to three groups T1D, AB and controls were used in this study, with relatively matching of race, gender and age. Our identification approach is based on the accurate mass and time (AMT) tag approach, which relies on the uniqueness of the measured molecular mass and LC elution time for a specific molecule in the context of a particular biological system. A schematic representation of experimental design and workflow is indicated in Fig.32. The strategy implicitly makes use of the fact that many possible species are masked from being identified in 1D-LC system because of undersampling issue in data dependent MS/MS scans, but they can be identified in high confidence when sample matrix is greatly simplified, such as using an offline LC to fractionate samples. Therefore, a species previously identified using the off-line 2D-LC-MS/MS approach will most likely be the same species observed at the same m/z and retention time in the 2nd dimensional LC-MS/MS.

Previously, pooled samples of these subjects were used to establish a comprehensive human serum lipid library containing the structural information, as well as the accurate mass and the reliable retention time. This informative serum lipid library served as the database for the feature identification purpose of this study. Moreover, utilizing the fragmentation pattern of lipid standards analyzed in the identical platform, the in-silico fragmentation of serum lipids was generated to assist in the high confident identification of DAISY samples. This strategy takes advantage of the accurate mass

measurements from high resolution MS, the reproducible retention time information obtained from high efficiency Accucore C30 column, and MS/MS level confirmation of lipids to provide extensive coverage and confidence in identification of lipid molecular species from serum. In total, 327 and 229 lipid species were commonly identified in positive and negative ion mode, respectively, with high confidence in every sample of this study, which belong to the following lipid classes: CE, DG, LPC, PC, PE, TG, Cer, SM and plasmanyl and plasmenyl lipids. The structures of these lipids were determined at the level of head groups, compositions and positions of fatty acyl chains. In comparison, a vast majority of earlier T1D studies using LC-MS based lipidomics only acquired the data in positive ion mode, which limit the level of identification to lipid class and total number of carbon and double bond for most of the glycerol phospholipids.

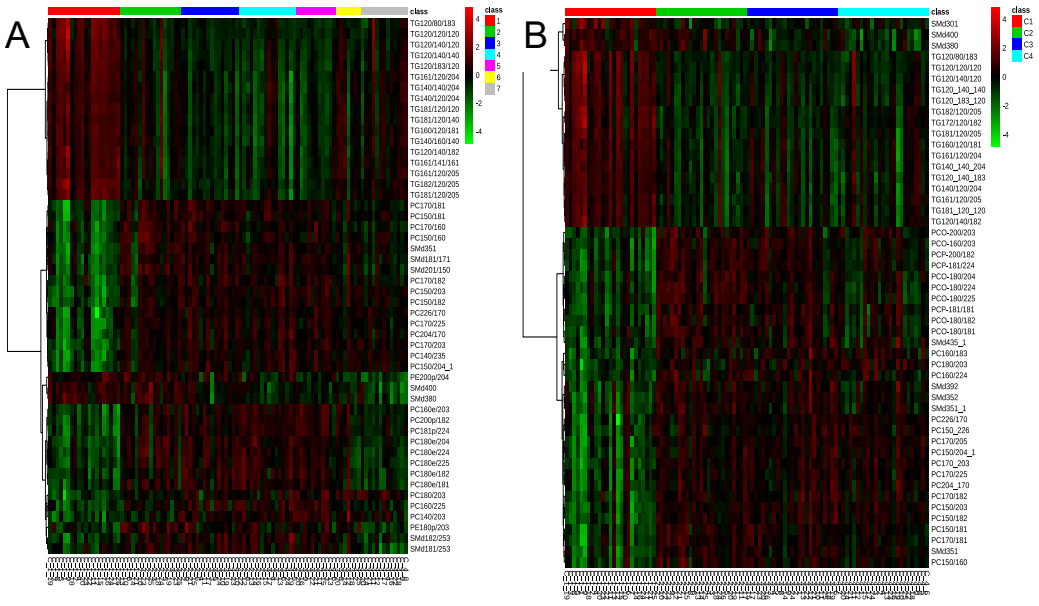

Figure 33. Hierarchical Clustering Plots Showing Age Dependence of Serum Lipidome, using Lipids Identified from Healthy Control Samples in Positive Ionization Mode. A , plotted in two year-intervals of age. Group 1: 0-2 years, group 2: 2-4 years, group 3: 4-6 years, group 4, 6-8 years, group 5, 8-10 years, group 6, 10-14 years, group 7, >14 years. B , plotted in sampling time points.

Influences Of Age On The Human Serum Lipidome

We analyzed serum lipids prospectively in three groups of samples: T1D, AB and Healthy Controls. Statistical modeling was applied to study the temporal changes of lipids in healthy children. Overall, more than 60% of healthy control serum lipids identified in this study had age-dependent expression trends (Fig. 32A). As shown in Fig.32, one could observe the changes that occurred after the subject reaching two years old. Whilst lipids in TG class showed downregulation following the maturity of the subjects, lipid species belonging to PC and SM classes showed upregulation. We observed a decreasing level of plasmalogen lipids after the first time point, and a dysregulated profile of PE. In addition, we performed heatmap analysis of the lipidomic changes according to the sampling time points, as matched to the time points of the T1D group (Fig. 32B), and similar lipid profile changes were observed with respect to age. Identical tests were done on the data collected from the negative ionization mode and similar trends of changes in lipid classes were observed (Fig. 33). This result highlighted the major challenge in a longitudinal study, i.e. whether the temporal changes observed for lipids truly reflect the underlying pathological conditions or are associated with age during a child's development. Hence, the data were statistically analyzed while taking age into consideration as detailed below.

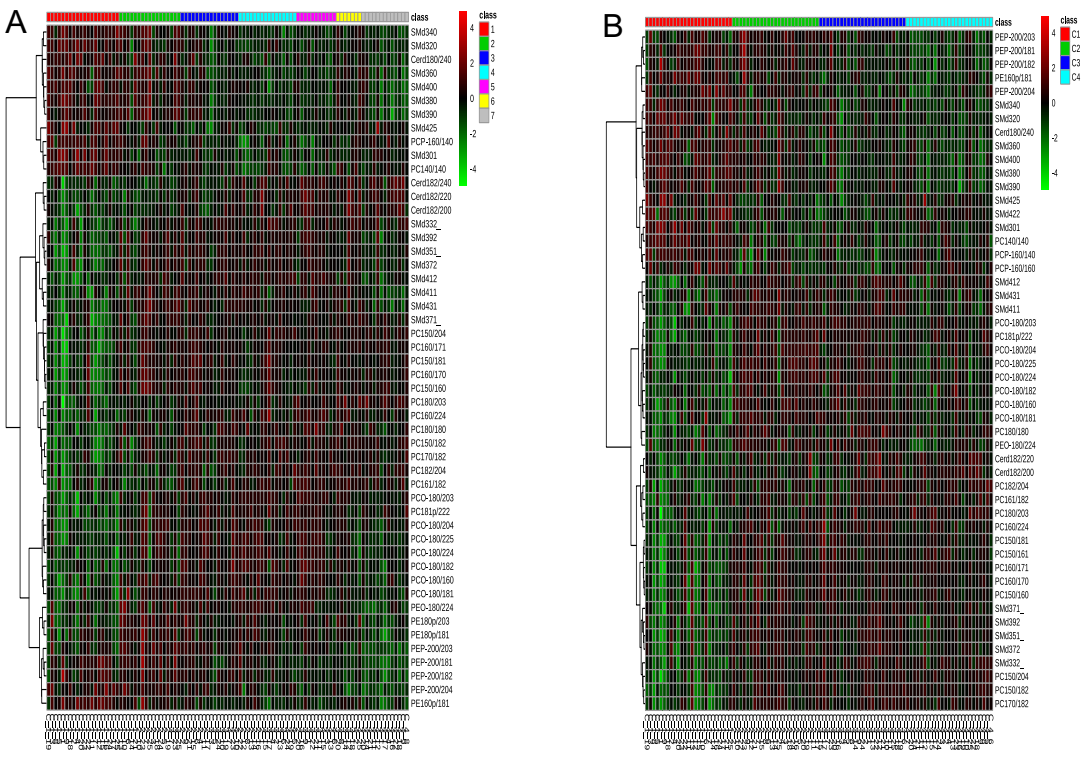

Figure 34. Hierarchical Clustering Plots Showing Age Dependence of Serum Lipidome, using Lipids Identified from Healthy Control Samples in Negative Ionization Mode. A , plotted in two year-intervals of age. Group 1: 0-2 years, group 2: 2-4 years, group 3: 4-6 years, group 4, 6-8 years, group 5, 8-10 years, group 6, 10-14 years, group 7, >14 years. B , plotted in sampling time points.

Distinct T1D Lipdome At A Young Age

We compared the serum lipidome of T1D, AB, and Healthy Controls at the first time point, which were acquired at the earliest time point possible for the individual subject considering the constraints of clinical enrollment. A volcano plot using t-test and FDR < 0.05 revealed a list of lipids with significant changes within four fold (Fig.34) In agreement with the literature, we observed a lower level of TG, but a higher level of SM and PC species in the T1D group.[24, 27] Similar comparison were also made between the two groups of samples at the other time points (2, 3 and 4); however, we didn't observe

any significant changes in these time points between the two groups. When we compared the two groups of samples belongs to AB and healthy control at different time points, significant changes were observed at time point 2. In contrast with observation in T1D when compared with healthy controls, AB groups has a higher level of TG and lower level of PC and SM (Fig. 35) . This is an interesting observation for AB group because a series of sample at time point 2 was collected a few months to a year prior to the appearance of the first autoantibody. Overall, the most significant changes were obtained in the time point one, which is promising to identify biomarkers for early diagnosis.

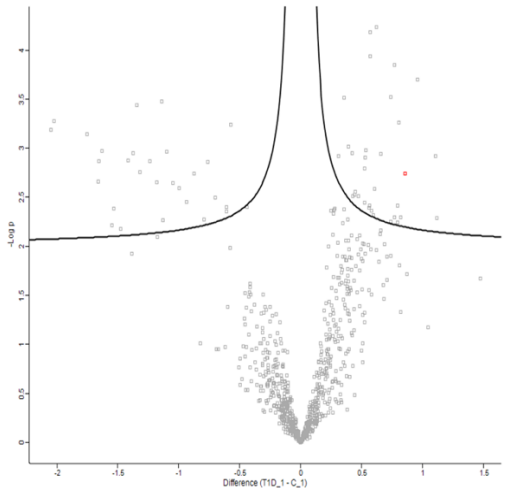

Figure 35. Volcano Plot Revealed a Significant Different Level of Lipids when comparing T1D with Control at the 1st Time Point. Each dot is one lipid species. Horizontal axis is the differences in term of lipid levels, and vertical axis is the p-value. Most of the TG have a lower abundance in T1D and can be seen on the upper left side of the plot. The PC and SM are observed on the upper right side.

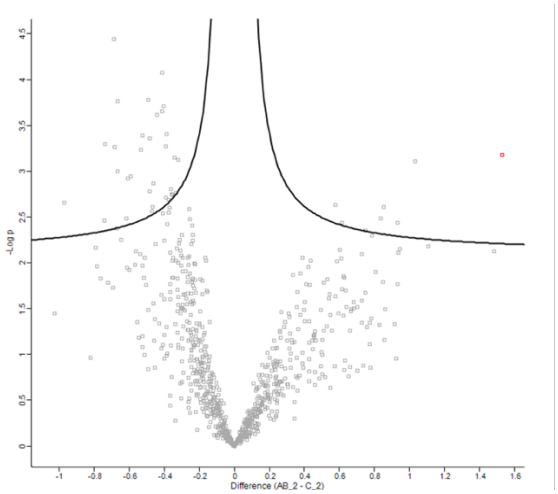

Figure 36. Volcano Plot Revealed a Significant Different Level of Lipids when comparing AB with Control at Time Point 2. Each dot is one lipid species. Horizontal axis is the differences in term of lipid levels, and vertical axis is the p-value. Most of the TG have a lower abundance in healthy control, and can be seen on the upper right side of the plot. The PC and SM are higher abundance in AB, and observed on the upper left side of the plot.

Although the total separation between three groups from <3 years of age wasn't achieved, PLS-DA plot shows the separation between T1D versus non-T1D (AB and healthy controls) (Fig. 36) . Based on the VIP score and the p-FDR value, we identified a panel of lipids in both positive and negative ion mode which distinguish T1D from the other two groups (Table 2). The average concentrations of these species were plotted in Fig. 37, which clearly showed these significantly changed lipids have a higher concentration in T1D compared to the other two groups in positive and negative mode, respectively, with healthy control samples having the lowest level of potential lipid markers listed in Table 2.

Table 2. A Panel of Lipids with Significant Differences in T1D Group as Compared to the AB and Healthy Control Groups. Data in both negative and positive modes were used in the analysis. Significant changes were designated as adjusted p-FDR <0.05 and VIP >1.3.

Mode	Accepted_Compound_ID	pfdr_p	VIP from PLSDA
negative	PC O-18:0/20:3	0.012	1.93
negative	PE 18:0p/20:3	0.012	2.17
negative	SM d43:1	0.012	1.88
negative	LPC 0:0/17:1	0.023	1.58
negative	LPC 15:0/0:0	0.023	1.84
negative	PC 16:0/22:4	0.023	1.56
negative	PE 18:0p/22:5	0.023	1.65
negative	PI 22:5/18:0	0.023	1.39
negative	SM d35:1	0.023	1.41
negative	PC 15:0/18:1	0.024	1.37
negative	PC 16:0/17:1	0.025	1.37
negative	LPC 17:0/0:0	0.025	1.64
negative	PC 15:0/16:1	0.025	1.31
negative	PC 15:0/18:2	0.025	1.35
negative	PC 18:0/20:3	0.025	1.31
negative	PC O-18:0/22:4	0.025	1.67
negative	PI 22:4/18:0	0.025	1.34
negative	SM d33:2	0.025	1.32
negative	SM d37:2	0.025	1.33
negative	SM d41:3	0.025	1.46
negative	SM d43:2	0.025	1.37
negative	PE P-20:0/20:3	0.025	1.99
negative	SM d43:3	0.025	1.32
negative	SM d43:2	0.038	1.94
negative	LPE 18:1	0.046	1.46
positive	PC 17:0_20:3	0.012	1.80
positive	PC 15:0/20:3	0.012	1.70
positive	PC P-18:1/22:4	0.015	1.68
positive	PC 16:0/22:4	0.023	1.61
positive	PC 17:0/22:5	0.023	1.40
positive	PC P-20:0/18:2	0.023	1.51
positive	PE 18:0_18:1	0.023	2.47
positive	PE P-18:0/20:3	0.023	1.81
positive	SM d45:5	0.023	1.42

positive	PC 17:0/20:5	0.023	1.40
positive	PC 18:0/20:3	0.024	1.46
positive	SM d35:2	0.024	1.37
positive	LPC 15:0/0:0	0.025	1.67
positive	LPC 17:0/0:0	0.025	1.53
positive	LPE 18:1	0.025	1.82
positive	PC 15:0/18:1	0.025	1.35
positive	PC 15:0/18:2	0.025	1.34
positive	PC 15:0/20:4	0.025	1.32
positive	PC 17:0/18:1	0.025	1.32
positive	PC 18:0/22:4	0.025	1.37
positive	PC 20:4_17:0	0.025	1.32
positive	PC O-16:0/20:3	0.025	1.67
positive	SM d37:2	0.025	1.31
positive	TG 12:0_14:0_14:0	0.025	1.37
positive	TG 18:1_12:0_12:0	0.025	1.44
positive	PC 18:0/22:5	0.025	1.35
positive	TG 18:1/12:0/14:0	0.028	1.45
positive	TG 16:0/12:0/18:1	0.028	1.34
positive	LPC 0:0/16:1	0.045	1.32
positive	TG 18:2/15:0/20:5	0.049	1.53

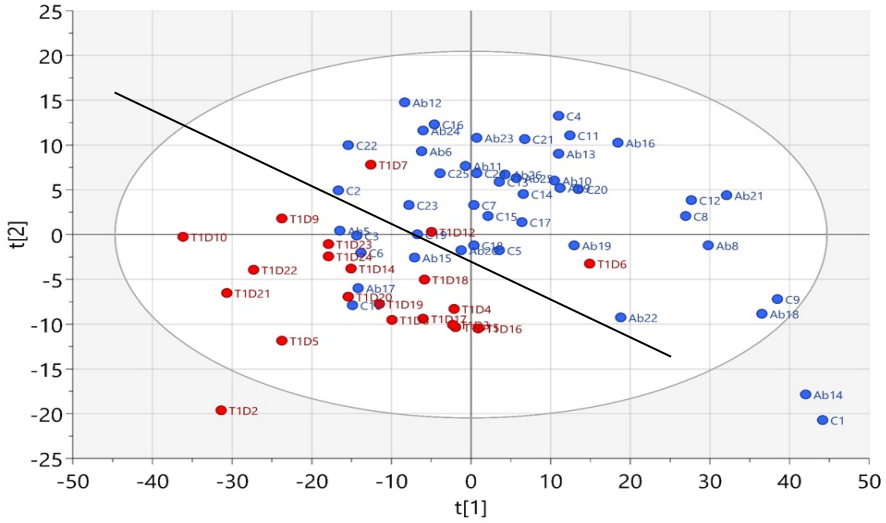

Figure 37. PLS-DA Plot showing Separation between T1D (red) and non-T1D groups at <3 years age, The Latter contains both AB and Healthy Controls (blue) .

Temporal Expression Patterns Of Serum Lipids In T1D, AB, And Healthy Controls

When comparing the temporal changes within each group, we recognized some patterns.The linear mixed model was used to observe the temporal change of each subject over time, with p-FDR<0.1, we identified 11 lipids with significant temporal changes in all groups. Comparing to the AB and Healthy controls, potential biomarkers in T1D group listed in Table 4 showed distinguished profile at the earliest time point. In the example in Fig.38, PI 22:5/18:6 and PC 18:0/20:3 were examined over 20 years of study. Both lipids indicated a higher level at the young age in T1D samples, and a gradual decrease chronologically. Both AB and healthy control groups showed an alternate profile observed during the development of these subjects.

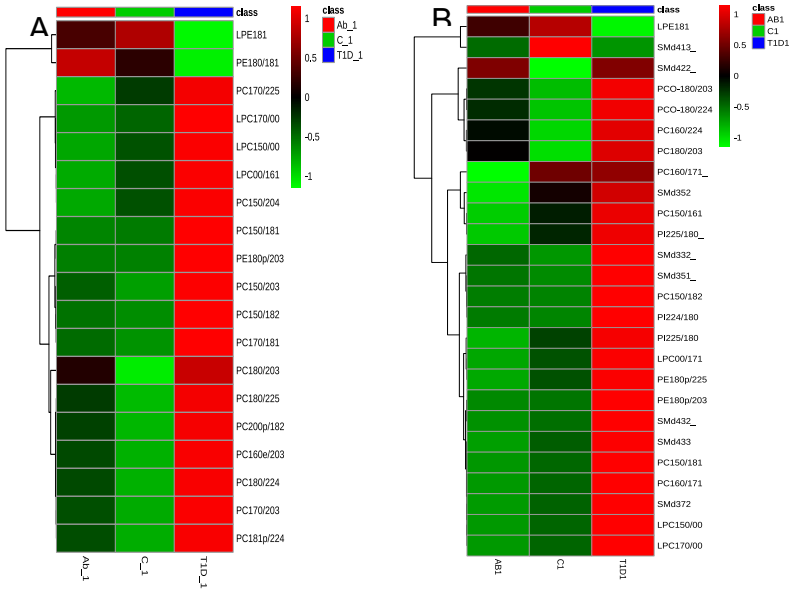

Figure 38. The Average Lipid Level of Potential Markers listed in Table 2. Heatmap revealed a significant higher level of lipids in T1D group observed in A) positive mode and B) negative ion mode.

Table 3. List of Candidate Lipids with a Temporal Change Across all the Subjects and Samples. Linear Mixed Model used The Adjust p-FDR <0.1 to identify lipids with significant changes. The level and trend of lipid in T1D were compared to Healthy Controls and AB.

Mode	Accepted_Compound_ID	pfdr_p	Starting Level in T1D	Trend in T1D
negative	Cer d18:2/20:0	0.083	high	slightly increase
negative	Cer d18:2/22:0	0.023	high	slightly increase
negative	PC 18:0/20:3	0.092	high	slightly increase
negative	PE 16:0p/20:4	0.083	low	decrease
negative	PE 18:0p/20:4	0.063	high	decrease
negative	PE P-20:0/20:4	0.021	low	decrease
positive	PE P-20:0/20:4	0.063	low	decrease
negative	PI 22:4/18:0	0.083	high	decrease
negative	PI 22:5/18:0	0.063	high	decrease
negative	SM d41:2	0.023	high	decrease
negative	SM d41:3	0.079	high	decrease

Lipid Profile Of Children Under The Age Of Three Can Predict The Development Of Islet Autoimmunity

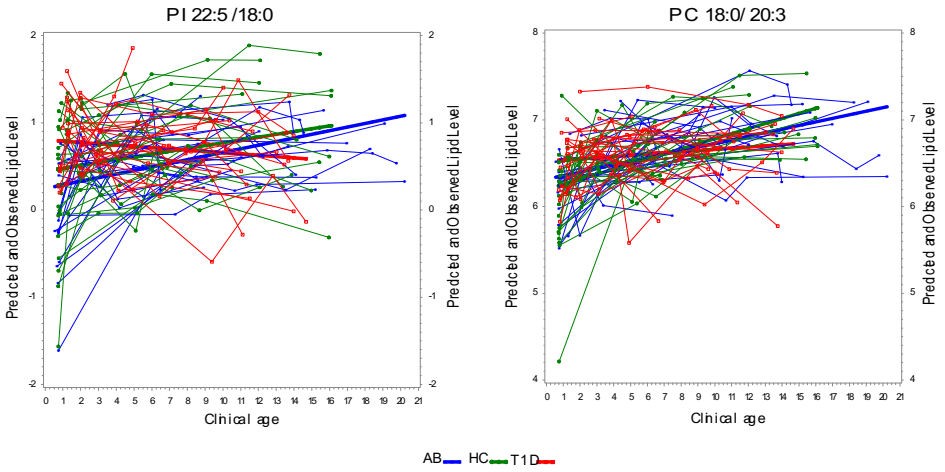

Figure 39. Temporal Change of PI 22:5/18:0 and PC 18:0/20:3 Recorded in Negative Ion Mode. Linear mixed model was performed with p-FDR<0.1. Each point is one sample, and the color of the line and point are color coded to the group. The plot revealed the normalized level of lipids vs the clinical age of sample. The predicted level of lipid in each plot is the linear regression line, with their slop reflects their alternation over time.

Additional analyses were performed to predict the onset of islet autoimmunity after the age of three when comparing healthy control group and the group developed islet autoimmunity (T1D and AB group). OPLS-DA scores plot (Fig. 39) showed the separation between controls and non-control T1D and AB , with a validated Q2=0.02, which passed the permutation test in predicting if the subject will develop the autoantibody after 3 years of age. With this data, we identified a panel of potential lipid markers that can predict if the patients will develop islet autoantibodies after 3 years of age (Table 4).

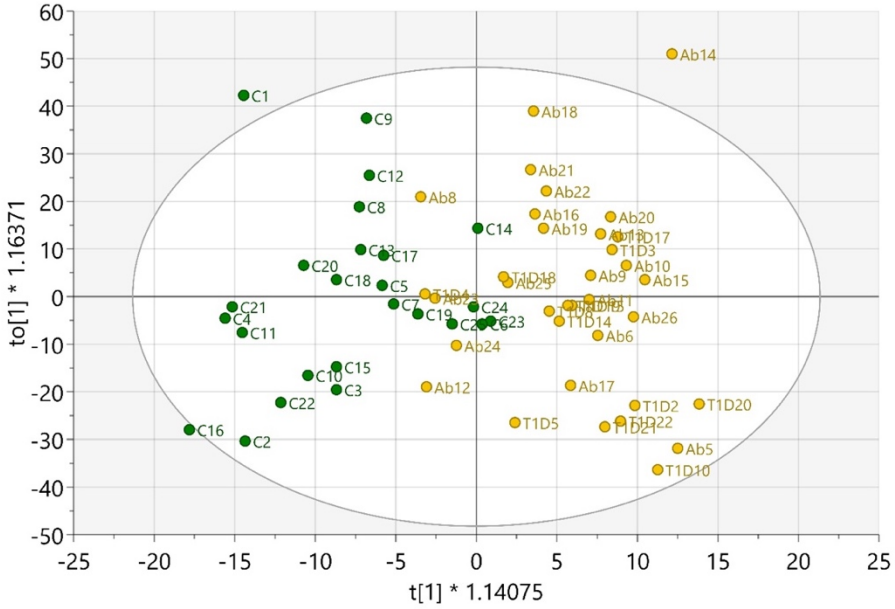

Figure 40. OPLS-DA Scores Plot of Control and non-control group (AB and T1D). Each dot is one subject. Subjects anticipated in this test contained sample that gave a negative antibody positivity prior to three years of age, but later give the positive result to the antibody assay when the subject is > 3 years old. Color coded to refect the group, Control group is green , non-control is yellow .

Table 4. List of Candidate Markers that can Predict the Appearance of Islet Autoantibodies after The Age of Three. VIP score >1.3, and the mean value for each group represents the up-or down-regulated level in each group.

Mode	Accepted_Compound_ID	Control_MEAN	non_Control_MEAN	VIP from OPLS-DA
negative	Cer d16:1/16:0	-2.37	-1.88	2.10
negative	Cer d16:1/24:0	2.85	3.07	2.36
negative	Cer d17:1/22:0	-0.79	-0.32	2.90
negative	Cer d18:1/18:0	-0.23	0.02	2.13
negative	Cer d18:2/20:0	-3.30	-2.82	3.01
negative	Cer d18:2/22:0	0.60	1.08	3.74
negative	Cer d18:2/24:0	1.94	2.08	1.85
negative	LPE 18:1	1.57	1.35	1.53
negative	LPI 20:4	-1.90	-2.11	1.63
negative	PC 16:0/22:4	5.23	5.38	1.77
negative	PC 18:0/18:0	-0.90	-0.60	2.48
negative	PC 18:0/20:2	3.71	3.96	2.32
negative	PC 18:0/20:3	6.17	6.37	2.09
negative	PC 18:0/22:3	-0.89	-0.63	2.36
negative	PC 22:0/18:2	-1.47	-1.09	1.59
negative	PC O-18:0/18:1	1.36	1.67	2.29
negative	PC O-18:0/22:4	1.23	1.36	1.58
negative	PC P-16:0/16:0	1.96	1.77	1.76
negative	PE 16:0p/20:4	4.10	3.85	2.43
negative	PE 16:0p/22:6	2.89	2.71	1.58
negative	SM d33:1	3.63	3.86	1.64
negative	SM d37:1	1.98	2.12	1.77
negative	SM d38:1	5.73	5.94	1.64
negative	SM d39:1	4.39	4.73	2.45
negative	SM d39:2	1.33	1.52	2.03

negative	SM d40:1	6.67	6.93	2.60
negative	SM d40:2	6.27	6.42	2.03
negative	SM d41:1	5.65	5.88	2.69
negative	SM d41:2	4.54	4.72	2.10
negative	SM d41:2	3.46	3.69	2.34
negative	SM d41:3	1.08	1.25	1.75
negative	SM d42:2	5.65	5.85	1.68
negative	SM d43:2	0.67	0.80	1.95
positive	Cer d18:2/24:0	-2.92	-2.65	2.11
positive	Cer d40:1	-2.48	-2.19	2.28
positive	Cer d41:1	-2.37	-2.20	1.93
positive	LPC 0:0/18:3	-2.40	-2.63	1.82
positive	LPC 18:2/0:0	4.51	4.22	2.03
positive	LPC 20:4/0:0	1.40	1.20	1.65
positive	LPE 16:0	-2.94	-3.09	1.62
positive	LPE 18:1	-1.84	-2.07	1.75
positive	LPE 18:2	-0.80	-1.13	1.92
positive	LPE 20:4	-1.82	-2.09	2.01
positive	PC 16:0/22:4	4.95	5.17	2.32
positive	PC 17:0_20:3	0.20	0.49	1.69
positive	PC 18:0/18:0	-1.59	-1.31	1.61
positive	PC 18:0/20:2	2.90	3.20	2.67
positive	PC 18:0/20:3	5.70	6.01	2.70
positive	PC 18:0/22:5	2.85	3.06	1.53
positive	PC 19:0/18:2	1.17	1.31	1.84
positive	PC O-20:0/20:3	-1.34	-1.04	1.88
positive	PE P-16:0/20:4	1.75	1.56	1.91
positive	PE P-16:0/22:6	0.58	0.40	1.62
positive	PE P-20:0/20:4	-0.76	-1.04	1.65

positive	SM d33:1	1.75	2.06	1.70
positive	SM d37:1	0.55	0.90	2.10
positive	SM d38:1	4.54	4.85	1.85
positive	SM d39:1	2.52	2.87	2.08
positive	SM d39:2	-1.16	-0.89	1.68
positive	SM d40:1	5.18	5.46	1.86
positive	SM d41:1	3.90	4.14	2.01
positive	SM d41:2	1.63	1.85	1.84
positive	SM d41:3	-0.33	-0.10	1.59
positive	SM d41:4	0.60	1.05	1.91
positive	SM d42:4	3.53	3.77	2.23
positive	SM d43:4	2.19	2.43	1.68
positive	SM d43:5	-0.27	0.03	1.55

Discussion

The AMT approach has been more widely used in proteomics for high throughput and accurate identification of peptides,[139, 141, 210, 211] very rarely it has been applied in lipidomics.[26] Using this approach and our in-house curated human serum library, we profiled lipidome level changes of serum lipids from three longitudinally collected sample sets related to T1D. To our knowledge, this is the first application of AMT approach to high throughput lipidomics, most of the lipids identified in our study contain the composition of fatty acyl chains and their *sn*-positions on the glycerol backbone, which provides at a high level of confidence in structural annotation of serum lipidome.

Dyslipidemia is well-established in diabetes mellitus. Previous work by others showed that most distinct changes of lipidome occurred in T1D children younger than 3

months old.[25] In this respect, we had similar findings in this DAISY cohort that most significant changes occurred at young age <3 years when comparing T1D and non-T1D groups. It is of note that it is difficult to observe change in lipids during the development of a chronic disease due to age as the major confounding factor, as we clearly demonstrated the lipidome levels are age dependent. Nonetheless, our data highly suggested the most pronounced changes happened at the earliest time point of patients, which is < 3 years of age. Oresic and co-workers found SM levels were low in T1D group compared to other groups at a younger age, and persistently lower over time when compared to the other groups.[25] In contrast, our data suggested a higher level of SM lipids at the younger age, decreasing during the development of the disease. The discrepancy may arise from the different cohort of samples were used, which differ in geographical location and other confounders, such as diets, genotypes, etc. This point can be further illustrated with two studies conducted by the same authors with opposite results. While one study revealed decreased levels of PC, SM and LPC in serum,[212] the second study showed increased SM and PC in T1D when compared to control samples.[213] These contradictions suggest the needed rigorousness in study design, including sample collection, but it is difficult to achieve for infant <1 year of age, i.e. most of the samples were collected non-fasting, and the diet-intake can significantly influence the serum lipidome. In this respect, previous study has shown children with different diets could result in higher concentration of odd chain TGs and polyunsaturated FA-containing phospholipids.[214] Hence, it is critical to have samples from the same study cohort for a fair and comprehensive comparison. Despite these limitations, we identified a panel of

lipids that can predict islet autoimmunity, as well as differentiate between three groups of samples earlier than 3 years of age.

Sample storage conditions also had a big influence on the integrity of samples.[215] Multiple studies had confirmed temperature and chemicals used in sample storage can affect degradation of lipids. The preanalytical variables include the storage condition immediately after sample collection, the storage condition pre- and post-transportation. Investigation on the variances of free-thaw cycles and sample storage condition found that a stable period for human plasma/serum sample is within 3 years at a temperature <-20°C, and <10 freeze-thaw cycles.[216] The samples used in our study were stored around 4-25 years inside -80°C freezer prior to transportation to our laboratory. Although we have minimized freeze-thaw cycles during sample preparation, we do not know to which extent long term storage can affect lipid stability. To our knowledge, effect of very long term storage on lipid degradation under deep freezing conditions has not been studied. Considering the heterogeneity of lipid levels within individuals and the limitations of long term sample storage in longitudinal cohorts, comparing the relative abundance of lipids cross-sectionally at different stages of disease development is still a valid approach for biomarker identification.

In summary, this research identified distinct changes in serum lipidome for subjects in the younger age who developed T1D or islet autoimmunity. It also suggests that, for better uncovering the longitudinal changes of different lipid profiles, a more rigorous age-matching between groups and with equal years of interval is desired to eliminate age as a confounding factor. While the list of lipid markers still needs to be

validated using other cohort of samples for their utilities in T1D diagnosis, nevertheless, the AMT approach we developed can be adapted to other large scale high throughput lipidomics studies, and the temporal changes of serum lipidome during childhood would also serve as a valuable resource for pediatric disease research.

CHAPTER VII

CONCLUDING REMARKS

Type 1 diabetes (T1D) is a well-known chronic disease occurs most frequently in children. Due to the unknown etiology and autoimmune nature of the disease, a late clinical diagnosis results in serious complications and financial burden. The current biomarker studies in T1D are mostly limited to cross-sectional comparisons at the disease onset, and in general do not reflect what happened at the early stages of this disorder. Recently, dysregulated lipid metabolism were observed in T1D, both at the overt disease stage and prior to development of islet autoimmunity, a key step in the natural progression of this autoimmune-mediated disease. Since function of lipids are determined by their structures, it is critical to comprehensively and accurately determine the structure of lipids.

In this dissertation, we developed novel analytical capabilities in structural elucidation of lipid molecules, particularly in determination of sn-position, and the location of unsaturation. A high throughput approach for lipidomics analysis was also developed to comprehensively quantify a large number of clinical samples, which has been used to profile the temporal changes of lipidome during the natural progression of T1D.

Chapter III established a novel workflow for accurate identification of lipids in human serum. By adding the additional separation dimension of mixed mode-LC, the

approach overcame the challenges in the one dimension RPLC-MS/MS approach and provided high confidence in structural identification, particularly for the isomeric and isobaric species existed within the same lipid class or between classes. The human serum lipids were identified with accurate mass and RPLC retention time, which were curated into an in-house data base for high throughput analysis of lipids from the same biological specimen. Identification of these lipid species were further confirmed at the fatty acyl level using tandem mass spectrometry in both positive and negative ion mode, with sn-positional assignment determined for most of the lipid molecular species. Chapter IV and V advanced further in structural elucidation of lipids by providing information on the location of C=C unsaturation. This was accomplished inside the mass analyzer through a specific gas phase ion chemistry between ozone and unsaturated lipid ions. This ozone-induced dissociation (OzID) process generates C=C location characteristic diagnostic fragmentation ions, which is highly valuable for structural elucidation at the level of C=C position. For the first time, we achieved the highest OzID efficiency with the protonated lipids in a high resolution traveling wave mass spectrometer, up to ~1000x more effective compared to previous reports. Moreover, the flexibility to implement OzID in a high gas pressure of the instrument made this technique compatible with LC separation for better resolving of isomeric unsaturated lipids. With OzID-MS, double bond positional isomers in human serum lipids can be elucidated. Using longitudinally collected human serum from individuals in T1D, AB and healthy control groups and the human serum lipid library curated in Chapter III, Chapter VI applied accurate mass and time tag approach for high throughput analysis and identification of candidate lipid markers that indicate

T1D progression. A significant difference was obtained in the lipid profile of T1D individuals at a younger age, however, the changes were normalized at later stages of this disease, which is in line with what reported by others using longitudinally collected samples.

In summary, we developed innovative methods for comprehensive characterization of lipids in human serum and high throughput analysis of human serum samples to identify T1D lipid biomarkers. While the panel of lipid markers still need to be validated in independent T1D cohorts for their values in predicting islet autoimmunity and early diagnosis of T1D, the advanced analytical capabilities we developed in C=C unsaturation determination and in AMT-based high throughput analysis of lipidome changes in human serum can be applied to other human diseases. In addition, the temporal changes of lipids during childhood development would also be valuable for researches in other pediatric diseases.

REFERENCES

1. Guariguata, L.; Whiting, D. R.; Hambleton, I.; Beagley, J.; Linnenkamp, U.; Shaw, J. E., Global estimates of diabetes prevalence for 2013 and projections for 2035. *Diabetes Res Clin Pract* **2014,** *103* (2), 137-49.
2. Zhang, P.; Zhang, X.; Brown, J.; Vistisen, D.; Sicree, R.; Shaw, J.; Nichols, G., Global healthcare expenditure on diabetes for 2010 and 2030. *Diabetes Res Clin Pract* **2010,** *87* (3), 293-301.
3. Huang, E. S.; Basu, A.; O'Grady, M.; Capretta, J. C., Projecting the future diabetes population size and related costs for the U.S. *Diabetes Care* **2009,** *32* (12), 2225-9.
4. Nokoff, N.; Rewers, M., Pathogenesis of type 1 diabetes: lessons from natural history studies of high-risk individuals. *Ann N Y Acad Sci* **2013,** *1281*, 1-15.
5. Vehik, K.; Hamman, R. F.; Lezotte, D.; Norris, J. M.; Klingensmith, G.; Bloch, C.; Rewers, M.; Dabelea, D., Increasing incidence of type 1 diabetes in 0- to 17-year-old Colorado youth. *Diabetes Care* **2007,** *30* (3), 503-9.
6. Atkinson, M. A.; Bluestone, J. A.; Eisenbarth, G. S.; Hebrok, M.; Herold, K. C.; Accili, D.; Pietropaolo, M.; Arvan, P. R.; Von Herrath, M.; Markel, D. S.; Rhodes, C. J., How does type 1 diabetes develop?: the notion of homicide or beta-cell suicide revisited. *Diabetes* **2011,** *60* (5), 1370-9.
7. Atkinson, M. A.; Eisenbarth, G. S., Type 1 diabetes: new perspectives on disease pathogenesis and treatment. *The Lancet* **2001,** *358* (9277), 221-229.
8. Atkinson, M. A.; Eisenbarth, G. S.; Michels, A. W., Type 1 diabetes. *The Lancet* **2014,** *383* (9911), 69-82.
9. Vehik, K.; Ajami, N. J.; Hadley, D.; Petrosino, J. F.; Burkhardt, B. R., The changing landscape of type 1 diabetes: recent developments and future frontiers. *Curr Diab Rep* **2013,** *13* (5), 642-50.
10. Skyler, J. S.; Ricordi, C., Stopping type 1 diabetes: attempts to prevent or cure type 1 diabetes in man. *Diabetes* **2011,** *60* (1), 1-8.
11. Miller, K. M.; Foster, N. C.; Beck, R. W.; Bergenstal, R. M.; DuBose, S. N.; DiMeglio, L. A.; Maahs, D. M.; Tamborlane, W. V.; Network, T. D. E. C., Current state of type 1 diabetes treatment in the U.S.: updated data from the T1D Exchange clinic registry. *Diabetes Care* **2015,** *38* (6), 971-8.
12. Ziegler, A. G.; Nepom, G. T., Prediction and pathogenesis in type 1 diabetes. *Immunity* **2010,** *32* (4), 468-78
13. Patterson, C.; Guariguata, L.; Dahlquist, G.; Soltesz, G.; Ogle, G.; Silink, M., Diabetes in the young - a global view and worldwide estimates of numbers of children with type 1 diabetes. *Diabetes Res Clin Pract* **2014,** *103* (2), 161-75.

14. Balderas, C.; Ruperez, F. J.; Ibanez, E.; Senorans, J.; Guerrero-Fernandez, J.; Casado, I. G.; Gracia-Bouthelier, R.; Garcia, A.; Barbas, C., Plasma and urine metabolic fingerprinting of type 1 diabetic children. *Electrophoresis* **2013,** *34* (19), 2882-90.
15. Lebastchi, J.; Herold, K. C., Immunologic and metabolic biomarkers of beta-cell destruction in the diagnosis of type 1 diabetes. *Cold Spring Harb Perspect Med* **2012,** *2* (6), a007708.
16. Daneman, D., Type 1 diabetes. *The Lancet* **2006,** *367* (9513), 847-858.
17. Strimbu, K.; Tavel, J. A., What are biomarkers? *Curr Opin HIV AIDS* **2010,** *5* (6), 463-6.
18. Bonifacio, E., Predicting type 1 diabetes using biomarkers. *Diabetes Care* **2015,** *38* (6), 989-96.
19. Heinonen, M. T.; Moulder, R.; Lahesmaa, R., New Insights and Biomarkers for Type 1 Diabetes: Review for Scandinavian Journal of Immunology. *Scand J Immunol* **2015,** *82* (3), 244-53.
20. Han, X., Lipidomics for precision medicine and metabolism: A personal view. *Biochim Biophys Acta Mol Cell Biol Lipids* **2017,** *1862* (8), 804-807.
21. Zhao, Y. Y.; Cheng, X. L.; Lin, R. C., Lipidomics applications for discovering biomarkers of diseases in clinical chemistry. *Int Rev Cell Mol Biol* **2014,** *313*, 1-26.
22. Oresic, M., Metabolomics in the studies of islet autoimmunity and type 1 diabetes. *Rev Diabet Stud* **2012,** *9* (4), 236-47.
23. Oresic, M.; Gopalacharyulu, P.; Mykkanen, J.; Lietzen, N.; Makinen, M.; Nygren, H.; Simell, S.; Simell, V.; Hyoty, H.; Veijola, R.; Ilonen, J.; Sysi-Aho, M.; Knip, M.; Hyotylainen, T.; Simell, O., Cord serum lipidome in prediction of islet autoimmunity and type 1 diabetes. *Diabetes* **2013,** *62* (9), 3268-74.
24. Pflueger, M.; Seppanen-Laakso, T.; Suortti, T.; Hyotylainen, T.; Achenbach, P.; Bonifacio, E.; Oresic, M.; Ziegler, A. G., Age- and islet autoimmunity-associated differences in amino acid and lipid metabolites in children at risk for type 1 diabetes. *Diabetes* **2011,** *60* (11), 2740-7.
25. Lamichhane, S.; Ahonen, L.; Dyrlund, T. S.; Kemppainen, E.; Siljander, H.; Hyoty, H.; Ilonen, J.; Toppari, J.; Veijola, R.; Hyotylainen, T.; Knip, M.; Oresic, M., Dynamics of Plasma Lipidome in Progression to Islet Autoimmunity and Type 1 Diabetes - Type 1 Diabetes Prediction and Prevention Study (DIPP). *Sci Rep* **2018,** *8* (1), 10635.
26. Sorensen, C. M.; Ding, J.; Zhang, Q.; Alquier, T.; Zhao, R.; Mueller, P. W.; Smith, R. D.; Metz, T. O., Perturbations in the lipid profile of individuals with newly diagnosed type 1 diabetes mellitus: lipidomics analysis of a Diabetes Antibody Standardization Program sample subset. *Clin Biochem* **2010,** *43* (12), 948-56.
27. Oresic, M.; Simell, S.; Sysi-Aho, M.; Nanto-Salonen, K.; Seppanen-Laakso, T.; Parikka, V.; Katajamaa, M.; Hekkala, A.; Mattila, I.; Keskinen, P.; Yetukuri, L.; Reinikainen, A.; Lahde, J.; Suortti, T.; Hakalax, J.; Simell, T.; Hyoty, H.; Veijola, R.; Ilonen, J.; Lahesmaa, R.; Knip, M.; Simell, O., Dysregulation of lipid and amino acid metabolism precedes islet autoimmunity in children who later progress to type 1 diabetes. *J Exp Med* **2008,** *205* (13), 2975-84.

28. Wenk, M. R., The emerging field of lipidomics. *Nat Rev Drug Discov* **2005,** *4* (7), 594-610.
29. Muro, E.; Atilla-Gokcumen, G. E.; Eggert, U. S., Lipids in cell biology: how can we understand them better? *Mol Biol Cell* **2014,** *25* (12), 1819-23.
30. Shevchenko, A.; Simons, K., Lipidomics: coming to grips with lipid diversity. *Nat Rev Mol Cell Biol* **2010,** *11* (8), 593-8.
31. Wymann, M. P.; Schneiter, R., Lipid signalling in disease. *Nat Rev Mol Cell Biol* **2008,** *9* (2), 162-76.
32. Kosicek, M.; Hecimovic, S., Phospholipids and Alzheimer's disease: alterations, mechanisms and potential biomarkers. *Int J Mol Sci* **2013,** *14* (1), 1310-22.
33. Huynh, K.; Martins, R. N.; Meikle, P. J., Lipidomic Profiles in Diabetes and Dementia. *J Alzheimers Dis* **2017,** *59* (2), 433-444.
34. Sutphen, R.; Xu, Y.; Wilbanks, G. D.; Fiorica, J.; Grendys, E. C.; LaPolla, J. P.; Arango, H.; Hoffman, M. S.; Martino, M.; Wakeley, K.; Griffin, D.; Blanco, R. W.; Cantor, A. B.; Xiao, Y.-j.; Krischer, J. P., Lysophospholipids Are Potential Biomarkers of Ovarian Cancer. *Cancer Epidemiology Biomarkers & Prevention* **2004,** *13* (7), 1185.
35. Nam, M.; Choi, M. S.; Jung, S.; Jung, Y.; Choi, J. Y.; Ryu, D. H.; Hwang, G. S., Lipidomic Profiling of Liver Tissue from Obesity-Prone and Obesity-Resistant Mice Fed a High Fat Diet. *Sci Rep* **2015,** *5*, 16984.
36. Yang, L.; Li, M.; Shan, Y.; Shen, S.; Bai, Y.; Liu, H., Recent advances in lipidomics for disease research. *J Sep Sci* **2016,** *39* (1), 38-50.
37. Fahy, E.; Subramaniam, S.; Brown, H. A.; Glass, C. K.; Merrill, A. H.; Murphy, R. C.; Raetz, C. R. H.; Russell, D. W.; Seyama, Y.; Shaw, W.; Shimizu, T.; Spener, F.; van Meer, G.; VanNieuwenhze, M. S.; White, S. H.; Witztum, J. L.; Dennis, E. A., A comprehensive classification system for lipids. *Journal of Lipid Research* **2005,** *46* (5), 839-862.
38. Fahy, E.; Subramaniam, S.; Murphy, R. C.; Nishijima, M.; Raetz, C. R.; Shimizu, T.; Spener, F.; van Meer, G.; Wakelam, M. J.; Dennis, E. A., Update of the LIPID MAPS comprehensive classification system for lipids. *J Lipid Res* **2009,** *50 Suppl*, S9-14.
39. Fahy, E.; Cotter, D.; Sud, M.; Subramaniam, S., Lipid classification, structures and tools. *Biochim Biophys Acta* **2011,** *1811* (11), 637-47.
40. Astarita, G.; Ollero, M., Lipidomics: An Evolving Discipline in Molecular Sciences. *International Journal of Molecular Sciences* **2015,** *16* (12), 7748-7752.
41. Brugger, B., Lipidomics: analysis of the lipid composition of cells and subcellular organelles by electrospray ionization mass spectrometry. *Annu Rev Biochem* **2014,** *83*, 79-98.
42. Gross, R. W.; Han, X., Lipidomics at the interface of structure and function in systems biology. *Chem Biol* **2011,** *18* (3), 284-91.
43. Lam, S. M.; Shui, G., Lipidomics as a principal tool for advancing biomedical research. *J Genet Genomics* **2013,** *40* (8), 375-90.

44. Meikle, P. J.; Wong, G.; Barlow, C. K.; Kingwell, B. A., Lipidomics: potential role in risk prediction and therapeutic monitoring for diabetes and cardiovascular disease. *Pharmacol Ther* **2014,** *143* (1), 12-23.
45. Nguyen, A.; Rudge, S. A.; Zhang, Q.; Wakelam, M. J. O., Using lipidomics analysis to determine signalling and metabolic changes in cells. *Current Opinion in Biotechnology* **2017,** *43*, 96-103.
46. Wenk, M. R., Lipidomics: new tools and applications. *Cell* **2010,** *143* (6), 888-95.
47. Lee, D. Y.; Kind, T.; Yoon, Y. R.; Fiehn, O.; Liu, K. H., Comparative evaluation of extraction methods for simultaneous mass-spectrometric analysis of complex lipids and primary metabolites from human blood plasma. *Anal Bioanal Chem* **2014,** *406* (28), 7275-86.
48. Reis, A.; Rudnitskaya, A.; Blackburn, G. J.; Mohd Fauzi, N.; Pitt, A. R.; Spickett, C. M., A comparison of five lipid extraction solvent systems for lipidomic studies of human LDL. *J Lipid Res* **2013,** *54* (7), 1812-24.
49. Folch, J.; Lees, M.; Sloane Stanley, G. H., A simple method for the isolation and purification of total lipides from animal tissues. *J Biol Chem* **1957,** *226* (1), 497-509.
50. Bligh, E. G.; Dyer, W. J., A rapid method of total lipid extraction and purification. *Can J Biochem Physiol* **1959,** *37* (8), 911-7.
51. Iverson, S. J.; Lang, S. L.; Cooper, M. H., Comparison of the Bligh and Dyer and Folch methods for total lipid determination in a broad range of marine tissue. *Lipids* **2001,** *36* (11), 1283-7.
52. Lofgren, L.; Stahlman, M.; Forsberg, G. B.; Saarinen, S.; Nilsson, R.; Hansson, G. I., The BUME method: a novel automated chloroform-free 96-well total lipid extraction method for blood plasma. *J Lipid Res* **2012,** *53* (8), 1690-700.
53. Matyash, V.; Liebisch, G.; Kurzchalia, T. V.; Shevchenko, A.; Schwudke, D., Lipid extraction by methyl-tert-butyl ether for high-throughput lipidomics. *J Lipid Res* **2008,** *49* (5), 1137-46.
54. Eggers, L. F.; Schwudke, D., Lipid Extraction: Basics of the Methyl-tert-Butyl Ether Extraction. In *Encyclopedia of Lipidomics*, Wenk, M. R., Ed. Springer Netherlands: Dordrecht, 2016; pp 1-3.
55. Lofgren, L.; Forsberg, G. B.; Stahlman, M., The BUME method: a new rapid and simple chloroform-free method for total lipid extraction of animal tissue. *Sci Rep* **2016,** *6*, 27688.
56. Verardo, V.; Gómez-Caravaca, A. M.; Montealegre, C.; Segura-Carretero, A.; Caboni, M. F.; Fernández-Gutiérrez, A.; Bendini, A., Optimization of a solid phase extraction method and hydrophilic interaction liquid chromatography coupled to mass spectrometry for the determination of phospholipids in virgin olive oil. *Food Research International* **2013,** *54* (2), 2083-2090.
57. Cajka, T.; Fiehn, O., Comprehensive analysis of lipids in biological systems by liquid chromatography-mass spectrometry. *Trends Analyt Chem* **2014,** *61*, 192-206.
58. Holcapek, M.; Jirasko, R.; Lisa, M., Recent developments in liquid chromatography-mass spectrometry and related techniques. *J Chromatogr A* **2012,** *1259*, 3-15.

59. Christie, W. W., Rapid separation and quantification of lipid classes by high performance liquid chromatography and mass (light-scattering) detection. *J Lipid Res* **1985,** *26* (4), 507-12.
60. Pham, T. H.; Zaeem, M.; Fillier, T. A.; Nadeem, M.; Vidal, N. P.; Manful, C.; Cheema, S.; Cheema, M.; Thomas, R. H., Targeting Modified Lipids during Routine Lipidomics Analysis using HILIC and C30 Reverse Phase Liquid Chromatography coupled to Mass Spectrometry. *Sci Rep* **2019,** *9* (1), 5048.
61. Abreu, S.; Solgadi, A.; Chaminade, P., Optimization of normal phase chromatographic conditions for lipid analysis and comparison of associated detection techniques. *J Chromatogr A* **2017,** *1514*, 54-71.
62. Christie, W. W., Separation of lipid classes by high-performance liquid chromatography with the "mass detector". *J Chromatogr* **1986,** *361*, 396-9.
63. Narvaez-Rivas, M.; Vu, N.; Chen, G. Y.; Zhang, Q., Off-line mixed-mode liquid chromatography coupled with reversed phase high performance liquid chromatography-high resolution mass spectrometry to improve coverage in lipidomics analysis. *Anal Chim Acta* **2017,** *954*, 140-150.
64. Graeve, M.; Janssen, D., Improved separation and quantification of neutral and polar lipid classes by HPLC-ELSD using a monolithic silica phase: application to exceptional marine lipids. *J Chromatogr B Analyt Technol Biomed Life Sci* **2009,** *877* (20-21), 1815-9.
65. McLaren, D. G.; Miller, P. L.; Lassman, M. E.; Castro-Perez, J. M.; Hubbard, B. K.; Roddy, T. P., An ultraperformance liquid chromatography method for the normal-phase separation of lipids. *Anal Biochem* **2011,** *414* (2), 266-72.
66. Hajek, R.; Jirasko, R.; Lisa, M.; Cifkova, E.; Holcapek, M., Hydrophilic Interaction Liquid Chromatography-Mass Spectrometry Characterization of Gangliosides in Biological Samples. *Anal Chem* **2017,** *89* (22), 12425-12432.
67. Cai, X.; Li, R., Concurrent profiling of polar metabolites and lipids in human plasma using HILIC-FTMS. *Sci Rep* **2016,** *6*, 36490.
68. Narvaez-Rivas, M.; Gallardo, E.; Rios, J. J.; Leon-Camacho, M., A new high-performance liquid chromatographic method with evaporative light scattering detector for the analysis of phospholipids. Application to Iberian pig subcutaneous fat. *J Chromatogr A* **2011,** *1218* (22), 3453-8.
69. Li, J.; Hu, C.; Zhao, X.; Dai, W.; Chen, S.; Lu, X.; Xu, G., Large-scaled human serum sphingolipid profiling by using reversed-phase liquid chromatography coupled with dynamic multiple reaction monitoring of mass spectrometry: method development and application in hepatocellular carcinoma. *J Chromatogr A* **2013,** *1320*, 103-10.
70. Aicheler, F.; Li, J.; Hoene, M.; Lehmann, R.; Xu, G.; Kohlbacher, O., Retention Time Prediction Improves Identification in Nontargeted Lipidomics Approaches. *Analytical Chemistry* **2015,** *87* (15), 7698-7704.
71. Ovcacikova, M.; Lisa, M.; Cifkova, E.; Holcapek, M., Retention behavior of lipids in reversed-phase ultrahigh-performance liquid chromatography-electrospray ionization mass spectrometry. *J Chromatogr A* **2016,** *1450*, 76-85.

72. Nakanishi, H.; Iida, Y.; Shimizu, T.; Taguchi, R., Separation and quantification of sn-1 and sn-2 fatty acid positional isomers in phosphatidylcholine by RPLC-ESIMS/MS. *J Biochem* **2010,** *147* (2), 245-56.
73. Narvaez-Rivas, M.; Zhang, Q., Comprehensive untargeted lipidomic analysis using core-shell C30 particle column and high field orbitrap mass spectrometer. *J Chromatogr A* **2016,** *1440*, 123-134.
74. Weir, J. M.; Wong, G.; Barlow, C. K.; Greeve, M. A.; Kowalczyk, A.; Almasy, L.; Comuzzie, A. G.; Mahaney, M. C.; Jowett, J. B.; Shaw, J.; Curran, J. E.; Blangero, J.; Meikle, P. J., Plasma lipid profiling in a large population-based cohort. *J Lipid Res* **2013,** *54* (10), 2898-908.
75. Lamichhane, S.; Ahonen, L.; Dyrlund, T. S.; Siljander, H.; Hyoty, H.; Ilonen, J.; Toppari, J.; Veijola, R.; Hyotylainen, T.; Knip, M.; Oresic, M., A longitudinal plasma lipidomics dataset from children who developed islet autoimmunity and type 1 diabetes. *Sci Data* **2018,** *5*, 180250.
76. Nie, H.; Liu, R.; Yang, Y.; Bai, Y.; Guan, Y.; Qian, D.; Wang, T.; Liu, H., Lipid profiling of rat peritoneal surface layers by online normal- and reversed-phase 2D LC QToF-MS. *J Lipid Res* **2010,** *51* (9), 2833-44.
77. Nzoughet, J. K.; Gallart-Ayala, H.; Biancotto, G.; Hennig, K.; Dervilly-Pinel, G.; Le Bizec, B., Hydrophilic interaction (HILIC) and reverse phase liquid chromatography (RPLC)–high resolution MS for characterizing lipids profile disruption in serum of anabolic implanted bovines. *Metabolomics* **2015,** *11* (6), 1884-1895.
78. Houjou, T.; Yamatani, K.; Imagawa, M.; Shimizu, T.; Taguchi, R., A shotgun tandem mass spectrometric analysis of phospholipids with normal-phase and/or reverse-phase liquid chromatography/electrospray ionization mass spectrometry. *Rapid Commun Mass Spectrom* **2005,** *19* (5), 654-66.
79. Ling, Y. S.; Liang, H. J.; Lin, M. H.; Tang, C. H.; Wu, K. Y.; Kuo, M. L.; Lin, C. Y., Two-dimensional LC-MS/MS to enhance ceramide and phosphatidylcholine species profiling in mouse liver. *Biomed Chromatogr* **2014,** *28* (9), 1284-93.
80. Rampler, E.; Criscuolo, A.; Zeller, M.; El Abiead, Y.; Schoeny, H.; Hermann, G.; Sokol, E.; Cook, K.; Peake, D. A.; Delanghe, B.; Koellensperger, G., A Novel Lipidomics Workflow for Improved Human Plasma Identification and Quantification Using RPLC-MSn Methods and Isotope Dilution Strategies. *Anal Chem* **2018,** *90* (11), 6494-6501.
81. Sandra, K.; Pereira Ados, S.; Vanhoenacker, G.; David, F.; Sandra, P., Comprehensive blood plasma lipidomics by liquid chromatography/quadrupole time-of-flight mass spectrometry. *J Chromatogr A* **2010,** *1217* (25), 4087-99.
82. Jensen, N. J.; Tomer, K. B.; Gross, M. L., FAB MS/MS for phosphatidylinositol, -glycerol, -ethanolamine and other complex phospholipids. *Lipids* **1987,** *22* (7), 480-9.
83. Han, X.; Gross, R. W., Electrospray ionization mass spectroscopic analysis of human erythrocyte plasma membrane phospholipids. *Proc Natl Acad Sci U S A* **1994,** *91* (22), 10635-9.
84. Fenn, J. B.; Mann, M.; Meng, C. K.; Wong, S. F.; Whitehouse, C. M., Electrospray ionization for mass spectrometry of large biomolecules. *Science* **1989,** *246* (4926), 64-71.

85. Han, X.; Gross, R. W., Global analyses of cellular lipidomes directly from crude extracts of biological samples by ESI mass spectrometry: a bridge to lipidomics. *J Lipid Res* **2003,** *44* (6), 1071-9.
86. Berry, K. A.; Hankin, J. A.; Barkley, R. M.; Spraggins, J. M.; Caprioli, R. M.; Murphy, R. C., MALDI imaging of lipid biochemistry in tissues by mass spectrometry. *Chem Rev* **2011,** *111* (10), 6491-512.
87. Fuchs, B.; Suss, R.; Schiller, J., An update of MALDI-TOF mass spectrometry in lipid research. *Prog Lipid Res* **2010,** *49* (4), 450-75.
88. Murphy, R. C.; Hankin, J. A.; Barkley, R. M., Imaging of lipid species by MALDI mass spectrometry. *J Lipid Res* **2009,** *50 Suppl*, S317-22.
89. Tanaka, K.; Yamada, M.; Tamiya-Koizumi, K.; Kannagi, R.; Aoyama, T.; Hara, A.; Kyogashima, M., Systematic analyses of free ceramide species and ceramide species comprising neutral glycosphingolipids by MALDI-TOF MS with high-energy CID. *Glycoconjugate Journal* **2011,** *28* (2), 67-87.
90. Petkovic, M.; Schiller, J.; Muller, J.; Muller, M.; Arnold, K.; Arnhold, J., The signal-to-noise ratio as the measure for the quantification of lysophospholipids by matrix-assisted laser desorption/ionisation time-of-flight mass spectrometry. *Analyst* **2001,** *126* (7), 1042-50.
91. Vrkoslav, V.; Mikova, R.; Cvacka, J., Characterization of natural wax esters by MALDI-TOF mass spectrometry. *J Mass Spectrom* **2009,** *44* (1), 101-10.
92. Dawson, G., Measuring brain lipids. *Biochim Biophys Acta* **2015,** *1851* (8), 1026-39.
93. O'Rourke, M. B.; Smith, C. C.; De La Monte, S. M.; Sutherland, G. T.; Padula, M. P., Higher Mass Accuracy MALDI-TOF/TOF Lipid Imaging of Human Brain Tissue in Alzheimer's Disease. *Curr Protoc Mol Biol* **2019,** *126* (1), e86.
94. Hong, J. H.; Kang, J. W.; Kim, D. K.; Baik, S. H.; Kim, K. H.; Shanta, S. R.; Jung, J. H.; Mook-Jung, I.; Kim, K. P., Global changes of phospholipids identified by MALDI imaging mass spectrometry in a mouse model of Alzheimer's disease. *J Lipid Res* **2016,** *57* (1), 36-45.
95. Petkovic, M.; Schiller, J.; Muller, M.; Benard, S.; Reichl, S.; Arnold, K.; Arnhold, J., Detection of individual phospholipids in lipid mixtures by matrix-assisted laser desorption/ionization time-of-flight mass spectrometry: phosphatidylcholine prevents the detection of further species. *Anal Biochem* **2001,** *289* (2), 202-16.
96. Fuchs, B.; Schiller, J., Application of MALDI-TOF mass spectrometry in lipidomics. *European Journal of Lipid Science and Technology* **2009,** *111* (1), 83-98.
97. Han, X.; Gross, R. W., Shotgun lipidomics: electrospray ionization mass spectrometric analysis and quantitation of cellular lipidomes directly from crude extracts of biological samples. *Mass Spectrom Rev* **2005,** *24* (3), 367-412.
98. Cui, Z.; Thomas, M. J., Phospholipid profiling by tandem mass spectrometry. *J Chromatogr B Analyt Technol Biomed Life Sci* **2009,** *877* (26), 2709-15.
99. Han, X.; Gross, R. W., Quantitative analysis and molecular species fingerprinting of triacylglyceride molecular species directly from lipid extracts of biological samples by electrospray ionization tandem mass spectrometry. *Anal Biochem* **2001,** *295* (1), 88-100.

100. Hsu, F.-F.; Turk, J., Electrospray ionization/tandem quadrupole mass spectrometric studies on phosphatidylcholines: The fragmentation processes. *Journal of the American Society for Mass Spectrometry* **2003,** *14* (4), 352-363.
101. Merrill, A. H., Jr.; Sullards, M. C.; Allegood, J. C.; Kelly, S.; Wang, E., Sphingolipidomics: high-throughput, structure-specific, and quantitative analysis of sphingolipids by liquid chromatography tandem mass spectrometry. *Methods* **2005,** *36* (2), 207-24.
102. Zehethofer, N.; Pinto, D. M., Recent developments in tandem mass spectrometry for lipidomic analysis. *Analytica Chimica Acta* **2008,** *627* (1), 62-70.
103. Zemski Berry, K. A.; Murphy, R. C., Electrospray ionization tandem mass spectrometry of glycerophosphoethanolamine plasmalogen phospholipids. *J Am Soc Mass Spectrom* **2004,** *15* (10), 1499-508.
104. Hsu, F. F.; Turk, J., Structural characterization of unsaturated glycerophospholipids by multiple-stage linear ion-trap mass spectrometry with electrospray ionization. *J Am Soc Mass Spectrom* **2008,** *19* (11), 1681-91.
105. Hsu, F. F.; Turk, J., Electrospray ionization with low-energy collisionally activated dissociation tandem mass spectrometry of glycerophospholipids: mechanisms of fragmentation and structural characterization. *J Chromatogr B Analyt Technol Biomed Life Sci* **2009,** *877* (26), 2673-95.
106. Hsu, F. F.; Turk, J., Electrospray ionization multiple-stage linear ion-trap mass spectrometry for structural elucidation of triacylglycerols: assignment of fatty acyl groups on the glycerol backbone and location of double bonds. *J Am Soc Mass Spectrom* **2010,** *21* (4), 657-69.
107. Hsu, F. F.; Turk, J.; Thukkani, A. K.; Messner, M. C.; Wildsmith, K. R.; Ford, D. A., Characterization of alkylacyl, alk-1-enylacyl and lyso subclasses of glycerophosphocholine by tandem quadrupole mass spectrometry with electrospray ionization. *J Mass Spectrom* **2003,** *38* (7), 752-63.
108. Ma, X.; Xia, Y., Pinpointing Double Bonds in Lipids by Paternò-Büchi Reactions and Mass Spectrometry. *Angewandte Chemie International Edition* **2014,** *53* (10), 2592-2596.
109. Feng, Y.; Chen, B.; Yu, Q.; Li, L., Identification of Double Bond Position Isomers in Unsaturated Lipids by m-CPBA Epoxidation and Mass Spectrometry Fragmentation. *Anal Chem* **2019,** *91* (3), 1791-1795.
110. Harrison, K. A.; Murphy, R. C., Direct mass spectrometric analysis of ozonides: application to unsaturated glycerophosphocholine lipids. *Anal Chem* **1996,** *68* (18), 3224-30.
111. Thomas, M. C.; Mitchell, T. W.; Blanksby, S. J., Ozonolysis of phospholipid double bonds during electrospray ionization: a new tool for structure determination. *J Am Chem Soc* **2006,** *128* (1), 58-9.
112. Thomas, M. C.; Mitchell, T. W.; Harman, D. G.; Deeley, J. M.; Murphy, R. C.; Blanksby, S. J., Elucidation of double bond position in unsaturated lipids by ozone electrospray ionization mass spectrometry. *Anal Chem* **2007,** *79* (13), 5013-22.
113. Criegee, R., Mechanism of Ozonolysis. *Angewandte Chemie International Edition in English* **1975,** *14* (11), 745-752.

114. Thomas, M. C.; Mitchell, T. W.; Harman, D. G.; Deeley, J. M.; Nealon, J. R.; Blanksby, S. J., Ozone-induced dissociation: elucidation of double bond position within mass-selected lipid ions. *Anal Chem* **2008,** *80* (1), 303-11.
115. Batarseh, A. M.; Abbott, S. K.; Duchoslav, E.; Alqarni, A.; Blanksby, S. J.; Mitchell, T. W., Discrimination of isobaric and isomeric lipids in complex mixtures by combining ultra-high pressure liquid chromatography with collision and ozone-induced dissociation. *International Journal of Mass Spectrometry* **2018,** *431*, 27-36.
116. Kozlowski, R. L.; Mitchell, T. W.; Blanksby, S. J., A rapid ambient ionization-mass spectrometry approach to monitoring the relative abundance of isomeric glycerophospholipids. *Sci Rep* **2015,** *5*, 9243.
117. Maccarone, A. T.; Duldig, J.; Mitchell, T. W.; Blanksby, S. J.; Duchoslav, E.; Campbell, J. L., Characterization of acyl chain position in unsaturated phosphatidylcholines using differential mobility-mass spectrometry. *J Lipid Res* **2014,** *55* (8), 1668-77.
118. Barrientos, R. C.; Vu, N.; Zhang, Q., Structural Analysis of Unsaturated Glycosphingolipids Using Shotgun Ozone-Induced Dissociation Mass Spectrometry. *Journal of The American Society for Mass Spectrometry* **2017,** *28* (11), 2330-2343.
119. Vu, N.; Brown, J.; Giles, K.; Zhang, Q., Ozone-induced dissociation on a traveling wave high-resolution mass spectrometer for determination of double-bond position in lipids. *Rapid Communications in Mass Spectrometry* **2017,** *31* (17), 1415-1423.
120. Blanksby, S. J.; Mitchell, T. W., Advances in mass spectrometry for lipidomics. *Annu Rev Anal Chem (Palo Alto Calif)* **2010,** *3*, 433-65.
121. Brown, S. H.; Mitchell, T. W.; Blanksby, S. J., Analysis of unsaturated lipids by ozone-induced dissociation. *Biochim Biophys Acta* **2011,** *1811* (11), 807-17.
122. Ellis, S. R.; Wu, C.; Deeley, J. M.; Zhu, X.; Truscott, R. J.; in het Panhuis, M.; Cooks, R. G.; Mitchell, T. W.; Blanksby, S. J., Imaging of human lens lipids by desorption electrospray ionization mass spectrometry. *J Am Soc Mass Spectrom* **2010,** *21* (12), 2095-104.
123. Kozlowski, R. L.; Campbell, J. L.; Mitchell, T. W.; Blanksby, S. J., Combining liquid chromatography with ozone-induced dissociation for the separation and identification of phosphatidylcholine double bond isomers. *Anal Bioanal Chem* **2015,** *407* (17), 5053-64.
124. Marshall, D. L.; Pham, H. T.; Bhujel, M.; Chin, J. S.; Yew, J. Y.; Mori, K.; Mitchell, T. W.; Blanksby, S. J., Sequential Collision- and Ozone-Induced Dissociation Enables Assignment of Relative Acyl Chain Position in Triacylglycerols. *Anal Chem* **2016,** *88* (5), 2685-92.
125. Poad, B. L. J.; Zheng, X.; Mitchell, T. W.; Smith, R. D.; Baker, E. S.; Blanksby, S. J., Online Ozonolysis Combined with Ion Mobility-Mass Spectrometry Provides a New Platform for Lipid Isomer Analyses. *Anal Chem* **2018,** *90* (2), 1292-1300.
126. Poad, B. L.; Pham, H. T.; Thomas, M. C.; Nealon, J. R.; Campbell, J. L.; Mitchell, T. W.; Blanksby, S. J., Ozone-induced dissociation on a modified tandem linear

ion-trap: observations of different reactivity for isomeric lipids. *J Am Soc Mass Spectrom* **2010,** *21* (12), 1989-99.
127. Nguyen, A.; Rudge, S. A.; Zhang, Q.; Wakelam, M. J. O., Using lipidomics analysis to determine signalling and metabolic changes in cells. *Curr Opin Biotechnol* **2017,** *43*, 96-103.
128. Li, X.; Xu, Z.; Lu, X.; Yang, X.; Yin, P.; Kong, H.; Yu, Y.; Xu, G., Comprehensive two-dimensional gas chromatography/time-of-flight mass spectrometry for metabonomics: Biomarker discovery for diabetes mellitus. *Anal Chim Acta* **2009,** *633* (2), 257-62.
129. Zarrouk, A.; Debbabi, M.; Bezine, M.; Karym, E. M.; Badreddine, A.; Rouaud, O.; Moreau, T.; Cherkaoui-Malki, M.; El Ayeb, M.; Nasser, B. J. C. A. R., Lipid Biomarkers in Alzheimer's Disease. *Curr Alzheimer Res* **2018,** *15* (4), 303-312.
130. Fox, T. E.; Bewley, M. C.; Unrath, K. A.; Pedersen, M. M.; Anderson, R. E.; Jung, D. Y.; Jefferson, L. S.; Kim, J. K.; Bronson, S. K.; Flanagan, J. M.; Kester, M., Circulating sphingolipid biomarkers in models of type 1 diabetes. *J Lipid Res* **2011,** *52* (3), 509-517.
131. Luppa, P. B.; Bietenbeck, A.; Beaudoin, C.; Giannetti, A., Clinically relevant analytical techniques, organizational concepts for application and future perspectives of point-of-care testing. *Biotechnology Advances* **2016,** *34* (3), 139-160.
132. Cajka, T.; Fiehn, O., Increasing lipidomic coverage by selecting optimal mobile-phase modifiers in LC–MS of blood plasma. *Metabolomics* **2016,** *12* (2).
133. Gao, X.; Zhang, Q.; Meng, D.; Isaac, G.; Zhao, R.; Fillmore, T. L.; Chu, R. K.; Zhou, J.; Tang, K.; Hu, Z.; Moore, R. J.; Smith, R. D.; Katze, M. G.; Metz, T. O., A reversed-phase capillary ultra-performance liquid chromatography-mass spectrometry (UPLC-MS) method for comprehensive top-down/bottom-up lipid profiling. *Anal Bioanal Chem* **2012,** *402* (9), 2923-33.
134. Kind, T.; Liu, K. H.; Lee, D. Y.; DeFelice, B.; Meissen, J. K.; Fiehn, O., LipidBlast in silico tandem mass spectrometry database for lipid identification. *Nat Methods* **2013,** *10* (8), 755-8.
135. Taguchi, R.; Ishikawa, M., Precise and global identification of phospholipid molecular species by an Orbitrap mass spectrometer and automated search engine Lipid Search. *J Chromatogr A* **2010,** *1217* (25), 4229-39.
136. Meng, D.; Zhang, Q.; Gao, X.; Wu, S.; Lin, G., LipidMiner: a software for automated identification and quantification of lipids from multiple liquid chromatography/mass spectrometry data files. *Rapid Commun Mass Spectrom* **2014,** *28* (8), 981-5.
137. Pluskal, T.; Castillo, S.; Villar-Briones, A.; Oresic, M., MZmine 2: modular framework for processing, visualizing, and analyzing mass spectrometry-based molecular profile data. *BMC Bioinformatics* **2010,** *11*, 395.
138. Conrads, T. P.; Anderson, G. A.; Veenstra, T. D.; Paša-Tolić, L.; Smith, R. D., Utility of Accurate Mass Tags for Proteome-Wide Protein Identification. *Analytical Chemistry* **2000,** *72* (14), 3349-3354.

139. Zimmer, J. S.; Monroe, M. E.; Qian, W. J.; Smith, R. D., Advances in proteomics data analysis and display using an accurate mass and time tag approach. *Mass Spectrom Rev* **2006,** *25* (3), 450-82.
140. Creek, D. J.; Jankevics, A.; Breitling, R.; Watson, D. G.; Barrett, M. P.; Burgess, K. E., Toward global metabolomics analysis with hydrophilic interaction liquid chromatography-mass spectrometry: improved metabolite identification by retention time prediction. *Anal Chem* **2011,** *83* (22), 8703-10.
141. Ding, J.; Sorensen, C. M.; Jaitly, N.; Jiang, H.; Orton, D. J.; Monroe, M. E.; Moore, R. J.; Smith, R. D.; Metz, T. O., Application of the accurate mass and time tag approach in studies of the human blood lipidome. *J Chromatogr B Analyt Technol Biomed Life Sci* **2008,** *871* (2), 243-52.
142. Rewers, M.; Bugawan, T. L.; Norris, J. M.; Blair, A.; Beaty, B.; Hoffman, M.; McDuffie, R. S., Jr.; Hamman, R. F.; Klingensmith, G.; Eisenbarth, G. S.; Erlich, H. A., Newborn screening for HLA markers associated with IDDM: diabetes autoimmunity study in the young (DAISY). *Diabetologia* **1996,** *39* (7), 807-12.
143. Norris, J. M.; Yin, X.; Lamb, M. M.; Barriga, K.; Seifert, J.; Hoffman, M.; Orton, H. D.; Baron, A. E.; Clare-Salzler, M.; Chase, H. P.; Szabo, N. J.; Erlich, H.; Eisenbarth, G. S.; Rewers, M., Omega-3 polyunsaturated fatty acid intake and islet autoimmunity in children at increased risk for type 1 diabetes. *JAMA* **2007,** *298* (12), 1420-8.
144. Wozny, K.; Lehmann, W. D.; Wozny, M.; Akbulut, B. S.; Brugger, B., A method for the quantitative determination of glycerophospholipid regioisomers by UPLC-ESI-MS/MS. *Anal Bioanal Chem* **2019,** *411* (4), 915-924.
145. Larsen, A.; Uran, S.; Jacobsen, P. B.; Skotland, T., Collision-induced dissociation of glycero phospholipids using electrospray ion-trap mass spectrometry. *Rapid Commun Mass Spectrom* **2001,** *15* (24), 2393-8.
146. Hvattum, E.; Hagelin, G.; Larsen, A., Study of mechanisms involved in the collision-induced dissociation of carboxylate anions from glycerophospholipids using negative ion electrospray tandem quadrupole mass spectrometry. *Rapid Commun Mass Spectrom* **1998,** *12* (19), 1405-9.
147. Pi, J.; Wu, X.; Feng, Y., Fragmentation patterns of five types of phospholipids by ultra-high-performance liquid chromatography electrospray ionization quadrupole time-of-flight tandem mass spectrometry. *Anal Methods* **2016,** *8* (6), 1319-1332.
148. Han, X.; Yang, K.; Gross, R. W., Multi-dimensional mass spectrometry-based shotgun lipidomics and novel strategies for lipidomic analyses. *Mass Spectrom Rev* **2012,** *31* (1), 134-78.
149. Holčapek, M.; Liebisch, G.; Ekroos, K., Lipidomic Analysis. *Anal Chem* **2018,** *90* (7), 4249-4257.
150. Liebisch, G.; Vizcaino, J. A.; Kofeler, H.; Trotzmuller, M.; Griffiths, W. J.; Schmitz, G.; Spener, F.; Wakelam, M. J., Shorthand notation for lipid structures derived from mass spectrometry. *J Lipid Res* **2013,** *54* (6), 1523-30.
151. Nakagawa, Y.; Horrocks, L. A. J. J. o. l. r., Separation of alkenylacyl, alkylacyl, and diacyl analogues and their molecular species by high performance liquid chromatography. *J Lipid Res* **1983,** *24* (9), 1268-1275.

152. Smith, P. B.; Snyder, A. P.; Harden, C. S., Characterization of bacterial phospholipids by electrospray ionization tandem mass spectrometry. *Anal Chem* **1995,** *67* (11), 1824-30.
153. Han, X.; Gross, R. W., Structural determination of picomole amounts of phospholipids via electrospray ionization tandem mass spectrometry. *J Am Soc Mass Spectrom* **1995,** *6* (12), 1202-1210.
154. Bird, S. S.; Marur, V. R.; Sniatynski, M. J.; Greenberg, H. K.; Kristal, B. S., Serum lipidomics profiling using LC-MS and high-energy collisional dissociation fragmentation: focus on triglyceride detection and characterization. *Anal Chem* **2011,** *83* (17), 6648-57.
155. Quehenberger, O.; Dennis, E. A., The human plasma lipidome. *N Engl J Med* **2011,** *365* (19), 1812-23.
156. Quehenberger, O.; Armando, A. M.; Brown, A. H.; Milne, S. B.; Myers, D. S.; Merrill, A. H.; Bandyopadhyay, S.; Jones, K. N.; Kelly, S.; Shaner, R. L.; Sullards, C. M.; Wang, E.; Murphy, R. C.; Barkley, R. M.; Leiker, T. J.; Raetz, C. R.; Guan, Z.; Laird, G. M.; Six, D. A.; Russell, D. W.; McDonald, J. G.; Subramaniam, S.; Fahy, E.; Dennis, E. A., Lipidomics reveals a remarkable diversity of lipids in human plasma. *J Lipid Res* **2010,** *51* (11), 3299-305.
157. Zhou, X.; Mao, J.; Ai, J.; Deng, Y.; Roth, M. R.; Pound, C.; Henegar, J.; Welti, R.; Bigler, S. A., Identification of plasma lipid biomarkers for prostate cancer by lipidomics and bioinformatics. *PLoS One* **2012,** *7* (11), e48889.
158. Liebisch, G.; Binder, M.; Schifferer, R.; Langmann, T.; Schulz, B.; Schmitz, G., High throughput quantification of cholesterol and cholesteryl ester by electrospray ionization tandem mass spectrometry (ESI-MS/MS). *Biochim Biophys Acta* **2006,** *1761* (1), 121-8.
159. Murphy, R. C.; Axelsen, P. H., Mass spectrometric analysis of long-chain lipids. *Mass Spectrom Rev* **2011,** *30* (4), 579-99.
160. Oresic, M.; Hanninen, V. A.; Vidal-Puig, A., Lipidomics: a new window to biomedical frontiers. *Trends Biotechnol* **2008,** *26* (12), 647-52.
161. Watson, A. D., Thematic review series: systems biology approaches to metabolic and cardiovascular disorders. Lipidomics: a global approach to lipid analysis in biological systems. *J Lipid Res* **2006,** *47* (10), 2101-11.
162. Brown, H. A.; Murphy, R. C., Working towards an exegesis for lipids in biology. *Nat Chem Biol* **2009,** *5* (9), 602-6.
163. Wang, M.; Wang, C.; Han, R. H.; Han, X., Novel advances in shotgun lipidomics for biology and medicine. *Prog Lipid Res* **2016,** *61*, 83-108.
164. Perillo, V. L.; Fernandez-Nievas, G. A.; Valles, A. S.; Barrantes, F. J.; Antollini, S. S., The position of the double bond in monounsaturated free fatty acids is essential for the inhibition of the nicotinic acetylcholine receptor. *Biochim Biophys Acta* **2012,** *1818* (11), 2511-20.
165. Bordoni, A.; Lopez-Jimenez, J. A.; Spano, C.; Biagi, P.; Horrobin, D. F.; Hrelia, S., Metabolism of linoleic and alpha-linolenic acids in cultured cardiomyocytes: effect of different N-6 and N-3 fatty acid supplementation. *Mol Cell Biochem* **1996,** *157* (1-2), 217-22.

166. Wang, C.; Wang, M.; Han, X., Applications of mass spectrometry for cellular lipid analysis. *Mol Biosyst* **2015,** *11* (3), 698-713.
167. Knittelfelder, O. L.; Weberhofer, B. P.; Eichmann, T. O.; Kohlwein, S. D.; Rechberger, G. N., A versatile ultra-high performance LC-MS method for lipid profiling. *J Chromatogr B Analyt Technol Biomed Life Sci* **2014,** *951-952*, 119-28.
168. Yang, K.; Cheng, H.; Gross, R. W.; Han, X., Automated lipid identification and quantification by multidimensional mass spectrometry-based shotgun lipidomics. *Anal Chem* **2009,** *81* (11), 4356-68.
169. Jensen, N.; Gross, M., A comparison of mass spectrometry methods for structural determination analysis of phospholipids. *Mass Spectrometry Reviews* **1988,** *1988* (7), 41-69.
170. Mitchell, T. W.; Pham, H.; Thomas, M. C.; Blanksby, S. J., Identification of double bond position in lipids: from GC to OzID. *J Chromatogr B Analyt Technol Biomed Life Sci* **2009,** *877* (26), 2722-35.
171. Yang, K.; Zhao, Z.; Gross, R. W.; Han, X., Systematic analysis of choline-containing phospholipids using multi-dimensional mass spectrometry-based shotgun lipidomics. *J Chromatogr B Analyt Technol Biomed Life Sci* **2009,** *877* (26), 2924-36.
172. Hsu, F. F.; Bohrer, A.; Turk, J., Formation of lithiated adducts of glycerophosphocholine lipids facilitates their identification by electrospray ionization tandem mass spectrometry. *J Am Soc Mass Spectrom* **1998,** *9* (5), 516-26.
173. Hsu, F. F.; Turk, J., Structural characterization of triacylglycerols as lithiated adducts by electrospray ionization mass spectrometry using low-energy collisionally activated dissociation on a triple stage quadrupole instrument. *J Am Soc Mass Spectrom* **1999,** *10* (7), 587-99.
174. Han, X., *Lipidomics: Comprehensive Mass Spectrometry of Lipids*. John Wiley & Sons: 2016.
175. Hsu, F. F.; Kuhlmann, F. M.; Turk, J.; Beverley, S. M., Multiple-stage linear ion-trap with high resolution mass spectrometry towards complete structural characterization of phosphatidylethanolamines containing cyclopropane fatty acyl chain in Leishmania infantum. *J Mass Spectrom* **2014,** *49* (3), 201-9.
176. Yan, Y.; Ubukata, M.; Cody, R. B.; Holy, T. E.; Gross, M. L., High-energy collision-induced dissociation by MALDI TOF/TOF causes charge-remote fragmentation of steroid sulfates. *J Am Soc Mass Spectrom* **2014,** *25* (8), 1404-11.
177. Pittenauer, E.; Allmaier, G., The renaissance of high-energy CID for structural elucidation of complex lipids: MALDI-TOF/RTOF-MS of alkali cationized triacylglycerols. *J Am Soc Mass Spectrom* **2009,** *20* (6), 1037-47.
178. Griffiths, W. J., Tandem mass spectrometry in the study of fatty acids, bile acids, and steroids. *Mass Spectrom Rev* **2003,** *22* (2), 81-152.
179. Ma, X.; Chong, L.; Tian, R.; Shi, R.; Hu, T. Y.; Ouyang, Z.; Xia, Y., Identification and quantitation of lipid C=C location isomers: A shotgun lipidomics approach enabled by photochemical reaction. *Proc Natl Acad Sci U S A* **2016,** *113* (10), 2573-8.
180. Ma, X.; Xia, Y., Pinpointing Double Bonds in Lipids by Paternò-Büchi Reactions and Mass Spectrometry. *Angewandte Chemie* **2014,** *126* (10), 2630-2634.

181. Deng, L.; Ibrahim, Y. M.; Baker, E. S.; Aly, N. A.; Hamid, A. M.; Zhang, X.; Zheng, X.; Garimella, S. V. B.; Webb, I. K.; Prost, S. A.; Sandoval, J. A.; Norheim, R. V.; Anderson, G. A.; Tolmachev, A. V.; Smith, R. D., Ion Mobility Separations of Isomers based upon Long Path Length Structures for Lossless Ion Manipulations Combined with Mass Spectrometry. *ChemistrySelect* **2016,** *1* (10), 2396-2399.
182. Stinson, C. A.; Xia, Y., A method of coupling the Paterno-Buchi reaction with direct infusion ESI-MS/MS for locating the C[double bond, length as m-dash]C bond in glycerophospholipids. *Analyst* **2016,** *141* (12), 3696-704.
183. Klein, D. R.; Brodbelt, J. S., Structural Characterization of Phosphatidylcholines Using 193 nm Ultraviolet Photodissociation Mass Spectrometry. *Anal Chem* **2017,** *89* (3), 1516-1522.
184. Pham, H. T.; Maccarone, A. T.; Thomas, M. C.; Campbell, J. L.; Mitchell, T. W.; Blanksby, S. J., Structural characterization of glycerophospholipids by combinations of ozone- and collision-induced dissociation mass spectrometry: the next step towards "top-down" lipidomics. *Analyst* **2014,** *139* (1), 204-14.
185. Giles, K.; Williams, J. P.; Campuzano, I., Enhancements in travelling wave ion mobility resolution. *Rapid Commun Mass Spectrom* **2011,** *25* (11), 1559-66.
186. Giles, K.; Pringle, S. D.; Worthington, K. R.; Little, D.; Wildgoose, J. L.; Bateman, R. H., Applications of a travelling wave-based radio-frequency-only stacked ring ion guide. *Rapid Commun Mass Spectrom* **2004,** *18* (20), 2401-14.
187. Pringle, S. D.; Giles, K.; Wildgoose, J. L.; Williams, J. P.; Slade, S. E.; Thalassinos, K.; Bateman, R. H.; Bowers, M. T.; Scrivens, J. H., An investigation of the mobility separation of some peptide and protein ions using a new hybrid quadrupole/travelling wave IMS/oa-ToF instrument. *International Journal of Mass Spectrometry* **2007,** *261* (1), 1-12.
188. Pham, H. T.; Maccarone, A. T.; Campbell, J. L.; Mitchell, T. W.; Blanksby, S. J., Ozone-induced dissociation of conjugated lipids reveals significant reaction rate enhancements and characteristic odd-electron product ions. *J Am Soc Mass Spectrom* **2013,** *24* (2), 286-96.
189. Martinez, R. I.; Herron, J. T., Stopped-flow studies of the mechanisms of ozone-alkene reactions in the gas phase: trans-2-butene. *J. Phys. Chem.* **1988,** *92* (16), 4644-4648.
190. Mason, S. A.; Arey, J.; Atkinson, R., Rate constants for the gas-phase reactions of NO3 radicals and O3 with C6-C14 1-alkenes and 2-methyl-1-alkenes at 296 +/- 2 K. *J Phys Chem A* **2009,** *113* (19), 5649-56.
191. Poad, B. L.; Green, M. R.; Kirk, J. M.; Tomczyk, N.; Mitchell, T. W.; Blanksby, S. J., High-Pressure Ozone-Induced Dissociation for Lipid Structure Elucidation on Fast Chromatographic Timescales. *Anal Chem* **2017,** *89* (7), 4223-4229.
192. Lains, I.; Kelly, R. S.; Miller, J. B.; Silva, R.; Vavvas, D. G.; Kim, I. K.; Murta, J. N.; Lasky-Su, J.; Miller, J. W.; Husain, D., Human Plasma Metabolomics Study across All Stages of Age-Related Macular Degeneration Identifies Potential Lipid Biomarkers. *Ophthalmology* **2018,** *125* (2), 245-254.
193. Burla, B.; Arita, M.; Arita, M.; Bendt, A. K.; Cazenave-Gassiot, A.; Dennis, E. A.; Ekroos, K.; Han, X.; Ikeda, K.; Liebisch, G.; Lin, M. K.; Loh, T. P.; Meikle, P.

J.; Oresic, M.; Quehenberger, O.; Shevchenko, A.; Torta, F.; Wakelam, M. J. O.; Wheelock, C. E.; Wenk, M. R., MS-based lipidomics of human blood plasma: a community-initiated position paper to develop accepted guidelines. *J Lipid Res* **2018,** *59* (10), 2001-2017.
194. Fernandis, A. Z.; Wenk, M. R., Lipid-based biomarkers for cancer. *J Chromatogr B Analyt Technol Biomed Life Sci* **2009,** *877* (26), 2830-5.
195. Razquin, C.; Toledo, E.; Clish, C. B.; Ruiz-Canela, M.; Dennis, C.; Corella, D.; Papandreou, C.; Ros, E.; Estruch, R.; Guasch-Ferre, M.; Gomez-Gracia, E.; Fito, M.; Yu, E.; Lapetra, J.; Wang, D.; Romaguera, D.; Liang, L.; Alonso-Gomez, A.; Deik, A.; Bullo, M.; Serra-Majem, L.; Salas-Salvado, J.; Hu, F. B.; Martinez-Gonzalez, M. A., Plasma Lipidomic Profiling and Risk of Type 2 Diabetes in the PREDIMED Trial. *Diabetes Care* **2018,** *41* (12), 2617-2624.
196. Nishimukai, M.; Maeba, R.; Yamazaki, Y.; Nezu, T.; Sakurai, T.; Takahashi, Y.; Hui, S. P.; Chiba, H.; Okazaki, T.; Hara, H., Serum choline plasmalogens, particularly those with oleic acid in sn-2, are associated with proatherogenic state. *J Lipid Res* **2014,** *55* (5), 956-65.
197. Anderson, N. L.; Anderson, N. G., The Human Plasma Proteome. *Molecular & Cellular Proteomics* **2002,** *1* (11), 845-867.
198. Williams, P. E.; Klein, D. R.; Greer, S. M.; Brodbelt, J. S., Pinpointing Double Bond and sn-Positions in Glycerophospholipids via Hybrid 193 nm Ultraviolet Photodissociation (UVPD) Mass Spectrometry. *J Am Chem Soc* **2017,** *139* (44), 15681-15690.
199. Baba, T.; Campbell, J. L.; Le Blanc, J. C. Y.; Baker, P. R. S., Distinguishing Cis and Trans Isomers in Intact Complex Lipids Using Electron Impact Excitation of Ions from Organics Mass Spectrometry. *Anal Chem* **2017,** *89* (14), 7307-7315.
200. Mitchell, T.; Blanksby, S.; Kozlowskia, R., Separation and identification of phosphatidylcholine regioisomers by combining liquid chromatography with a fusion of collision-and ozone-induced dissociation. *Eur J Mass Spectrom (Chichester)* **2015,** *21* (3), 191-200.
201. Giles, K., Travelling wave ion mobility. *International Journal for Ion Mobility Spectrometry* **2013,** *16* (1), 1-3.
202. Poad, B. L. J.; Pham, H. T.; Thomas, M. C.; Nealon, J. R.; Campbell, J. L.; Mitchell, T. W.; Blanksby, S. J., Ozone-Induced Dissociation on a Modified Tandem Linear Ion-Trap: Observations of Different Reactivity for Isomeric Lipids. *Journal of the American Society for Mass Spectrometry* **2010,** *21* (12), 1989-1999.
203. Atkinson, M. A., The pathogenesis and natural history of type 1 diabetes. *Cold Spring Harb Perspect Med* **2012,** *2* (11).
204. van Belle, T. L.; Coppieters, K. T.; von Herrath, M. G., Type 1 diabetes: etiology, immunology, and therapeutic strategies. *Physiol Rev* **2011,** *91* (1), 79-118.
205. Atkinson, M. A.; von Herrath, M.; Powers, A. C.; Clare-Salzler, M., Current concepts on the pathogenesis of type 1 diabetes--considerations for attempts to prevent and reverse the disease. *Diabetes Care* **2015,** *38* (6), 979-88.
206. Kershnar, A. K.; Daniels, S. R.; Imperatore, G.; Palla, S. L.; Petitti, D. B.; Pettitt, D. J.; Marcovina, S.; Dolan, L. M.; Hamman, R. F.; Liese, A. D.; Pihoker, C.;

Rodriguez, B. L., Lipid abnormalities are prevalent in youth with type 1 and type 2 diabetes: the SEARCH for Diabetes in Youth Study. *J Pediatr* **2006,** *149* (3), 314-9.
207. La Torre, D.; Seppanen-Laakso, T.; Larsson, H. E.; Hyotylainen, T.; Ivarsson, S. A.; Lernmark, A.; Oresic, M.; DiPi, S. S. G., Decreased cord-blood phospholipids in young age-at-onset type 1 diabetes. *Diabetes* **2013,** *62* (11), 3951-6.
208. Hyotylainen, T.; Oresic, M., Analytical Lipidomics in Metabolic and Clinical Research. *Trends Endocrinol Metab* **2015,** *26* (12), 671-673.
209. Snell-Bergeon, J. K.; Smith, J.; Dong, F.; Baron, A. E.; Barriga, K.; Norris, J. M.; Rewers, M., Early childhood infections and the risk of islet autoimmunity: the Diabetes Autoimmunity Study in the Young (DAISY). *Diabetes Care* **2012,** *35* (12), 2553-8.
210. Smith, R. D.; Anderson, G. A.; Lipton, M. S.; Pasa-Tolic, L.; Shen, Y.; Conrads, T. P.; Veenstra, T. D.; Udseth, H. R., An accurate mass tag strategy for quantitative and high-throughput proteome measurements. *Proteomics* **2002,** *2* (5), 513-23.
211. Stanley, J. R.; Adkins, J. N.; Slysz, G. W.; Monroe, M. E.; Purvine, S. O.; Karpievitch, Y. V.; Anderson, G. A.; Smith, R. D.; Dabney, A. R., A statistical method for assessing peptide identification confidence in accurate mass and time tag proteomics. *Anal Chem* **2011,** *83* (16), 6135-40.
212. Ziegler, O.; Mejean, L.; Igau, B.; Fruchart, J. C.; Drouin, P.; Fievet, C., Accessibility of human apolipoprotein B-100 epitopes in insulin-dependent diabetes: relation with the surface lipid environment of atherogenic particles. *Diabetes Metab* **1996,** *22* (3), 179-84.
213. Bagdade, J. D.; Subbaiah, P. V., Abnormal high-density lipoprotein composition in women with insulin-dependent diabetes. *J Lab Clin Med* **1989,** *113* (2), 235-40.
214. Warensjo, E.; Smedman, A.; Stegmayr, B.; Hallmans, G.; Weinehall, L.; Vessby, B.; Johansson, I., Stroke and plasma markers of milk fat intake--a prospective nested case-control study. *Nutr J* **2009,** *8*, 21.
215. Rudy, M. D.; Kainz, M. J.; Graeve, M.; Colombo, S. M.; Arts, M. T., Handling and Storage Procedures Have Variable Effects on Fatty Acid Content in Fishes with Different Lipid Quantities. *PLoS One* **2016,** *11* (8), e0160497.
216. Cuhadar, S.; Koseoglu, M.; Atay, A.; Dirican, A., The effect of storage time and freeze-thaw cycles on the stability of serum samples. *Biochem Med (Zagreb)* **2013,** *23* (1), 70-7.

APPENDIX A

SUPPLEMENTARY TABLE

Table S1. Human Serum Lipid Library Including Accurate Mass and RPLC Retention Time.

Compound ID	Compound name	Class	Calc Mass	Formula	RPLC retention time (min)
1	Cer(d16:0/22:0)	Cer	595.59003	C38H77O3N11	15.88
2	Cer(d16:1/16:0)	Cer	509.4808	C32 H63 O3 N1	10.44
3	Cer(d16:1/24:0)	Cer	621.606	C40 H79 O3 N1	16.73
4	Cer(d17:1/16:0)	Cer	523.4964	C33 H65 O3 N1	11.25
5	Cer(d17:1/18:0)	Cer	551.5277	C35 H69 O3 N1	12.91
6	Cer(d17:1/22:0)	Cer	607.5903	C39 H77 O3 N1	16.12
7	Cer(d17:1/24:0)	Cer	635.6216	C41 H81 O3 N1	17.15
8	Cer(d18:0/16:0)	Cer	539.5277	C34 H69 O3 N1	12.65
9	Cer(d18:0/18:0)	Cer	567.559	C36 H73 O3 N1	14.26
10	Cer(d18:0/22:0)	Cer	623.6216	C40 H81 O3 N1	16.99
11	Cer(d18:0/24:0)	Cer	651.6529	C42 H85 O3 N1	17.92
12	Cer(d18:1/16:0)	Cer	537.5121	C34 H67 O3 N1	12.07
13	Cer(d18:1/18:0)	Cer	565.5434	C36 H71 O3 N1	13.70
14	Cer(d18:1/20:0)	Cer	593.5747	C38 H75 O3 N1	15.28
15	Cer(d18:1/22:0)	Cer	621.606	C40 H79 O3 N1	16.42
16	Cer(d18:1/24:0)	Cer	649.6373	C42 H83 O3 N1	17.62
17	Cer(d18:2/16:0)	Cer	535.4964	C34 H65 O3 N1	10.69
18	Cer(d18:2/18:0)	Cer	563.5277	C36 H69 O3 N1	12.36
19	Cer(d18:2/20:0)	Cer	591.559	C38 H73 O3 N1	14.02
20	Cer(d18:2/22:0)	Cer	619.5903	C40 H77 O3 N1	15.59
21	Cer(d18:2/24:0)	Cer	647.6216	C42 H81 O3 N1	16.85
22	Cer(d34:0)	Cer	539.5277	C34 H69 O3 N1	12.96
23	Cer(d36:0)	Cer	567.559	C36 H73 O3 N1	14.26
24	Cer(d38:0)	Cer	595.5903	C38 H77 O3 N1	16.05
25	Cer(d40:0)	Cer	623.6216	C40 H81 O3 N1	17.19
26	Cer(d40:1)	Cer	621.606	C40 H79 O3 N1	16.62
27	Cer(d42:3)	Cer	645.606	C42H79O3N1	15.40
28	Cer(d44:1)	Cer	677.6686	C44 H87 O3 N1	17.99
29	CE(18:1)	ChE	650.60015	C45 H78 O2	21.22
30	CE(18:2)	ChE	648.5845	C45 H76 O2	20.75
31	CE(20:3)	ChE	674.60015	C47 H78 O2	20.83
32	CE(20:4)	ChE	672.5845	C47 H76 O2	20.45

33	CE(22:6)	ChE	696.5845	C49 H76 O2	20.20
34	DG(12:0/18:2)	DG	536.4441	C33 H60 O5	10.52
35	DG(16:0/0:0/18:2)	DG	592.5067	C37 H68 O5	13.72
36	DG(16:0/18:1)	DG	594.5223	C37 H70 O5	14.89
37	DG(16:1/18:1)	DG	592.5067	C37 H68 O5	13.48
38	DG(16:1/18:2)	DG	590.491	C37 H66 O5	12.26
39	DG(16:1/18:3)	DG	588.4754	C37 H64 O5	11.20
40	DG(18:0/18:1)	DG	622.5536	C39 H74 O5	16.29
41	DG(18:1/0:0/16:0)	DG	594.5223	C37 H70 O5	14.99
42	DG(18:1/0:0/18:1)	DG	620.538	C39 H72 O5	15.06
43	DG(18:1/18:1)	DG	620.538	C39 H72 O5	15.24
44	DG(18:1/18:3)	DG	616.5067	C39 H68 O5	12.76
45	DG(18:1/20:3)	DG	640.5067	C41 H68 O5	13.67
46	DG(18:1/20:4)	DG	642.5223	C41 H70 O5	15.21
47	DG(18:1/20:4)	DG	642.5223	C41 H70 O5	13.42
48	DG(18:1/22:4)	DG	670.5536	C43 H74 O5	14.52
49	DG(18:1/22:5)	DG	668.538	C43 H72 O5	13.98
50	DG(18:1/22:6)	DG	666.5223	C43 H70 O5	12.99
51	DG(18:2/0:0/18:1)	DG	618.5223	C39 H70 O5	13.79
52	DG(18:2/0:0/18:2)	DG	616.5067	C39 H68 O5	12.57
53	DG(18:2/18:1)	DG	618.5223	C39 H70 O5	14.03
54	DG(18:2/18:3)	DG	614.491	C39 H66 O5	11.53
55	DG(18:2/20:4)	DG	640.5067	C41 H68 O5	13.67
56	DG(18:2/20:5)	DG	638.491	C41 H66 O5	11.18
57	DG(18:2/22:4)	DG	668.538	C43 H72 O5	13.35
58	DG(18:2/22:5)	DG	666.5223	C43 H70 O5	12.78
59	DG(20:2/18:2)	DG	644.538	C41 H72 O5	16.46
60	DG(20:3/18:1)	DG	644.538	C41 H72 O5	14.14
61	DG(22:6/18:2)	DG	664.5067	C43 H68 O5	11.82
62	LPC(0:0/14:0)	LPC	467.3012	C22 H46 O7 N1 P1	1.54
63	LPC(0:0/15:0)	LPC	481.3168	C23 H48 O7 N1 P1	1.86
64	LPC(0:0/16:1)	LPC	493.3168	C24 H48 O7 N1 P1	1.79
65	LPC(0:0/17:0)	LPC	509.3481	C25 H52 O7 N1 P1	2.60
66	LPC(0:0/17:1)	LPC	507.3325	C25 H50 O7 N1 P1	2.16
67	LPC(0:0/18:0)	LPC	523.3638	C26 H54 O7 N1 P1	3.46
68	LPC(0:0/18:1)	LPC	521.3481	C26 H52 O7 N1 P1	2.42
69	LPC(0:0/18:2)	LPC	519.3325	C26 H50 O7 N1 P1	1.84

70	LPC(0:0/18:3)	LPC	517.3168	C26 H48 O7 N1 P1	1.62
71	LPC(0:0/20:0)	LPC	551.3951	C28 H58 O7 N1 P1	5.28
72	LPC(0:0/20:1)	LPC	549.3794	C28 H56 O7 N1 P1	3.61
73	LPC(0:0/20:2)	LPC	547.3638	C28 H54 O7 N1 P1	2.64
74	LPC(0:0/20:3)	LPC	545.3481	C28 H52 O7 N1 P1	2.08
75	LPC(0:0/20:4)	LPC	543.3325	C28 H50 O7 N1 P1	1.79
76	LPC(0:0/20:5)	LPC	541.3168	C28 H48 O7 N1 P1	1.55
77	LPC(0:0/22:5)	LPC	569.3481	C30 H52 O7 N1 P1	1.90
78	LPC(0:0/22:6)	LPC	567.3325	C30 H50 O7 N1 P1	1.68
79	LPC(0:0/P-16:1)	LPC	477.3219	C24 H48 O6 N1 P1	2.25
80	LPC(0:0/P-18:1)	LPC	505.3532	C26 H52 O6 N1 P1	3.03
81	LPC(0:0/P-18:2)	LPC	503.3376	C26 H50 O6 N1 P1	2.63
82	LPC(12:0/0:0)	LPC	439.2699	C20 H42 O7 N1 P1	1.24
83	LPC(14:0/0:0)	LPC	467.3012	C22 H46 O7 N1 P1	1.66
84	LPC(14:1/0:0)	LPC	465.2855	C22 H44 O7 N1 P1	1.32
85	LPC(15:0/0:0)	LPC	481.3168	C23 H48 O7 N1 P1	2.01
86	LPC(16:0/0:0)	LPC	495.3325	C24 H50 O7 N1 P1	2.45
87	LPC(16:1/0:0)	LPC	493.3168	C24 H48 O7 N1 P1	2.67
88	LPC(16:2/0:0)	LPC	491.3012	C24 H46 O7 N1 P1	1.52
89	LPC(17:0/0:0)	LPC	509.3481	C25 H52 O7 N1 P1	3.05
90	LPC(17:1/0:0)	LPC	507.3325	C25 H50 O7 N1 P1	2.53
91	LPC(18:0/0:0)	LPC	523.3638	C26 H54 O7 N1 P1	3.78
92	LPC(18:1/0:0)	LPC	521.3481	C26 H52 O7 N1 P1	2.63
93	LPC(18:2/0:0)	LPC	519.3325	C26 H50 O7 N1 P1	1.98
94	LPC(18:3/0:0)	LPC	517.3168	C26 H48 O7 N1 P1	1.10
95	LPC(20:0/0:0)	LPC	551.3951	C28 H58 O7 N1 P1	5.71
96	LPC(20:1/0:0)	LPC	549.3794	C28 H56 O7 N1 P1	3.91
97	LPC(20:2/0:0)	LPC	547.3638	C28 H54 O7 N1 P1	2.86
98	LPC(20:3/0:0)	LPC	545.3481	C28 H52 O7 N1 P1	2.23
99	LPC(20:4/0:0)	LPC	543.3325	C28 H50 O7 N1 P1	1.90
100	LPC(22:0/0:0)	LPC	579.4264	C30 H62 O7 N1 P1	7.46
101	LPC(22:2/0:0)	LPC	575.3951	C30 H58 O7 N1 P1	4.25
102	LPC(22:5/0:0)	LPC	569.3481	C30 H52 O7 N1 P1	2.27
103	LPC(22:6/0:0)	LPC	567.3325	C30 H50 O7 N1 P1	1.81
104	LPC(O-16:0/0:0)	LPC	481.3532	C24 H52 O6 N1 P1	2.94
105	LPC(O-18:0/0:0)	LPC	509.3845	C26 H56 O6 N1 P1	4.56
106	LPC(O-20:0/0:0)	LPC	537.4158	C28 H60 O6 N1 P1	6.63

107	LPC(P-16:0/0:0)	LPC	479.3376	C24 H50 O6 N1 P1	2.85
108	LPC(P-18:0/0:0)	LPC	507.3689	C26 H54 O6 N1 P1	3.12
109	LPC(P-18:1/0:0)	LPC	505.3532	C26 H52 O6 N1 P1	2.30
110	LPC(P-18:2/0:0)	LPC	503.3376	C26 H50 O6 N1 P1	2.40
111	LPC(P-20:0/0:0)	LPC	535.4002	C28 H58 O6 N1 P1	4.66
112	LPC(P-20:1/0:0)	LPC	533.3845	C28 H56 O6 N1 P1	3.41
113	LPE(14:0)	LPE	425.2542	C19 H40 O7 N1 P1	1.73
114	LPE(16:0)	LPE	453.2855	C21 H44 O7 N1 P1	2.38
115	LPE(16:1)	LPE	451.2699	C21 H42 O7 N1 P1	1.87
116	LPE(17:0)	LPE	467.3012	C22 H46 O7 N1 P1	3.22
117	LPE(18:0)	LPE	481.3168	C23 H48 O7 N1 P1	4.00
118	LPE(18:1)	LPE	479.3012	C23 H46 O7 N1 P1	2.58
119	LPE(18:2)	LPE	477.2855	C23 H44 O7 N1 P1	1.93
120	LPE(18:3)	LPE	475.2699	C23 H42 O7 N1 P1	1.67
121	LPE(20:2)	LPE	505.3168	C25 H48 O7 N1 P1	3.02
122	LPE(20:3)	LPE	503.3012	C25 H46 O7 N1 P1	2.35
123	LPE(20:4)	LPE	501.2855	C25 H44 O7 N1 P1	1.87
124	LPE(20:5)	LPE	499.2699	C25 H42 O7 N1 P1	1.61
125	LPE(22:4)	LPE	529.3168	C27 H48 O7 N1 P1	2.69
126	LPE(22:5)	LPE	527.3012	C27 H46 O7 N1 P1	2.37
127	LPE(22:6)	LPE	525.2855	C27 H44 O7 N1 P1	1.88
128	LPG(16:0)	LPG	484.2801	C22 H45 O9 N0 P1	2.31
129	LPG(18:0)	LPG	512.3114	C24 H49 O9 N0 P1	3.54
130	LPG(18:2)	LPG	508.2801	C24 H45 O9 N0 P1	1.87
131	LPI(18:0)	LPI	600.3275	C27 H53 O12 N0 P1	3.25
132	LPI(18:1)	LPI	598.3118	C27 H51 O12 N0 P1	2.28
133	LPI(18:2)	LPI	596.2962	C27 H49 O12 N0 P1	1.75
134	LPI(20:3)	LPI	622.3118	C29 H51 O12 N0 P1	1.96
135	LPI(20:4)	LPI	620.2962	C29 H49 O12 N0 P1	1.70
136	PC(12:0/18:2)	PC	701.4996	C38 H72 O8 N1 P1	8.00
137	PC(14:0/14:0)	PC	677.4996	C36 H72 O8 N1 P1	8.94
138	PC(14:0/15:0)	PC	691.5152	C37 H74 O8 N1 P1	9.34
139	PC(14:0/17:0)	PC	719.5465	C39 H78 O8 N1 P1	10.88
140	PC(14:0/18:2)	PC	729.5309	C40 H76 O8 N1 P1	9.43
141	PC(14:0/20:3)	PC	755.5465	C42 H78 O8 N1 P1	9.78

142	PC(14:0/20:4)	PC	753.5309	C42 H76 O8 N1 P1	9.24
143	PC(14:0_12:0)	PC	649.4683	C34 H68 O8 N1 P1	7.50
144	PC(14:0_16:1)	PC	703.5152	C38 H74 O8 N1 P1	9.10
145	PC(15:0/14:0)	PC	691.5152	C37 H74 O8 N1 P1	9.66
146	PC(15:0/16:0)	PC	719.5465	C39 H78 O8 N1 P1	11.22
147	PC(15:0/16:1)	PC	717.5309	C39 H76 O8 N1 P1	9.85
148	PC(15:0/18:1)	PC	745.5622	C41 H80 O8 N1 P1	11.37
149	PC(15:0/18:2)	PC	743.5465	C41 H78 O8 N1 P1	10.19
150	PC(15:0/20:3)	PC	769.5622	C43 H80 O8 N1 P1	10.59
151	PC(15:0/20:4)	PC	767.5465	C43 H78 O8 N1 P1	9.99
152	PC(15:0/22:5)	PC	793.5622	C45 H80 O8 N1 P1	10.11
153	PC(15:0_22:6)	PC	791.5465	C45 H78 O8 N1 P1	9.63
154	PC(16:0/14:0)	PC	705.5309	C38 H76 O8 N1 P1	10.45
155	PC(16:0/15:0)	PC	719.5465	C39 H78 O8 N1 P1	10.88
156	PC(16:0/16:0)	PC	733.5622	C40 H80 O8 N1 P1	11.99
157	PC(16:0/16:1)	PC	731.5465	C40 H78 O8 N1 P1	10.61
158	PC(16:0/17:0)	PC	747.5778	C41 H82 O8 N1 P1	12.45
159	PC(16:0/17:1)	PC	745.5622	C41 H80 O8 N1 P1	12.22
160	PC(16:0/17:1)	PC	745.5622	C41 H80 O8 N1 P1	12.23
161	PC(16:0/18:1)	PC	759.5778	C42 H82 O8 N1 P1	12.13
162	PC(16:0/18:2)	PC	757.5622	C42 H80 O8 N1 P1	10.95
163	PC(16:0/18:3)	PC	755.5465	C42 H78 O8 N1 P1	10.20
164	PC(16:0/19:1)	PC	773.5935	C43 H84 O8 N1 P1	12.91
165	PC(16:0/19:2)	PC	771.5778	C43 H82 O8 N1 P1	11.53
166	PC(16:0/20:3)	PC	783.5778	C44 H82 O8 N1 P1	11.35
167	PC(16:0/20:5)	PC	779.5465	C44 H78 O8 N1 P1	9.81
168	PC(16:0/22:4)	PC	809.5935	C46 H84 O8 N1 P1	11.82
169	PC(16:0/22:5)	PC	807.5778	C46 H82 O8 N1 P1	10.85
170	PC(16:0_20:4)	PC	781.5622	C44 H80 O8 N1 P1	10.75
171	PC(16:1/18:1)	PC	757.5622	C42 H80 O8 N1 P1	11.21
172	PC(16:1/18:2)	PC	755.5465	C42 H78 O8 N1 P1	9.61
173	PC(16:1/18:2)	PC	755.5465	C42 H78 O8 N1 P1	9.60
174	PC(16:1/18:3)	PC	753.5309	C42 H76 O8 N1 P1	8.88
175	PC(16:1/20:3)	PC	781.5622	C44 H80 O8 N1 P1	9.92
176	PC(16:1/20:4)	PC	779.5465	C44 H78 O8 N1 P1	9.40
177	PC(16:1/20:5)	PC	777.5309	C44 H76 O8 N1 P1	8.50
178	PC(16:2/18:2)	PC	753.5309	C42 H76 O8 N1 P1	9.24

179	PC(17:0/16:0)	PC	747.5778	C41 H82 O8 N1 P1	12.79
180	PC(17:0/18:1)	PC	773.5935	C43 H84 O8 N1 P1	12.91
181	PC(17:0/18:2)	PC	771.5778	C43 H82 O8 N1 P1	11.77
182	PC(17:0/20:2)	PC	799.6091	C45 H86 O8 N1 P1	12.99
183	PC(17:0/20:5)	PC	793.5622	C45 H80 O8 N1 P1	10.38
184	PC(17:0/22:5)	PC	821.5935	C47 H84 O8 N1 P1	11.63
185	PC(17:0_20:3)	PC	797.5935	C45 H84 O8 N1 P1	11.91
186	PC(17:0_20:3)	PC	797.5935	C45 H84 O8 N1 P1	12.17
187	PC(17:0_20:4)	PC	795.5778	C45 H82 O8 N1 P1	11.27
188	PC(17:1/18:2)	PC	769.5622	C43 H80 O8 N1 P1	10.35
189	PC(17:1/20:4)	PC	793.5622	C45 H80 O8 N1 P1	10.38
190	PC(18:0/16:0)	PC	761.5935	C42 H84 O8 N1 P1	13.57
191	PC(18:0/18:0)	PC	789.6248	C44 H88 O8 N1 P1	15.06
192	PC(18:0/18:1)	PC	787.6091	C44 H86 O8 N1 P1	13.69
193	PC(18:0/18:2)	PC	785.5935	C44 H84 O8 N1 P1	12.55
194	PC(18:0/18:3)	PC	783.5778	C44 H82 O8 N1 P1	11.87
195	PC(18:0/20:2)	PC	813.6248	C46 H88 O8 N1 P1	13.89
196	PC(18:0/20:4)	PC	809.5935	C46 H84 O8 N1 P1	12.34
197	PC(18:0/20:5)	PC	807.5778	C46 H82 O8 N1 P1	11.36
198	PC(18:0/22:3)	PC	839.6404	C48 H90 O8 N1 P1	14.49
199	PC(18:0/22:4)	PC	837.6248	C48 H88 O8 N1 P1	13.38
200	PC(18:0/22:5)	PC	835.6091	C48 H86 O8 N1 P1	12.92
201	PC(18:1/18:1)	PC	785.5935	C44 H84 O8 N1 P1	12.26
202	PC(18:1/18:2)	PC	783.5778	C44 H82 O8 N1 P1	11.35
203	PC(18:1/20:3)	PC	809.5935	C46 H84 O8 N1 P1	11.82
204	PC(18:1/20:4)	PC	807.5778	C46 H82 O8 N1 P1	11.12
205	PC(18:1/22:0)	PC	843.6717	C48 H94 O8 N1 P1	16.49
206	PC(18:1/22:4)	PC	835.6091	C48 H86 O8 N1 P1	11.97
207	PC(18:1/22:5)	PC	833.5935	C48 H84 O8 N1 P1	11.21
208	PC(18:1/22:6)	PC	831.5778	C48 H82 O8 N1 P1	10.51
209	PC(18:1_22:2)	PC	839.6404	C48 H90 O8 N1 P1	13.98
210	PC(18:2/18:2)	PC	781.5622	C44 H80 O8 N1 P1	9.92
211	PC(18:2/20:3)	PC	807.5778	C46 H82 O8 N1 P1	10.33
212	PC(18:2/20:4)	PC	805.5622	C46 H80 O8 N1 P1	9.72
213	PC(18:2p/20:2)	PC	793.5985	C46 H84 O7 N1 P1	13.53
214	PC(18:3/16:1)	PC	753.5309	C42 H76 O8 N1 P1	8.68
215	PC(18:3/18:2)	PC	779.5465	C44 H78 O8 N1 P1	8.96

216	PC(18:3/18:3)	PC	777.5309	C44 H76 O8 N1 P1	8.06
217	PC(18:4/20:3)	PC	803.5465	C46 H78 O8 N1 P1	9.29
218	PC(19:0/18:2)	PC	799.6091	C45 H86 O8 N1 P1	13.35
219	PC(20:0/18:2)	PC	813.6248	C46 H88 O8 N1 P1	14.15
220	PC(20:0/18:2)	PC	813.6248	C46 H88 O8 N1 P1	14.13
221	PC(20:0/20:3)	PC	839.6404	C48 H90 O8 N1 P1	14.49
222	PC(20:0/20:4)	PC	837.6248	C48 H88 O8 N1 P1	13.92
223	PC(20:0/22:6)	PC	861.6248	C50 H88 O8 N1 P1	13.54
224	PC(20:1/18:2)	PC	811.6091	C46 H86 O8 N1 P1	12.69
225	PC(20:1/20:4)	PC	835.6091	C48 H86 O8 N1 P1	12.41
226	PC(20:1/22:6)	PC	859.6091	C50 H86 O8 N1 P1	11.94
227	PC(20:1_18:1)	PC	813.6248	C46 H88 O8 N1 P1	13.65
228	PC(20:2/20:1)	PC	839.6404	C48 H90 O8 N1 P1	14.20
229	PC(20:3/20:4)	PC	831.5778	C48 H82 O8 N1 P1	10.24
230	PC(20:4/20:3)	PC	831.5778	C48 H82 O8 N1 P1	10.09
231	PC(20:4/20:4)	PC	829.5622	C48 H80 O8 N1 P1	9.41
232	PC(20:4/22:6)	PC	853.5622	C50 H80 O8 N1 P1	9.09
233	PC(20:4_17:0)	PC	795.5778	C45 H82 O8 N1 P1	11.56
234	PC(20:5/18:2)	PC	803.5465	C46 H78 O8 N1 P1	8.80
235	PC(22:0/18:2)	PC	841.6561	C48 H92 O8 N1 P1	15.62
236	PC(22:0/20:4)	PC	865.6561	C50 H92 O8 N1 P1	15.41
237	PC(22:4/20:4)	PC	857.5935	C50 H84 O8 N1 P1	10.51
238	PC(22:5/20:4)	PC	855.5778	C50 H82 O8 N1 P1	10.02
239	PC(22:6/17:0)	PC	819.5778	C47 H82 O8 N1 P1	10.87
240	PC(22:6/18:0)	PC	833.5935	C48 H84 O8 N1 P1	11.96
241	PC(22:6_16:0)	PC	805.5622	C46 H80 O8 N1 P1	10.39
242	PC(24:0/18:2)	PC	869.6874	C50 H96 O8 N1 P1	16.81
243	PC(24:0/20:4)	PC	893.6874	C52 H96 O8 N1 P1	16.65
244	PC(24:0/20:5)	PC	891.6717	C52 H94 O8 N1 P1	16.81
245	PC(O-16:0/14:0)	PC	691.5516	C38 H78 O7 N1 P1	11.43
246	PC(O-16:0/16:0)	PC	719.5829	C40 H82 O7 N1 P1	13.00
247	PC(O-16:0/16:1)	PC	717.5672	C40 H80 O7 N1 P1	11.63
248	PC(O-16:0/18:1)	PC	745.5985	C42 H84 O7 N1 P1	13.08
249	PC(O-16:0/18:2)	PC	743.5829	C42 H82 O7 N1 P1	11.94
250	PC(O-16:0/20:3)	PC	769.5985	C44 H84 O7 N1 P1	12.32
251	PC(O-16:0/20:4)	PC	767.5829	C44 H82 O7 N1 P1	11.71
252	PC(O-16:0/22:4)	PC	795.6142	C46 H86 O7 N1 P1	12.79

253	PC(O-16:0/22:5)	PC	791.5829	C46 H82 O7 N1 P1	11.53
254	PC(O-16:0/22:6)	PC	791.5829	C46 H82 O7 N1 P1	11.30
255	PC(O-18:0/16:0)	PC	747.6142	C42 H86 O7 N1 P1	14.58
256	PC(O-18:0/18:1)	PC	773.6298	C44 H88 O7 N1 P1	14.69
257	PC(O-18:0/18:2)	PC	771.6142	C44 H86 O7 N1 P1	13.55
258	PC(O-18:0/20:3)	PC	797.6298	C46 H88 O7 N1 P1	13.93
259	PC(O-18:0/20:4)	PC	795.6142	C46 H86 O7 N1 P1	13.32
260	PC(O-18:0/22:4)	PC	823.6455	C48 H90 O7 N1 P1	14.36
261	PC(O-18:0/22:5)	PC	821.6298	C48 H88 O7 N1 P1	13.25
262	PC(O-18:0/22:6)	PC	819.6142	C48 H86 O7 N1 P1	12.91
263	PC(O-20:0/18:2)	PC	799.6455	C46 H90 O7 N1 P1	15.11
264	PC(O-20:0/20:4)	PC	823.6455	C48 H90 O7 N1 P1	14.87
265	PC(O-20:0/22:4)	PC	851.6768	C50 H94 O7 N1 P1	15.81
266	PC(O-20:0/22:6)	PC	847.6455	C50 H90 O7 N1 P1	14.47
267	PC(O-20:e/18:1)	PC	801.6611	C46 H92 O7 N1 P1	16.10
268	PC(P-16:0/14:0)	PC	689.5359	C38 H76 O7 N1 P1	11.19
269	PC(P-16:0/16:0)	PC	717.5672	C40 H80 O7 N1 P1	12.78
270	PC(P-16:0/18:1)	PC	743.5829	C42 H82 O7 N1 P1	12.87
271	PC(P-16:0/18:2)	PC	741.5672	C42 H80 O7 N1 P1	11.69
272	PC(P-16:0/20:2)	PC	769.5985	C44 H84 O7 N1 P1	14.59
273	PC(P-16:0/20:3)	PC	767.5829	C44 H82 O7 N1 P1	13.11
274	PC(P-16:0/20:4)	PC	765.5672	C44 H80 O7 N1 P1	11.44
275	PC(P-16:0/22:6)	PC	789.5672	C46 H80 O7 N1 P1	11.04
276	PC(P-16:1/20:3)	PC	765.5672	C44 H80 O7 N1 P1	11.91
277	PC(P-16:1/21:4)	PC	777.5672	C45 H80 O7 N1 P1	10.88
278	PC(P-16:1/24:7)	PC	813.5672	C48 H80 O7 N1 P1	10.55
279	PC(P-18:0/16:0)	PC	745.5985	C42 H84 O7 N1 P1	13.05
280	PC(P-18:0/18:1)	PC	771.6142	C44 H86 O7 N1 P1	13.19
281	PC(P-18:0/18:2)	PC	769.5985	C44 H84 O7 N1 P1	11.99
282	PC(P-18:0/20:4)	PC	793.5985	C46 H84 O7 N1 P1	11.77
283	PC(P-18:0/22:4)	PC	821.6298	C48 H88 O7 N1 P1	12.83
284	PC(P-18:0/22:5)	PC	819.6142	C48 H86 O7 N1 P1	11.87
285	PC(P-18:0/22:6)	PC	817.5985	C48 H84 O7 N1 P1	11.37
286	PC(P-18:1/18:1)	PC	769.5985	C44 H84 O7 N1 P1	12.97
287	PC(P-18:1/18:2)	PC	767.5829	C44 H82 O7 N1 P1	12.05
288	PC(P-18:1/20:4)	PC	791.5829	C46 H82 O7 N1 P1	11.53
289	PC(P-18:1/22:2)	PC	823.6455	C48 H90 O7 N1 P1	14.88

290	PC(P-18:1/22:4)	PC	819.6142	C48 H86 O7 N1 P1	13.94
291	PC(P-18:1/22:5)	PC	817.5985	C48 H84 O7 N1 P1	11.64
292	PC(P-18:1/24:7)	PC	841.5985	C50 H84 O7 N1 P1	11.87
293	PC(P-20:0/18:2)	PC	797.6298	C46 H88 O7 N1 P1	13.94
294	PC(P-20:0/20:4)	PC	821.6298	C48 H88 O7 N1 P1	13.56
295	PC(P-20:0/22:4)	PC	849.6611	C50 H92 O7 N1 P1	14.28
296	PE(16:0/18:1)	PE	717.5309	C39 H76 O8 N1 P1	12.56
297	PE(16:0/18:2)	PE	715.5152	C39 H74 O8 N1 P1	11.38
298	PE(16:0/20:4)	PE	739.5152	C41 H74 O8 N1 P1	11.16
299	PE(16:0/20:5)	PE	737.4996	C41 H72 O8 N1 P1	10.18
300	PE(16:0/22:4)	PE	767.5465	C43 H78 O8 N1 P1	12.22
301	PE(16:1/18:1)	PE	715.5152	C39 H74 O8 N1 P1	11.15
302	PE(17:0/18:2)	PE	729.5309	C40 H76 O8 N1 P1	12.18
303	PE(17:0_18:1)	PE	731.5465	C40 H78 O8 N1 P1	13.34
304	PE(17:1/20:4)	PE	751.5152	C42 H74 O8 N1 P1	10.96
305	PE(17:1/22:6)	PE	775.5152	C44 H74 O8 N1 P1	10.59
306	PE(17:1_18:2)	PE	727.5152	C40 H74 O8 N1 P1	11.21
307	PE(18:0/16:0)	PE	719.5465	C39 H78 O8 N1 P1	13.99
308	PE(18:0/20:3)	PE	769.5622	C43 H80 O8 N1 P1	13.52
309	PE(18:0/20:4)	PE	767.5465	C43 H78 O8 N1 P1	12.76
310	PE(18:0/20:5)	PE	765.5309	C43 H76 O8 N1 P1	11.77
311	PE(18:0/22:4)	PE	795.5778	C45 H82 O8 N1 P1	13.77
312	PE(18:0/22:5)	PE	793.5622	C45 H80 O8 N1 P1	13.33
313	PE(18:0_18:1)	PE	745.5622	C41 H80 O8 N1 P1	14.10
314	PE(18:1/18:1)	PE	743.5465	C41 H78 O8 N1 P1	12.67
315	PE(18:1/20:2)	PE	769.5622	C43 H80 O8 N1 P1	13.35
316	PE(18:1/22:5)	PE	791.5465	C45 H78 O8 N1 P1	11.87
317	PE(18:1/22:6)	PE	789.5309	C45 H76 O8 N1 P1	10.89
318	PE(18:1_18:2)	PE	741.5309	C41 H76 O8 N1 P1	11.49
319	PE(18:2/18:2)	PE	739.5152	C41 H74 O8 N1 P1	10.30
320	PE(18:2/20:4)	PE	763.5152	C43 H74 O8 N1 P1	10.08
321	PE(18:2_18:0)	PE	743.5465	C41 H78 O8 N1 P1	12.98
322	PE(20:1/20:4)	PE	793.5622	C45 H80 O8 N1 P1	12.59
323	PE(22:6/16:0)	PE	763.5152	C43 H74 O8 N1 P1	10.78
324	PE(22:6/18:0)	PE	791.5465	C45 H78 O8 N1 P1	12.37
325	PE(O-16:0/18:2)	PE	701.5359	C39 H76 O7 N1 P1	12.41
326	PE(O-16:0/20:4)	PE	725.5359	C41 H76 O7 N1 P1	12.24

327	PE(O-16:0/22:4)	PE	753.5672	C43 H80 O7 N1 P1	13.23
328	PE(O-16:0/22:6)	PE	749.5359	C43 H76 O7 N1 P1	11.76
329	PE(O-18:0/18:1)	PE	731.5829	C41 H82 O7 N1 P1	15.11
330	PE(O-18:0/18:2)	PE	729.5672	C41 H80 O7 N1 P1	14.00
331	PE(O-18:0/22:4)	PE	781.5985	C45 H84 O7 N1 P1	14.76
332	PE(O-18:0/22:6)	PE	777.5672	C45 H80 O7 N1 P1	13.38
333	PE(P-16:0/18:0)	PE	703.5516	C39 H78 O7 N1 P1	13.53
334	PE(P-16:0/18:3)	PE	697.5046	C39 H72 O7 N1 P1	11.13
335	PE(P-16:0/20:4)	PE	723.5203	C41 H74 O7 N1 P1	11.90
336	PE(P-16:0/20:5)	PE	721.5046	C41 H72 O7 N1 P1	10.90
337	PE(P-16:0/22:6)	PE	747.5203	C43 H74 O7 N1 P1	11.49
338	PE(P-16:0p/18:1)	PE	701.5359	C39 H76 O7 N1 P1	13.35
339	PE(P-16:0p/18:2)	PE	699.5203	C39 H74 O7 N1 P1	12.16
340	PE(P-18:0/16:0)	PE	703.5516	C39 H78 O7 N1 P1	14.79
341	PE(P-18:0/18:1)	PE	729.5672	C41 H80 O7 N1 P1	14.87
342	PE(P-18:0/18:2)	PE	727.5516	C41 H78 O7 N1 P1	13.75
343	PE(P-18:0/20:1)	PE	757.5985	C43 H84 O7 N1 P1	16.11
344	PE(P-18:0/20:3)	PE	753.5672	C43 H80 O7 N1 P1	14.27
345	PE(P-18:0/20:4)	PE	751.5516	C43 H78 O7 N1 P1	13.50
346	PE(P-18:0/22:5)	PE	777.5672	C45 H80 O7 N1 P1	14.05
347	PE(P-18:0/22:7)	PE	773.5359	C45 H76 O7 N1 P1	11.85
348	PE(P-18:1/18:1)	PE	727.5516	C41 H78 O7 N1 P1	13.43
349	PE(P-18:1/18:2)	PE	725.5359	C41 H76 O7 N1 P1	12.24
350	PE(P-18:1/20:3)	PE	751.5516	C43 H78 O7 N1 P1	12.98
351	PE(P-18:1/20:4)	PE	749.5359	C43 H76 O7 N1 P1	11.99
352	PE(P-18:1/22:5)	PE	775.5516	C45 H78 O7 N1 P1	13.10
353	PE(P-18:1/22:6)	PE	773.5359	C45 H76 O7 N1 P1	11.59
354	PE(P-18:2/18:2)	PE	723.5203	C41 H74 O7 N1 P1	11.05
355	PE(P-18:2/20:4)	PE	747.5203	C43 H74 O7 N1 P1	10.79
356	PE(P-18:2/22:6)	PE	771.5203	C45 H74 O7 N1 P1	10.40
357	PE(P-20:0/18:1)	PE	757.5985	C43 H84 O7 N1 P1	16.24
358	PE(P-20:0/18:2)	PE	755.5829	C43 H82 O7 N1 P1	15.27
359	PE(P-20:0/20:3)	PE	781.5985	C45 H84 O7 N1 P1	15.59
360	PE(P-20:0/20:4)	PE	779.5829	C45 H82 O7 N1 P1	15.02
361	PE(P-20:0/22:5)	PE	805.5985	C47 H84 O7 N1 P1	15.52
362	PE(P-20:0/22:6)	PE	803.5829	C47 H82 O7 N1 P1	14.64
363	PE(P-20:1/18:1)	PE	755.5829	C43 H82 O7 N1 P1	14.82

364	PE(P-20:1/20:4)	PE	777.5672	C45 H80 O7 N1 P1	13.75
365	PE(P-20:1/22:6)	PE	801.5672	C47 H80 O7 N1 P1	13.05
366	PG(16:0/18:1)	PG	748.5254	C40 H77 O10 N0 P1	11.55
367	PG(16:0/18:2)	PG	746.5098	C40 H75 O10 N0 P1	10.48
368	PG(16:0/20:4)	PG	770.5098	C42 H75 O10 N0 P1	10.30
369	PG(18:0/18:1)	PG	776.5567	C42 H81 O10 N0 P1	13.07
370	PG(18:1/18:2)	PG	772.5254	C42 H77 O10 N0 P1	10.61
371	PI(16:0/16:0)	PI	810.5258	C41 H79 O13 N0 P1	11.11
372	PI(16:0/18:1)	PI	836.5415	C43 H81 O13 N0 P1	11.27
373	PI(16:0/18:2)	PI	834.5258	C43 H79 O13 N0 P1	10.14
374	PI(16:0/20:3)	PI	860.5415	C45 H81 O13 N0 P1	10.27
375	PI(17:0/18:2)	PI	848.5415	C44 H81 O13 N0 P1	10.91
376	PI(17:0/20:3)	PI	874.5571	C46 H83 O13 N0 P1	11.30
377	PI(17:0/20:4)	PI	872.5415	C46 H81 O13 N0 P1	10.74
378	PI(17:0_18:1)	PI	850.5571	C44 H83 O13 N0 P1	12.04
379	PI(18:0/18:2)	PI	862.5571	C45 H83 O13 N0 P1	11.69
380	PI(18:0/20:3)	PI	888.5728	C47 H85 O13 N0 P1	12.09
381	PI(18:0/20:4)	PI	886.5571	C47 H83 O13 N0 P1	11.49
382	PI(18:0_18:1)	PI	864.5728	C45 H85 O13 N0 P1	12.81
383	PI(18:1/18:1)	PI	862.5571	C45 H83 O13 N0 P1	11.39
384	PI(18:1_18:2)	PI	860.5415	C45 H81 O13 N0 P1	10.27
385	PI(18:2/18:2)	PI	858.5258	C45 H79 O13 N0 P1	9.15
386	PI(18:2/20:4)	PI	882.5258	C47 H79 O13 N0 P1	9.63
387	PI(20:2/18:0)	PI	862.5571	C45 H83 O13 N0 P1	11.83
388	PI(20:4/16:0)	PI	858.5258	C45 H79 O13 N0 P1	9.97
389	PI(20:4/18:1)	PI	884.5415	C47 H81 O13 N0 P1	10.33

390	PI(20:4/20:1)	PI	912.5728	C49 H85 O13 N0 P1	11.56
391	PI(22:4/18:0)	PI	914.5884	C49 H87 O13 N0 P1	12.53
392	PI(22:5/16:0)	PI	884.5415	C47 H81 O13 N0 P1	10.57
393	PI(22:5/18:0)	PI	912.5728	C49 H85 O13 N0 P1	12.10
394	PI(22:6/16:0)	PI	882.5258	C47 H79 O13 N0 P1	9.63
395	PI(22:6/18:1)	PI	908.5415	C49 H81 O13 N0 P1	9.99
396	PS(20:0/20:4)	PS	839.5676	C46 H82 O10 N1 P1	12.40
397	PS(20:0p/18:2)	PS	799.5727	C44 H82 O9 N1 P1	13.34
398	PS(20:0p/20:4)	PS	823.5727	C46 H82 O9 N1 P1	13.10
399	PS(38:6p)	PS	791.5101	C44 H74 O9 N1 P1	11.90
400	SM(d17:1/23:3)	SM	780.6145	C45 H85 O6 N2 P1	14.08
401	SM(d22:1/18:2)	SM	782.6302	C45 H87 O6 N2 P1	12.60
402	SM(d28:0)	SM	620.4893	C33 H69 O6 N2 P1	6.62
403	SM(d28:1)	SM	618.4737	C33 H67 O6 N2 P1	5.78
404	SM(d29:1)	SM	632.4893	C34 H69 O6 N2 P1	6.67
405	SM(d30:0)	SM	648.5206	C35 H73 O6 N2 P1	7.90
406	SM(d30:1)	SM	646.505	C35 H71 O6 N2 P1	7.32
407	SM(d30:2)	SM	644.4893	C35 H69 O6 N2 P1	6.13
408	SM(d31:1)	SM	660.5206	C36 H73 O6 N2 P1	8.02
409	SM(d32:0)	SM	676.5519	C37 H77 O6 N2 P1	9.38
410	SM(d32:1)	SM	674.5363	C37 H75 O6 N2 P1	8.79
411	SM(d32:2)	SM	672.5206	C37 H73 O6 N2 P1	7.55
412	SM(d32:4)	SM	668.4893	C37 H69 O6 N2 P1	7.34
413	SM(d33:0)	SM	690.5676	C38 H79 O6 N2 P1	10.17
414	SM(d33:1)	SM	688.5519	C38 H77 O6 N2 P1	9.57
415	SM(d33:2)	SM	686.5363	C38 H75 O6 N2 P1	9.02
416	SM(d33:2)	SM	686.5363	C38 H75 O6 N2 P1	8.35
417	SM(d33:4)	SM	682.505	C38 H71 O6 N2 P1	8.02
418	SM(d34:0)	SM	704.5832	C39 H81 O6 N2 P1	10.99
419	SM(d34:1)	SM	702.5676	C39 H79 O6 N2 P1	10.36
420	SM(d34:2)	SM	700.5519	C39 H77 O6 N2 P1	9.04
421	SM(d34:3)	SM	698.5363	C39 H75 O6 N2 P1	7.95
422	SM(d34:3)	SM	698.5363	C39 H75 O6 N2 P1	9.38
423	SM(d34:4)	SM	696.5206	C39 H73 O6 N2 P1	8.81

424	SM(d34:5)	SM	694.505	C39 H71 O6 N2 P1	7.55
425	SM(d35:0)	SM	718.5989	C40 H83 O6 N2 P1	11.47
426	SM(d35:0)	SM	718.5989	C40 H83 O6 N2 P1	11.82
427	SM(d35:1)	SM	716.5832	C40 H81 O6 N2 P1	11.21
428	SM(d35:1)	SM	716.5832	C40 H81 O6 N2 P1	10.84
429	SM(d35:2)	SM	714.5676	C40 H79 O6 N2 P1	9.86
430	SM(d35:2)	SM	714.5676	C40 H79 O6 N2 P1	10.17
431	SM(d35:3)	SM	712.5519	C40 H77 O6 N2 P1	8.70
432	SM(d35:4)	SM	710.5363	C40 H75 O6 N2 P1	9.57
433	SM(d36:0)	SM	732.6145	C41 H85 O6 N2 P1	12.63
434	SM(d36:1)	SM	730.5989	C41 H83 O6 N2 P1	12.01
435	SM(d36:2)	SM	728.5832	C41 H81 O6 N2 P1	10.67
436	SM(d36:3)	SM	726.5676	C41 H79 O6 N2 P1	9.47
437	SM(d36:4)	SM	724.5519	C41 H77 O6 N2 P1	8.17
438	SM(d36:5)	SM	722.5363	C41 H75 O6 N2 P1	9.24
439	SM(d36:5)	SM	722.5363	C41 H75 O6 N2 P1	9.04
440	SM(d37:0)	SM	746.6302	C42 H87 O6 N2 P1	13.48
441	SM(d37:1)	SM	744.6145	C42 H85 O6 N2 P1	12.94
442	SM(d37:1)	SM	744.6145	C42 H85 O6 N2 P1	12.48
443	SM(d37:2)	SM	742.5989	C42 H83 O6 N2 P1	11.53
444	SM(d37:2)	SM	742.5989	C42 H83 O6 N2 P1	11.26
445	SM(d37:3)	SM	740.5832	C42 H81 O6 N2 P1	10.01
446	SM(d37:4)	SM	738.5676	C42 H79 O6 N2 P1	11.21
447	SM(d37:4)	SM	738.5676	C42 H79 O6 N2 P1	10.84
448	SM(d37:5)	SM	736.5519	C42 H77 O6 N2 P1	9.85
449	SM(d38:0)	SM	760.6458	C43 H89 O6 N2 P1	14.29
450	SM(d38:1)	SM	758.6302	C43 H87 O6 N2 P1	13.76
451	SM(d38:1)	SM	758.6302	C43 H87 O6 N2 P1	13.63
452	SM(d38:2)	SM	756.6145	C43 H85 O6 N2 P1	12.35
453	SM(d38:3)	SM	754.5989	C43 H83 O6 N2 P1	11.04
454	SM(d38:3)	SM	754.5989	C43 H83 O6 N2 P1	10.75
455	SM(d38:4)	SM	752.5832	C43 H81 O6 N2 P1	9.51
456	SM(d38:5)	SM	750.5676	C43 H79 O6 N2 P1	10.67
457	SM(d38:6)	SM	748.5519	C43 H77 O6 N2 P1	9.47
458	SM(d39:0)	SM	774.6615	C44 H91 O6 N2 P1	15.11
459	SM(d39:1)	SM	772.6458	C44 H89 O6 N2 P1	14.58
460	SM(d39:2)	SM	770.6302	C44 H87 O6 N2 P1	13.18

461	SM(d39:2)	SM	770.6302	C44 H87 O6 N2 P1	12.83
462	SM(d39:3)	SM	768.6145	C44 H85 O6 N2 P1	11.97
463	SM(d39:3)	SM	768.6145	C44 H85 O6 N2 P1	11.76
464	SM(d39:3)	SM	768.6145	C44 H85 O6 N2 P1	11.52
465	SM(d39:4)	SM	766.5989	C44 H83 O6 N2 P1	12.47
466	SM(d39:4)	SM	766.5989	C44 H83 O6 N2 P1	12.93
467	SM(d39:5)	SM	764.5832	C44 H81 O6 N2 P1	11.25
468	SM(d40:0)	SM	788.6771	C45 H93 O6 N2 P1	15.73
469	SM(d40:1)	SM	786.6615	C45 H91 O6 N2 P1	15.20
470	SM(d40:2)	SM	784.6458	C45 H89 O6 N2 P1	13.60
471	SM(d40:2)	SM	784.6458	C45 H89 O6 N2 P1	14.08
472	SM(d40:3)	SM	782.6302	C45 H87 O6 N2 P1	12.29
473	SM(d40:4)	SM	780.6145	C45 H85 O6 N2 P1	13.95
474	SM(d40:4)	SM	780.6145	C45 H85 O6 N2 P1	10.97
475	SM(d40:5)	SM	778.5989	C45 H83 O6 N2 P1	10.42
476	SM(d40:6)	SM	776.5832	C45 H81 O6 N2 P1	10.76
477	SM(d40:7)	SM	774.5676	C45 H79 O6 N2 P1	9.05
478	SM(d41:1)	SM	800.6771	C46 H93 O6 N2 P1	15.59
479	SM(d41:2)	SM	798.6615	C46 H91 O6 N2 P1	14.77
480	SM(d41:2)	SM	798.6615	C46 H91 O6 N2 P1	14.31
481	SM(d41:3)	SM	796.6458	C46 H89 O6 N2 P1	13.04
482	SM(d41:4)	SM	794.6302	C46 H87 O6 N2 P1	14.59
483	SM(d41:5)	SM	792.6145	C46 H85 O6 N2 P1	10.81
484	SM(d42:1)	SM	814.6928	C47 H95 O6 N2 P1	16.52
485	SM(d42:2)	SM	812.6771	C47 H93 O6 N2 P1	15.52
486	SM(d42:2)	SM	812.6771	C47 H93 O6 N2 P1	15.01
487	SM(d42:3)	SM	810.6615	C47 H91 O6 N2 P1	13.79
488	SM(d42:4)	SM	808.6458	C47 H89 O6 N2 P1	12.71
489	SM(d42:4)	SM	808.6458	C47 H89 O6 N2 P1	15.33
490	SM(d42:4)	SM	808.6458	C47 H89 O6 N2 P1	12.51
491	SM(d42:5)	SM	806.6302	C47 H87 O6 N2 P1	11.59
492	SM(d42:6)	SM	804.6145	C47 H85 O6 N2 P1	10.57
493	SM(d42:6)	SM	804.6145	C47 H85 O6 N2 P1	10.29
494	SM(d42:7)	SM	802.5989	C47 H83 O6 N2 P1	9.94
495	SM(d42:7)	SM	802.5989	C47 H83 O6 N2 P1	11.19
496	SM(d42:7)	SM	802.5989	C47 H83 O6 N2 P1	9.29
497	SM(d42:8)	SM	800.5832	C47 H81 O6 N2 P1	16.82

498	SM(d43:1)	SM	828.7084	C48 H97 O6 N2 P1	17.07
499	SM(d43:1)	SM	828.7084	C48 H97 O6 N2 P1	16.82
500	SM(d43:2)	SM	826.6928	C48 H95 O6 N2 P1	15.40
501	SM(d43:2)	SM	826.6928	C48 H95 O6 N2 P1	15.71
502	SM(d43:2)	SM	826.6928	C48 H95 O6 N2 P1	16.20
503	SM(d43:3)	SM	824.6771	C48 H93 O6 N2 P1	14.55
504	SM(d43:3)	SM	824.6771	C48 H93 O6 N2 P1	14.19
505	SM(d43:4)	SM	822.6615	C48 H91 O6 N2 P1	15.93
506	SM(d43:4)	SM	822.6615	C48 H91 O6 N2 P1	13.48
507	SM(d43:5)	SM	820.6458	C48 H89 O6 N2 P1	14.32
508	SM(d43:6)	SM	818.6302	C48 H87 O6 N2 P1	13.42
509	SM(d43:7)	SM	816.6145	C48 H85 O6 N2 P1	11.95
510	SM(d43:8)	SM	814.5989	C48 H83 O6 N2 P1	10.81
511	SM(d44:1)	SM	842.7241	C49 H99 O6 N2 P1	17.31
512	SM(d44:1)	SM	842.7241	C49 H99 O6 N2 P1	17.05
513	SM(d44:1)	SM	842.7241	C49 H99 O6 N2 P1	17.54
514	SM(d44:2)	SM	840.7084	C49 H97 O6 N2 P1	16.77
515	SM(d44:2)	SM	840.7084	C49 H97 O6 N2 P1	16.06
516	SM(d44:2)	SM	840.7084	C49 H97 O6 N2 P1	16.31
517	SM(d44:3)	SM	838.6928	C49 H95 O6 N2 P1	15.26
518	SM(d44:4)	SM	836.6771	C49 H93 O6 N2 P1	14.03
519	SM(d44:5)	SM	834.6615	C49 H91 O6 N2 P1	12.88
520	SM(d44:6)	SM	832.6458	C49 H89 O6 N2 P1	11.61
521	SM(d44:6)	SM	832.6458	C49 H89 O6 N2 P1	12.03
522	SM(d44:7)	SM	830.6302	C49 H87 O6 N2 P1	10.74
523	SM(d44:7)	SM	830.6302	C49 H87 O6 N2 P1	12.21
524	SM(d44:7)	SM	830.6302	C49 H87 O6 N2 P1	13.06
525	SM(d44:8)	SM	828.6145	C49 H85 O6 N2 P1	11.27
526	SM(d44:8)	SM	828.6145	C49 H85 O6 N2 P1	11.58
527	SM(d45:4)	SM	850.6928	C50 H95 O6 N2 P1	17.07
528	SM(d45:4)	SM	850.6928	C50 H95 O6 N2 P1	16.82
529	SM(d45:5)	SM	848.6771	C50 H93 O6 N2 P1	16.21
530	SM(d45:5)	SM	848.6771	C50 H93 O6 N2 P1	15.71
531	SM(d45:5)	SM	848.6771	C50 H93 O6 N2 P1	15.41
532	SM(d45:6)	SM	846.6615	C50 H91 O6 N2 P1	14.54
533	SM(d45:6)	SM	846.6615	C50 H91 O6 N2 P1	14.20
534	SM(d46:5)	SM	862.6928	C51 H95 O6 N2 P1	16.31

535	SM(d46:6)	SM	860.6771	C51 H93 O6 N2 P1	15.28
536	SM(d46:7)	SM	858.6615	C51 H91 O6 N2 P1	14.07
537	SM(d46:8)	SM	856.6458	C51 H89 O6 N2 P1	12.89
538	TG(10:0_10:0_12:0)	TG	582.4859	C35 H66 O6	13.55
539	TG(10:0_10:0_18:1)	TG	664.5642	C41 H76 O6	16.42
540	TG(10:0_10:0_18:2)	TG	662.5485	C41 H74 O6	15.40
541	TG(10:0_10:0_18:3)	TG	660.5329	C41 H72 O6	14.38
542	TG(10:0_12:0_12:0)	TG	610.5172	C37 H70 O6	14.94
543	TG(10:0_12:0_14:1)	TG	636.5329	C39 H72 O6	15.20
544	TG(10:0_12:0_18:1)	TG	692.5955	C43 H80 O6	17.34
545	TG(10:0_12:0_18:2)	TG	690.5798	C43 H78 O6	16.52
546	TG(10:0_12:0_18:3)	TG	688.5642	C43 H76 O6	15.69
547	TG(10:0_12:0_20:4)	TG	714.5798	C45 H78 O6	17.33
548	TG(10:0_12:0_20:5)	TG	712.5642	C45 H76 O6	16.52
549	TG(10:0_18:1_22:6)	TG	820.6581	C53 H88 O6	17.84
550	TG(10:0_18:2_18:2)	TG	770.6424	C49 H86 O6	17.67
551	TG(10:0_18:2_18:3)	TG	768.6268	C49 H84 O6	17.05
552	TG(10:0_18:3_18:3)	TG	766.6111	C49 H82 O6	17.71
553	TG(10:0_18:3_22:6)	TG	816.6268	C53 H84 O6	17.29
554	TG(12:0_12:0_12:0)	TG	638.5485	C39 H74 O6	16.24
555	TG(12:0_12:0_14:0)	TG	666.5798	C41 H78 O6	17.28
556	TG(12:0_12:0_17:1)	TG	706.6111	C44 H82 O6	17.77
557	TG(12:0_12:0_18:2)	TG	718.6111	C45 H82 O6	17.45
558	TG(12:0_12:0_18:3)	TG	716.5955	C45 H80 O6	16.81
559	TG(12:0_12:0_18:3)	TG	716.5955	C45 H80 O6	18.12
560	TG(12:0_12:0_20:4)	TG	742.6111	C47 H82 O6	18.12
561	TG(12:0_12:0_20:5)	TG	740.5955	C47 H80 O6	17.45
562	TG(12:0_14:0_14:0)	TG	694.6111	C43 H82 O6	18.12
563	TG(12:0_14:0_18:2)	TG	746.6424	C47 H86 O6	18.25
564	TG(12:0_14:0_18:3)	TG	744.6268	C47 H84 O6	17.71
565	TG(12:0_14:0_18:3)	TG	744.6268	C47 H84 O6	18.82
566	TG(12:0_14:0_20:4)	TG	770.6424	C49 H86 O6	18.81
567	TG(12:0_14:1_20:5)	TG	766.6111	C49 H82 O6	17.59
568	TG(12:0_17:1_18:2)	TG	786.6737	C50 H90 O6	18.61
569	TG(12:0_18:2_18:2)	TG	798.6737	C51 H90 O6	18.36
570	TG(12:0_18:2_18:3)	TG	796.6581	C51 H88 O6	17.85
571	TG(12:0_18:2_20:5)	TG	820.6581	C53 H88 O6	18.37

572	TG(12:0_18:2_22:6)	TG	846.6737	C55 H90 O6	17.89
573	TG(12:0_18:3_18:3)	TG	794.6424	C51 H86 O6	17.29
574	TG(12:0_18:3_20:5)	TG	818.6424	C53 H86 O6	17.84
575	TG(14:0_14:0_20:4)	TG	798.6737	C51 H90 O6	19.39
576	TG(14:0_14:0_22:6)	TG	822.6737	C53 H90 O6	18.50
577	TG(14:0_17:1_18:2)	TG	814.705	C52 H94 O6	19.21
578	TG(14:0_18:2_18:3)	TG	824.6894	C53 H92 O6	18.56
579	TG(14:0_18:2_20:5)	TG	848.6894	C55 H92 O6	18.99
580	TG(14:0_18:3_20:4)	TG	848.6894	C55 H92 O6	19.31
581	TG(14:0_20:5_20:5)	TG	870.6737	C57 H90 O6	18.36
582	TG(15:0_10:0_14:0)	TG	680.5955	C42 H80 O6	17.57
583	TG(15:0_10:0_18:1)	TG	734.6424	C46 H86 O6	18.35
584	TG(15:0_12:0_14:0)	TG	708.6268	C44 H84 O6	18.36
585	TG(15:0_12:0_14:0)	TG	708.6268	C44 H84 O6	18.50
586	TG(15:0_12:0_18:1)	TG	762.6737	C48 H90 O6	18.99
587	TG(15:0_12:0_18:2)	TG	760.6581	C48 H88 O6	18.59
588	TG(15:0_14:0_14:0)	TG	736.6581	C46 H88 O6	18.99
589	TG(15:0_14:0_16:0)	TG	764.6894	C48 H92 O6	19.56
590	TG(15:0_14:0_18:1)	TG	790.705	C50 H94 O6	19.66
591	TG(15:0_14:0_18:2)	TG	788.6894	C50 H92 O6	19.15
592	TG(15:0_14:0_18:3)	TG	786.6737	C50 H90 O6	18.78
593	TG(15:0_16:0_16:0)	TG	792.7207	C50 H96 O6	20.07
594	TG(15:0_16:0_18:1)	TG	818.7363	C52 H98 O6	20.04
595	TG(15:0_16:0_18:2)	TG	816.7207	C52 H96 O6	19.65
596	TG(15:0_16:1_18:3)	TG	812.6894	C52 H92 O6	19.01
597	TG(15:0_18:1_18:1)	TG	844.752	C54 H100 O6	18.91
598	TG(15:0_18:1_18:2)	TG	842.7363	C54 H98 O6	19.73
599	TG(15:0_18:1_20:5)	TG	864.7207	C56 H96 O6	19.62
600	TG(15:0_18:1_22:6)	TG	890.7363	C58 H98 O6	19.35
601	TG(15:0_18:2_18:2)	TG	840.7207	C54 H96 O6	19.29
602	TG(15:0_18:2_18:3)	TG	838.705	C54 H94 O6	19.69
603	TG(15:0_18:2_20:5)	TG	862.705	C56 H94 O6	19.30
604	TG(15:0_18:2_22:6)	TG	888.7207	C58 H96 O6	18.91
605	TG(15:0_8:0_16:0)	TG	680.5955	C42 H80 O6	17.74
606	TG(16:0_10:0_22:6)	TG	794.6424	C51 H86 O6	17.80
607	TG(16:0_12:0_18:1)	TG	776.6894	C49 H92 O6	19.39
608	TG(16:0_12:0_18:3)	TG	772.6581	C49 H88 O6	19.41

609	TG(16:0_14:0_14:0)	TG	750.6737	C47 H90 O6	19.29
610	TG(16:0_14:0_18:1)	TG	804.7207	C51 H96 O6	19.91
611	TG(16:0_14:0_18:3)	TG	800.6894	C51 H92 O6	19.09
612	TG(16:0_14:0_20:4)	TG	826.705	C53 H94 O6	19.30
613	TG(16:0_14:0_22:6)	TG	850.705	C55 H94 O6	19.11
614	TG(16:0_14:1_18:3)	TG	798.6737	C51 H90 O6	18.71
615	TG(16:0_16:0_16:0)	TG	806.7363	C51 H98 O6	20.40
616	TG(16:0_16:0_17:0)	TG	820.752	C52 H100 O6	20.51
617	TG(16:0_16:0_17:1)	TG	818.7363	C52 H98 O6	20.54
618	TG(16:0_16:0_18:1)	TG	832.752	C53 H100 O6	20.37
619	TG(16:0_16:0_20:4)	TG	854.7363	C55 H98 O6	19.83
620	TG(16:0_16:0_20:5)	TG	852.7207	C55 H96 O6	20.01
621	TG(16:0_16:0_24:0)	TG	918.8615	C59 H114 O6	21.88
622	TG(16:0_16:1_18:1)	TG	830.7363	C53 H98 O6	20.00
623	TG(16:0_16:1_18:2)	TG	828.7207	C53 H96 O6	19.65
624	TG(16:0_17:0_18:1)	TG	846.7676	C54 H102 O6	20.48
625	TG(16:0_17:1_18:1)	TG	844.752	C54 H100 O6	20.53
626	TG(16:0_18:1_18:1)	TG	858.7676	C55 H102 O6	20.35
627	TG(16:0_18:1_20:4)	TG	880.752	C57 H100 O6	20.34
628	TG(16:0_18:1_20:5)	TG	878.7363	C57 H98 O6	19.98
629	TG(16:0_18:2_18:2)	TG	854.7363	C55 H98 O6	19.55
630	TG(16:0_18:2_18:3)	TG	852.7207	C55 H96 O6	19.19
631	TG(16:0_18:2_20:4)	TG	878.7363	C57 H98 O6	19.37
632	TG(16:0_18:2_20:5)	TG	876.7207	C57 H96 O6	19.59
633	TG(16:0_18:2_22:4)	TG	906.7676	C59 H102 O6	19.81
634	TG(16:0_18:2_22:5)	TG	904.752	C59 H100 O6	19.64
635	TG(16:0_18:2_22:6)	TG	902.7363	C59 H98 O6	19.20
636	TG(16:0_18:3_20:5)	TG	874.705	C57 H94 O6	19.18
637	TG(16:0_20:4_22:6)	TG	926.7363	C61 H98 O6	19.02
638	TG(16:0_20:5_22:6)	TG	924.7207	C61 H96 O6	18.61
639	TG(16:0_20:5_22:6)	TG	924.7207	C61 H96 O6	19.21
640	TG(16:0_22:5_22:6)	TG	952.752	C63 H100 O6	19.22
641	TG(16:0_22:6_22:6)	TG	950.7363	C63 H98 O6	18.81
642	TG(16:1_12:0_20:4)	TG	796.6581	C51 H88 O6	18.91
643	TG(16:1_12:0_20:5)	TG	794.6424	C51 H86 O6	18.27
644	TG(16:1_14:1_16:1)	TG	772.6581	C49 H88 O6	18.27
645	TG(16:1_17:1_18:1)	TG	842.7363	C54 H98 O6	18.28

646	TG(16:1_18:2_18:2)	TG	852.7207	C55 H96 O6	19.02
647	TG(16:1_18:2_18:3)	TG	850.705	C55 H94 O6	18.80
648	TG(16:1_18:2_22:6)	TG	900.7207	C59 H96 O6	18.61
649	TG(16:1_18:3_20:5)	TG	872.6894	C57 H92 O6	18.80
650	TG(16:2_18:2_18:3)	TG	848.6894	C55 H92 O6	18.36
651	TG(17:0_18:1_18:1)	TG	872.7833	C56 H104 O6	20.56
652	TG(17:0_18:1_18:2)	TG	870.7676	C56 H102 O6	20.11
653	TG(17:0_18:1_20:4)	TG	894.7676	C58 H102 O6	20.07
654	TG(17:0_18:2_20:4)	TG	892.752	C58 H100 O6	19.64
655	TG(18:0_12:0_16:0)	TG	778.705	C49 H94 O6	19.93
656	TG(18:0_16:0_16:0)	TG	834.7676	C53 H102 O6	20.82
657	TG(18:0_16:0_17:0)	TG	848.7833	C54 H104 O6	20.92
658	TG(18:0_16:0_18:0)	TG	862.7989	C55 H106 O6	21.20
659	TG(18:0_16:0_18:1)	TG	860.7833	C55 H104 O6	20.79
660	TG(18:0_16:0_20:4)	TG	882.7676	C57 H102 O6	20.79
661	TG(18:0_16:0_22:6)	TG	906.7676	C59 H102 O6	20.16
662	TG(18:0_17:0_18:0)	TG	876.8146	C56 H108 O6	21.31
663	TG(18:0_17:0_18:1)	TG	874.7989	C56 H106 O6	20.96
664	TG(18:0_17:0_20:4)	TG	896.7833	C58 H104 O6	20.54
665	TG(18:0_18:0_18:0)	TG	890.8302	C57 H110 O6	21.56
666	TG(18:0_18:0_18:1)	TG	888.8146	C57 H108 O6	21.17
667	TG(18:0_18:1_18:1)	TG	886.7989	C57 H106 O6	20.77
668	TG(18:0_18:1_20:0)	TG	916.8459	C59 H112 O6	21.53
669	TG(18:0_18:1_20:4)	TG	908.7833	C59 H104 O6	20.29
670	TG(18:0_18:1_20:4)	TG	908.7833	C59 H104 O6	20.75
671	TG(18:0_18:1_22:0)	TG	944.8772	C61 H116 O6	21.86
672	TG(18:0_18:1_22:5)	TG	934.7989	C61 H106 O6	20.43
673	TG(18:0_18:1_22:6)	TG	932.7833	C61 H104 O6	20.13
674	TG(18:0_18:1_22:6)	TG	932.7833	C61 H104 O6	20.51
675	TG(18:0_18:1_24:0)	TG	972.9085	C63 H120 O6	22.16
676	TG(18:0_20:0_22:0)	TG	974.9241	C63 H122 O6	22.45
677	TG(18:0_20:4_22:4)	TG	958.7989	C63 H106 O6	20.11
678	TG(18:0_20:4_22:6)	TG	954.7676	C63 H102 O6	19.59
679	TG(18:0_22:0_22:0)	TG	1002.9554	C65 H126 O6	22.73
680	TG(18:1_12:0_12:0)	TG	720.6268	C45 H84 O6	18.12
681	TG(18:1_12:0_14:0)	TG	748.6581	C47 H88 O6	18.82
682	TG(18:1_12:0_18:1)	TG	802.705	C51 H94 O6	19.40

683	TG(18:1_12:0_18:2)	TG	800.6894	C51 H92 O6	18.90
684	TG(18:1_12:0_20:5)	TG	822.6737	C53 H90 O6	18.89
685	TG(18:1_14:0_17:1)	TG	816.7207	C52 H96 O6	20.08
686	TG(18:1_14:0_18:1)	TG	830.7363	C53 H98 O6	19.89
687	TG(18:1_14:0_18:2)	TG	828.7207	C53 H96 O6	19.47
688	TG(18:1_14:0_18:3)	TG	826.705	C53 H94 O6	18.99
689	TG(18:1_14:0_20:4)	TG	852.7207	C55 H96 O6	19.87
690	TG(18:1_17:1_18:1)	TG	870.7676	C56 H102 O6	18.90
691	TG(18:1_17:1_18:2)	TG	868.752	C56 H100 O6	20.10
692	TG(18:1_18:1_18:1)	TG	884.7833	C57 H104 O6	20.34
693	TG(18:1_18:1_18:2)	TG	882.7676	C57 H102 O6	19.95
694	TG(18:1_18:1_22:0)	TG	942.8615	C61 H114 O6	21.51
695	TG(18:1_18:1_22:4)	TG	934.7989	C61 H106 O6	20.16
696	TG(18:1_18:1_22:5)	TG	932.7833	C61 H104 O6	19.80
697	TG(18:1_18:1_22:6)	TG	930.7676	C61 H102 O6	20.16
698	TG(18:1_18:2_18:2)	TG	880.752	C57 H100 O6	19.55
699	TG(18:1_18:2_20:2)	TG	908.7833	C59 H104 O6	20.16
700	TG(18:1_18:2_20:4)	TG	904.752	C59 H100 O6	19.39
701	TG(18:1_18:2_20:4)	TG	904.752	C59 H100 O6	20.08
702	TG(18:1_18:2_22:0)	TG	940.8459	C61 H112 O6	21.23
703	TG(18:1_18:2_22:5)	TG	930.7676	C61 H102 O6	19.40
704	TG(18:1_18:2_22:6)	TG	928.752	C61 H100 O6	18.72
705	TG(18:1_18:3_24:0)	TG	966.8615	C63 H114 O6	21.32
706	TG(18:1_20:3_20:4)	TG	930.7676	C61 H102 O6	20.28
707	TG(18:1_20:4_20:4)	TG	928.752	C61 H100 O6	19.82
708	TG(18:1_20:4_22:0)	TG	964.8459	C63 H112 O6	21.09
709	TG(18:1_20:4_24:0)	TG	992.8772	C65 H116 O6	21.46
710	TG(18:2_14:1_17:1)	TG	812.6894	C52 H92 O6	18.75
711	TG(18:2_17:1_18:2)	TG	866.7363	C56 H98 O6	19.30
712	TG(18:2_17:1_22:6)	TG	914.7363	C60 H98 O6	18.90
713	TG(18:2_18:2_18:2)	TG	878.7363	C57 H98 O6	19.11
714	TG(18:2_18:2_20:4)	TG	902.7363	C59 H98 O6	18.95
715	TG(18:2_18:2_22:6)	TG	926.7363	C61 H98 O6	18.71
716	TG(18:2_18:2_22:6)	TG	926.7363	C61 H98 O6	19.37
717	TG(18:2_20:4_22:6)	TG	950.7363	C63 H98 O6	18.50
718	TG(18:2_22:6_22:6)	TG	974.7363	C65 H98 O6	18.27
719	TG(18:3_14:1_18:2)	TG	822.6737	C53 H90 O6	18.13

720	TG(18:3_17:1_18:2)	TG	864.7207	C56 H96 O6	18.88
721	TG(18:3_18:2_18:2)	TG	876.7207	C57 H96 O6	18.68
722	TG(18:3_18:2_18:3)	TG	874.705	C57 H94 O6	18.23
723	TG(18:3_18:2_18:3)	TG	874.705	C57 H94 O6	18.59
724	TG(18:3_18:2_20:5)	TG	898.705	C59 H94 O6	18.06
725	TG(18:3_18:2_20:5)	TG	898.705	C59 H94 O6	18.69
726	TG(18:3_18:2_20:5)	TG	898.705	C59 H94 O6	19.00
727	TG(18:3_18:2_22:6)	TG	924.7207	C61 H96 O6	18.26
728	TG(18:3_18:3_20:3)	TG	900.7207	C59 H96 O6	18.80
729	TG(18:3_18:3_20:5)	TG	896.6894	C59 H92 O6	18.21
730	TG(20:0_18:1_18:1)	TG	914.8302	C59 H110 O6	20.72
731	TG(20:0_18:1_18:1)	TG	914.8302	C59 H110 O6	21.14
732	TG(20:0_18:1_18:2)	TG	912.8146	C59 H108 O6	20.84
733	TG(20:1_18:1_18:1)	TG	912.8146	C59 H108 O6	20.72
734	TG(20:5_14:1_18:2)	TG	846.6737	C55 H90 O6	18.55
735	TG(20:5_17:1_18:2)	TG	888.7207	C58 H96 O6	18.74
736	TG(20:5_17:1_18:2)	TG	888.7207	C58 H96 O6	19.31
737	TG(20:5_18:2_18:2)	TG	900.7207	C59 H96 O6	19.38
738	TG(20:5_18:2_22:6)	TG	948.7207	C63 H96 O6	18.04
739	TG(20:5_18:2_22:6)	TG	948.7207	C63 H96 O6	18.70
740	TG(22:0_18:2_18:2)	TG	938.8302	C61 H110 O6	20.93
741	TG(22:5_17:1_18:2)	TG	916.752	C60 H100 O6	19.35
742	TG(22:5_18:2_18:2)	TG	928.752	C61 H100 O6	19.19
743	TG(24:0_18:2_20:5)	TG	988.8459	C65 H112 O6	21.31
744	TG(8:0_10:0_10:0)	TG	526.4233	C31 H58 O6	10.44
745	TG(8:0_10:0_12:0)	TG	554.4546	C33 H62 O6	12.01
746	TG(8:0_10:0_18:2)	TG	634.5172	C39 H70 O6	13.99
747	TG(8:0_10:0_20:5)	TG	656.5016	C41 H68 O6	13.99
748	TG(8:0_12:0_18:3)	TG	660.5329	C41 H72 O6	16.41
749	TG(8:0_14:0_20:5)	TG	712.5642	C45 H76 O6	16.84
750	TG(8:0_18:2_18:2)	TG	742.6111	C47 H82 O6	16.85
751	TG(8:0_18:2_18:3)	TG	740.5955	C47 H80 O6	16.10
752	TG(8:0_8:0_10:0)	TG	498.392	C29 H54 O6	8.97
753	TG(8:0_8:0_8:0)	TG	470.3607	C27 H50 O6	7.58